SELECTIVE PAIR LUMINESCENCE OF MAGNESIUM IN GALLIUM ARSENIDE

DISSERTATION

Jeffrey R. Cavins
Captain, USAF

AFIT/DS/ENP/88-2

DEPARTMENT OF THE AIR FORCE
AIR UNIVERSITY
AIR FORCE INSTITUTE OF TECHNOLOGY

Wright-Patterson Air Force Base, Ohio

AFIT/DS/ENP/88-2

SELECTIVE PAIR LUMINESCENCE OF MAGNESIUM IN GALLIUM ARSENIDE

DISSERTATION

Jeffrey R. Cavins
Captain, USAF

AFIT/DS/ENP/88-2

AFIT/DS/ENP/88-2

SELECTIVE PAIR LUMINESCENCE OF MAGNESIUM IN GALLIUM ARSENIDE

DISSERTATION

Presented to the Faculty of the School of Engineering

of the Air Force Institute of Technology

Air University

In Partial Fulfillment of the

Requirements for the Degree of

Doctor of Philosophy

Jeffrey R. Cavins, B.S., M.S.

Captain, USAF

December 1988

AFIT/DS/ENP/88-2

SELECTIVE PAIR LUMINESCENCE OF MAGNESIUM IN GALLIUM ARSENIDE

Jeffrey R. Cavins, B. S., M. S.
Captain, USAF

Approved:

Yung Kee Yeo 12/5/88
Chairman

Robert L Hengehold 12/5/88

Yoon B Roh 12/5/88

Edward S. Kolesar 12/5/88

Ronald C. Rey 12/5/88

Accepted:

J S Przemieniecki 5 Dec. 1988
Dean, School of Engineering

Preface

The purpose of this research is to investigate Mg implanted VPE GaAs using both photoluminescent and selective pair luminescent techniques. The luminescence from below band gap optical pumping is a relatively new diagnostic in the study of semiconductors, and the results for Mg acceptor and ion implanted layers gave new information on acceptor energy levels in GaAs.

There are a great many people who contribute both directly and indirectly to a research project such as this. First and foremost, I would like to thank Dr. Yung Kee Yeo and Dr. Robert L. Hengehold, my research advisers, without whose patience and insistent pushing I would never have finished this project. I am grateful to Dr. Won Roh for his valuable advice. The Physics Department Laboratory Staff were the greatest; thanks to Bill Evans, Walt Pemberton, and Rick Patton for keeping me supplied and my equipment working.

And finally thanks to my wife Deborah, for her understanding, and for pushing me forward when my motivation lagged, to my son, Mark, whose timely arrival provided the extra time I needed to finish the research, and to Nikki and Brian, who will get their Dad back when this is over.

Table of Contents

List of Figures

List of Tables

List of Symbols

Å = Angstrom

BE = Bound Exciton

cm = Centimeter

CW = Continuous Wave

°C = Degrees Celsius

DAP = Donor-Acceptor Pair

eV = Electron Volt

FB = Free to Bound

gm = Gram

IR = Infrared

K = Degrees of Kelvin

meV = Milli-Electron Volt

mm = Millimeter

mW = Milliwatt

PL = Photoluminescence

SPL = Selective Pair Luminescence

W = Watt

μm = Micrometer (Micron)

Abstract

Photoluminescence (PL) and selective pair luminescence (SPL) studies were performed on vapor phase epitaxial (VPE) GaAs. The GaAs included both undoped and Mg ion implanted samples with fluences of 10^{12}, $5x10^{12}$, 10^{13}, $5x10^{13}$, and 10^{14} Mg/cm^2, respectively.

PL from the unimplanted samples indicated Zn was the dominant impurity with slight traces of C and Si also evident. In addition, the SPL spectra contained three peaks at 17.2, 20.0, and 21.1 meV, which coincide with the values expected for the $2P_{3/2}$, $2S_{3/2}$, and $2P_{5/2}\Gamma_8$ states of Mg, respectively. This assignment was confirmed during SPL measurements of the ion implanted samples. The effect of the Mg implant on the relative intensities of the Mg related SPL transitions was small but discernible. Photoluminescence of the ion implanted materials showed strong Mg impurity spectra; however, the Zn impurity spectra was still dominant.

Additionally, a parametric study was performed on the effects of temperature and laser pump intensity on the SPL spectra. Temperature behavior of the SPL spectra was similar to the PL with the strongest SPL transitions visible at temperatures as high as 30 K. Analysis of the intensity

behavior of the SPL spectra indicated pump intensity should be minimized (less than 70 mW/cm^2) for best results.

SELECTIVE PAIR LUMINESCENCE OF MAGNESIUM IN GALLIUM ARSENIDE

Chapter I

Introduction

The Air Force and industry have been studying GaAs for many years as both a replacement and complement to Si in electronics. The material properties for GaAs (Table I)(2) make it superior to Si in many military applications. The larger band gap allows GaAs to operate at considerably higher temperatures than Si, before thermal carrier generation becomes a serious problem. The higher majority carrier mobility and shorter minority carrier lifetime of GaAs allows it to be used in devices in which high switching speeds are needed such as high speed integrated circuits and microwave devices. Also, the direct band gap of GaAs allows the construction of devices which were not possible with indirect band gap Si.

The continued research in GaAs is further fueled by research in and use of the many alloys such as $Al_xGa_{1-x}As$ and $Ga_xIn_{1-x}As$ to produce many hybrid structures. More recently the interest in superlattice and quantum well structures has spurred the construction of new devices using GaAs and its

alloys. The structures are used in such devices as semiconductor lasers and new optical detectors.

The use of GaAs, however, is not without problems. The major problem arises from the high vapor pressure of the As at elevated temperatures. One of the standard techniques for doping Si semiconductors is through diffusion doping at high temperatures. This technique does not work for GaAs since it decomposes at higher temperatures. Thus, one of the standard techniques adopted by many researchers has been ion implantation. Ion implantation itself is not without difficulty since the implantation causes a considerable amount of lattice damage which requires annealing to repair.

Many studies of doping and annealing techniques have been performed. The major optical technique for characterizing the effect of the implant and annealing has been photoluminescence (PL). PL has the ability to reveal the types of impurities present in a semiconductor material on a qualitative basis, which is not possible with electrical measurements.

Problem Statement.

Photoluminescence has been the technique of choice for many years for identification of impurities and the associated impurity energy levels, qualitative measurements of the effects of ion implantation and annealing, and the

Table I: Properties of GaAs

(at room temperature unless specified otherwise)

Properties	Value
Band Gap at 4.2 °K	1.5194 eV
Lattice Constant	5.6533 Å
Crystal Density	5.360 gm/cm^3
Melting Point	1238 °C
Linear Thermal Expansion Coefficient	6.4x10^{-6}/°C
Specific Heat C_p	0.08 cal/g-deg K
Debye Temperature	370 K
LO Phonon Energy	36.25 meV
TO Phonon Energy	33.29 meV
Electron Effective Mass*	0.0665 m_o
Hole Effective Mass*	0.48 m_o

* m_o = electron rest mass

effects of variations in the growth conditions on the crystal. Unfortunately, PL has some limitations. Many impurities have energy levels that are very close in energy, and with line broadening, distinguishing between one impurity and another may become very difficult if not impossible in many cases. In addition, if a given impurity is optically dominant in the material it can mask other impurities that are present, preventing detection of the minority impurities. In some crystals, such as crystals

with Cr compensation, the PL signal is weak and of poor quality causing difficulties in impurity identification.

Selective pair luminescence (SPL) is a relatively new technique for producing optical luminescence in semiconductor crystals. Instead of pumping the material with above band gap photons the way PL does, SPL uses below band gap photons to pump the material. In this manner only selected luminescent transitions in the material are pumped. Other transitions which compete with the transitions of interest can be removed from the spectra by pumping below their formation energies. A reduction in competing transition such as exciton and free-to-bound (FB) transitions can greatly enhance the resolution of donor-acceptor pair (DAP) transitions. Discrete pumping of the excited states of DAP transitions can allow us to observe multiple spectral lines from a given impurity. The discrete pumping also allows us to observe very narrow linewidth transitions from the DAP excited states since only pairs of a given separation are pumped, as opposed to all possible separations as in PL. The multiple sharp transitions for individual impurities combined with a reduction in competing transitions yield much more information about the material with improved sensitivity.

In order for SPL to be useful as a diagnostic, it is necessary to build a database of transitions for known impurities in GaAs. Several SPL studies have already been

accomplished concerning GaAs with Zn, C, Si, and Ge impurities as well as the 1.44 eV transition associated with antisites, and the series of transitions between 1.504 ev and 1.511 eV (1,16,27,33,58,69). However, this leaves a number of impurities, such as Mg, Be, and Cd available for investigation. In addition, I found no evidence that the optimum conditions for observing SPL has been presented in the open literature. For example, the limitations on temperature and pump intensity are not clearly documented in any piece of research. Since SPL uses a below band gap excitation source, the pump energy will penetrate much deeper into the material than the PL source, which uses above band gap excitation. With with near band edge pumping energy, penetration could be as shallow as several microns to as deep as all the way through the material. This technique has been used successfully in the past on bulk grown material and epilayer material of 20 to 30 μm thickness (33:1332).

This research is oriented to studying the excited states of Mg acceptors through SPL. Mg doping is accomplished through ion implantation. Additional analysis was performed for determining the limitations in observing SPL based on implant energy and dose. Also, the effects of temperature and pump intensity were monitored to determine the functional ranges over which the SPL can be observed.

Sequence of Events.

Chapter II, "Theory and Background," contains the background information necessary to understand the observations of the luminescence from the GaAs. It contains the information on band structure, radiative transitions in semiconductors, theory of excited acceptor states, theory behind SPL, and previous observations of PL and SPL in GaAs.

Chapter III, "Experiment," describes the experimental apparatus and procedures used in the PL and SPL measurements.

Chapter IV, "Results and Discussion," contains the results of the PL and SPL from the samples. The information is presented starting with the unimplanted epilayers, covering first the PL then the SPL measurements. The implanted samples are then discussed individually starting with lowest dose, lowest implant energy sample continuing to the highest dose, highest implant energy sample. Following the individual analysis of the samples is a section containing a comparison of the samples and evaluating the overall results of the experiment.

Chapter V , "Conclusions and Recommendations," covers the major conclusions obtained from the present research and recommendations for further research in this area.

Chapter II

Background and Theory

This chapter will detail the basic theory behind radiative transitions in GaAs, including the basic theory of acceptor states in zincblende semiconductors. Following the basic theory will be a section on previous work done in PL and SPL and a tabulation of these results.

Theory

GaAs is a semiconductor with a zincblende crystalline structure. Zincblende is a structure consisting of two interlocking face-centered cubic (FCC) lattices. One FCC lattice is composed entirely of Ga, the other FCC lattice contains only As. The two FCC lattices are separated along the FCC body diagonal by one quarter of its length. The energy band diagram of zincblende structures is shown in Figure 1. GaAs is a direct band gap material and that the Γ_8 band is degenerate near $\vec{k}$=0,0,0.

Radiative Transitions. When above band gap photons strike a semiconductor material, absorption of the photon will produce an electron-hole pair by moving an electron from the valence band to the conduction band, and leaving behind a hole in the valence band.

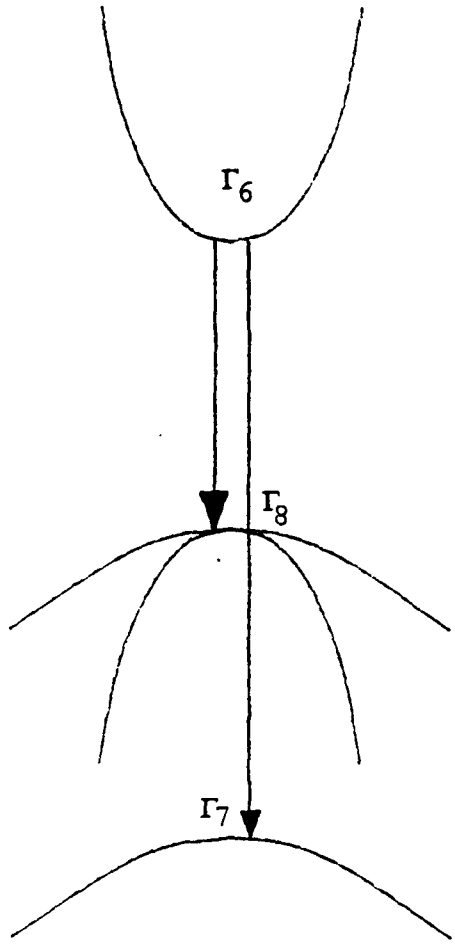

Figure 1: Energy Band Diagram for GaAs near $\vec{k}$=0,0,0.

Once the free charges are created in the bands a number of processes can occur. Auger recombination can occur, in which case no luminescence will be produced. An Auger recombination is a process in which nonradiative recombination occurs. Recombination of the electron-hole pair gives up the excess energy to mechanical processes in the material such as an increase in the kinetic energy of other free charges (73). The free charges will produce a variety of radiative transitions after thermalization depending upon the condition of the material. The basic transitions are shown in Figure 2. The transitions can be partitioned into four basic types: band to band, exciton, free to bound (FB), and donor-acceptor pair (DAP) transitions.

Band to band transitions are simply the direct recombination of an electron in the conduction band with a hole in the valence band.

The exciton structures are more complicated than the other radiative transitions. An exciton is a pseudo-atom formed by the pairing of an electron and hole into a stable atom-like structure. The binding of the electron and hole reduces the energy of the system by (5:628):

$$E_{ex} = (m^*/m)(1/\epsilon_o^2)13.605 \text{ eV}, \qquad (1)$$

where

ϵ_o = is the bulk relative dielectric constant of the material,

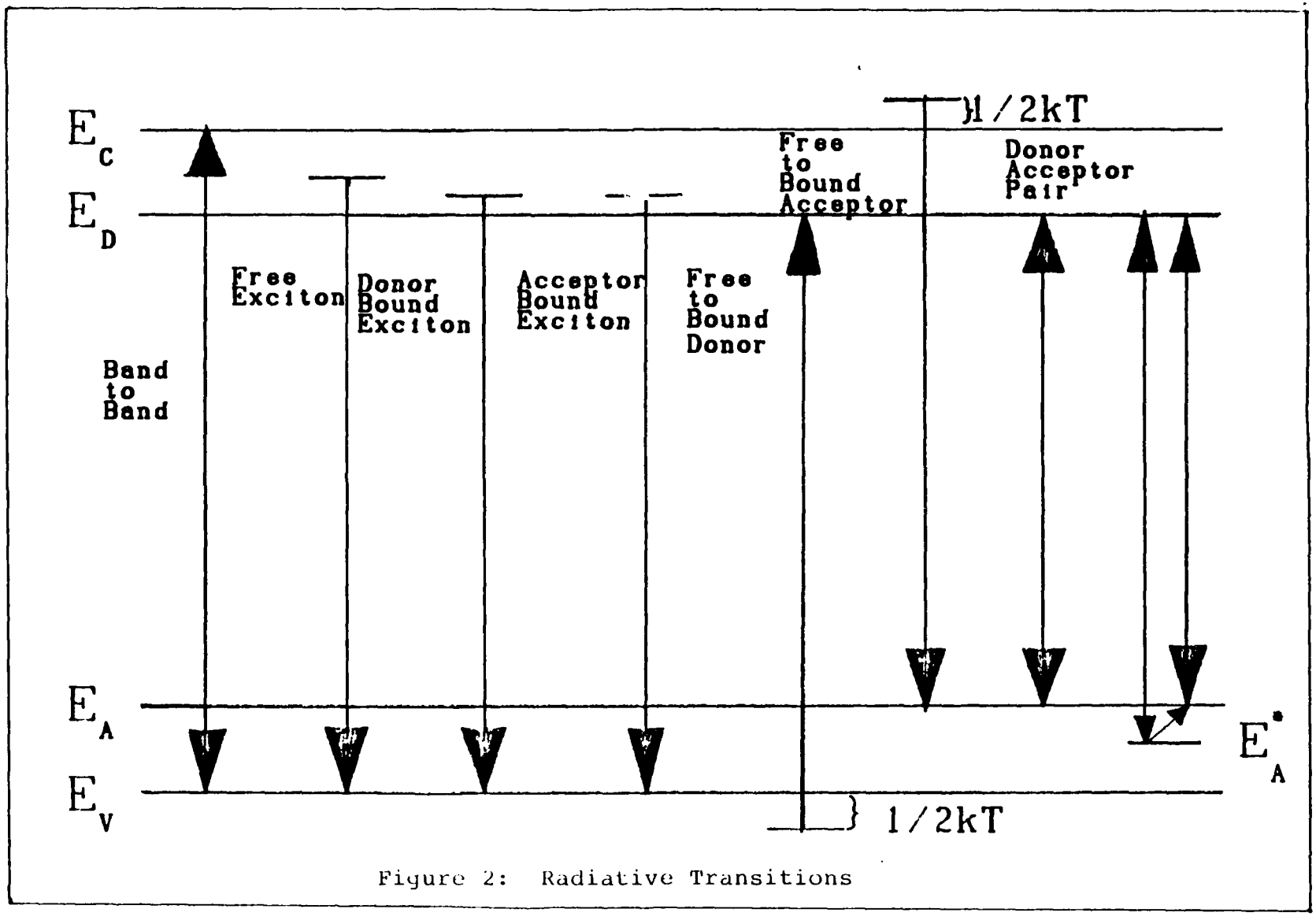

Figure 2: Radiative Transitions

m^* = the reduced effective mass of the electron-hole pair.

m = electron rest mass.

The reduced effective mass of the electron-hole pair is:

$$1/m^* = 1/m_e + 1/m_h, \tag{2}$$

where

m_e = the electron effective mass,

m_h = the hole effective mass.

The recombination energy of the free exciton is given by:

$$E = E_g - E_{ex}, \tag{3}$$

The free exciton is not the only exciton transition in the material. The impurities in the material produce localized potential wells and it is possible for the free exciton to become trapped in these potentials. This situation produces a set of transitions for excitons bound to neutral donors, ionized donors, neutral acceptors, and ionized acceptors, not to mention exciton-defect structures (73). The following set of equations apply to impurity bound excitons in GaAs (13:994-995):

Neutral Donor Bound Exciton

$$E = E_g - E_{ex} - 0.13E_D, \tag{4}$$

where E_D is the binding energy of an isolated donor.

Ionized Donor Bound Exciton

$$E = E_g - E_D - 0.06E_D, \tag{5}$$

Neutral Acceptor Bound Exciton

$$E = E_g - E_{ex} - 0.07E_A, \quad (6)$$

Ionized Acceptor Bound Exciton

$$E = E_g - E_A - 0.4E_A, \quad (7)$$

where E_A is the binding energy of an isolated acceptor.

The excitonic transitions in GaAs are very shallow, and can only be observed when kT is less than the binding energy of the exciton complex.

Other types of transitions include the free-to-bound (FB) transitions. The FB transitions are basically the recombination of a free charge with a neutral impurity site. This can either be a hole with a neutral donor or an electron with a neutral acceptor. The energy of the FB transition is given by:

$$E = E_g - E_{A(D)} + kT/2 \pm nE_{ph}, \quad (8)$$

where

$E_{A(D)}$ = the ground state binding energy of the acceptor or the donor, respectively,

kT/2 = the thermal energy of the free charge,

n = the number of phonons involved in the transition,

E_{ph} = the energy of the phonon in the material.

The basic temperature limitation in observing FB transitions is the binding energy of the impurity. For GaAs E_D is 5.8 meV while E_A is greater than 26.0 meV. This means that acceptor transitions are visible up to relatively high

temperatures, while donor transitions, being relatively shallow, are only visible at low temperatures.

The other type of transition is the donor acceptor pair (DAP) transition. The DAP transition occurs when the electron on a neutral donor becomes coupled to a hole on a neutral acceptor by the Coulomb interaction between the charges. Recombination of the pair will emit radiation corresponding to the energy difference between the donor and acceptor plus the Coulomb interaction term. The relation for this process is shown in equation 9.

$$E = E_g - (E_A + E_D) + e^2/\epsilon_o R + J(R), \qquad (9)$$

where

e = the electronic charge,

R = the separation distance of the donor-acceptor pair sites,

J(R) = the wave function overlap correction term.

The wave function overlap correction term is a modification to the equation to take into account the perturbation in the energy that occurs when the impurities are so close together that the overlap of the individual impurity wave functions is significant. The overlap becomes significant when the pair separation is on the order of (or less than) the classical Bohr radius for the shallowest impurity in the DAP. For GaAs, the donor is the shallowest impurity with a classical Bohr radius of about 100 Å. For single crystal GaAs, the allowed ranges for the pair

separations corresponds to a discrete set of transitions allowed by the lattice sites. This means that for shorter range pairs, discrete transitions should be seen for each allowed pair separation. For longer range pairs, the energy difference becomes so small that the transitions merge into a single featureless peak (73). In fact, discrete DAP transitions have been observed in GaAs (47). The allowed pair separations for a zincblende crystal are given by two different equations (1:3553). For pairs formed where one impurity is on a different type of site (i.e., one on Ga and the other on As) the pair separation is given by:

$$R = a_o \, (m/2 - 5/16)^{1/2}, \qquad (10)$$

where

a_o = the lattice constant which is 5.6533 Å for GaAs.

m = is the lattice shell number.

For pairs formed by impurities on the same type of site (i.e. both on Ga or both on As) the pair separation is given by:

$$R = a_o \, (m/2)^{1/2}, \qquad (11)$$

DAP spectra exhibit the following characteristics during recombination (73):

1. The DAP spectra shift to higher energy with increasing pump intensity.
2. Narrowing of the DAP band occurs with increasing pump intensity.

3. The pair spectra shifts to higher energies as the donor concentration increases.
4. A rapid decrease in intensity occurs as the temperature is increased from 25 K to 35 K.
5. The DAP spectra shifts to higher energies as the temperature increases from 25 K to 35 K.

As can be seen, the properties of the DAP spectra are complex, but understanding of the DAP process is necessary since DAP transitions are the fundamental process observed in SPL.

In addition to the simpler transitions, a number of other radiative transitions occur which are related to more complex processes in the crystal. The spectra emitted from antisites, as well as other crystal defects, arise from quite complex relationships, and most are not well understood.

Acceptor Excited States. The commonly cited reference for the theory of acceptor states in zincblende and diamond structure materials is the work of Baldereschi and Lipari (7,8,9,10). This work represents an extension of work originally performed by Luttinger in 1956 (36). The general approach of this work is to use an effective mass Hamiltonian to solve for the acceptor energy levels. This approximation assumes a Coulombic behavior for the potential. Near the impurity core, however, the potential

deviates strongly from the Coulomb behavior and the approximation fails to provide good results (7:2697).

The Hamiltonian with the effective mass approximation is given by (7:2698):

$$H = (\gamma_1 + 5\gamma_2/2)(p^2/2m_o) - (\gamma_2/m_o)(p_x^2J_x^2 + p_y^2J_y^2 + p_z^2J_z^2) - (2\gamma_3/m_o)[(p_xp_y)(J_xJ_y) + (p_yp_z)(J_yJ_z) + (p_zp_x)(J_zJ_x)] - e^2/\epsilon_o r, \quad (12)$$

where

$\{ab\}$ = $(ab + ba)/2$,

m_o = free electron mass,

γ_1, γ_2, γ_3 = Luttinger valence band parameters,

$\vec{p}$ = linear momentum operator for holes,

$\vec{J}$ = angular momentum operator corresponding to spin 3/2.

The Luttinger valence band parameters describe the hole dispersion relation near the center of the Brillouin zone. The Hamiltonian in equation (12) is valid for crystals with diamond or zincblende structure with strong spin-orbit coupling. The first term in the Hamiltonian is the particle kinetic energy, the second and third terms are attributable to spin-orbit interaction, and the fourth term is the external Coulomb potential.

Introduction of the following second-rank Cartesian tensors can be used to simplify equation (12):

$$P_{ik} = 3p_ip_k - \delta_{ik}p^2, \quad (13)$$

$$J_{ik} = (3/2)(J_iJ_k + J_kJ_i) - \delta_{ik}J^2, \quad (14)$$

These tensor quantities are symmetric and have a vanishing trace. Rewriting equation (12) in terms of (13) and (14) yields a more compact version of the Hamiltonian. That is,

$$H = \gamma_1 p^2/2m_o - e^2/\epsilon_o r - (1/9m_o)[\gamma_3 - (\gamma_3 - \gamma_2)\delta_{ik}]P_{ik}J_{ik}. \quad (15)$$

This equation is a reducible second rank Cartesian tensor which can be broken down into an irreducible spherical tensor. That is,

$$H = (\gamma_1 p^2/2m_o - e^2/\epsilon_o r) - (3\gamma_3 + 2\gamma_2)(P^{(2)}\cdot J^{(2)})/45m_o + (\gamma_3 - \gamma_2)\{[P^{(2)}X\ J^{(2)}]^{(4)}_{-4} + \sqrt{70}/5[P^{(2)}X\ J^{(2)}]^{(4)}_{0} + [P^{(2)}X\ J^{(2)}]^{(4)}_{4}\}/18m_o, \quad (16)$$

where

$P^{(2)}, J^{(2)}$ = are the results of decomposing P_{ik} and J_{ik} into irreducible spherical tensors of rank 2.

This Hamiltonian is functionally the same as equation (15), except that it is now broken into terms with spherical and cubic symmetry. The first two terms are spherically invariant in addition to having cubic symmetry, while the last term is strictly cubic. It now becomes convenient to introduce two new terms:

$$\mu = (6\gamma_3 + 4\gamma_2)/5\gamma_1, \quad (17)$$

and

$$\delta = (\gamma_3 - \gamma_2)/\gamma_1, \quad (18)$$

The term μ is the strength of the spin-orbit interaction, and the term δ is a measure of the cubic contribution to the Hamiltonian. It is also appropriate to introduce two new

units for energy and length, the effective Rydberg (R_o) and the Bohr radius (a_o), respectively (7:2698). That is,

$$R_o = e^4 m_o / 2\hbar^2 \epsilon_o^2 \gamma_1, \tag{19}$$

$$a_o = \hbar^2 \epsilon_o \gamma_1 / e^2 m_o, \tag{20}$$

Rewriting the Hamiltonian in terms of these quantities yields:

$$H = p^2/\hbar^2 - 2/r - \mu(P^{(2)}\cdot J^{(2)})/9\hbar^2 + \delta \{[P^{(2)}XJ^{(2)}]^{(4)}_4 + \sqrt{70}/5[P^{(2)}XJ^{(2)}]^{(4)}_0 + [P^{(2)}XJ^{(2)}]^{(4)}_{-4}\}/9\hbar^2 \tag{21}$$

Ignoring the purely cubic terms as being small in relation to the spherical contributions, we have the spherical Hamiltonian:

$$H_{sph} = (1/\hbar^2)[p^2 - \mu(P^{(2)}\cdot J^{(2)})/9] - 2/r. \tag{22}$$

Analysis of the the Hamiltonian shows that it can be thought of as a hydrogen atom perturbed by the spherical term $(P^{(2)}\cdot J^{(2)})$.

For $\mu = 0$, the Hamiltonian becomes simply the hydrogen atom Hamiltonian. For $\mu = 0$ the spin orbit term must be included and solution of the equation become more difficult. For strong spin-orbit coupling, the total angular momentum $\vec{F} = \vec{L} + \vec{J}$ is a constant of the motion for the spherically symmetric Hamiltonian. In addition, the spin-orbit term only couples hydrogenic states for which $\Delta L = 0, \pm 2$. This allows the following general expressions for the most common wave functions to be written as:

$$\Phi(S_{3/2}) = f_0(r)\,|L=0,J=3/2,F=3/2,F_z\rangle + g_0(r)\,|L=2,J=3/2,F=3/2,F_z\rangle, \quad (23)$$

$$\Phi(P_{1/2}) = f_1(r)\,|L=1,J=3/2,F=1/2,F_z\rangle, \quad (24)$$

$$\Phi(P_{3/2}) = f_2(r)\,|L=1,J=3/2,F=3/2,F_z\rangle + g_2(r)\,|L=3,J=3/2,F=3/2,F_z\rangle, \quad (25)$$

$$\Phi(P_{5/2}) = f_3(r)\,|L=1,J=3/2,F=5/2,F_z\rangle + g_3(r)\,|L=3,J=3/2,F=5/2,F_z\rangle. \quad (26)$$

Where the $|L,J,F,F_z\rangle$ are eigenfunctions of the total angular momentum, and $f_i(r)$ and $g_i(r)$ are the general radial wave functions. Calculation of the Hamiltonian matrix elements is done through the reduced matrix element technique and can be written as:

$$\langle L',J,F,M|\,(P^{(2)}.J^{(2)})\,|L,J,F,M\rangle = (-1)^{L+J+F} \begin{Bmatrix} F & J & L' \\ 2 & L & J \end{Bmatrix} X\ (J||J^{(2)}||J)\,(L'||P^{(2)}||L). \quad (27)$$

The details of the 6-j symbol (in brackets) and the reduced matrix elements in the above equation are available in the appendix of reference 7. The matrix element of the hydrogenic term is given by:

$$\langle L',J,F,M|\,p^2/\hbar^2 - 2/r\,|L,J,F,M\rangle = [-(1/r^2)d\ (r^2d\ /dr)/dr + L(L+1)/r^2 - 2/r]\,\delta_{LL'}. \quad (28)$$

As a result of this analysis a complete system of differential equations are realized which are valid for the $S_{3/2}$, $P_{1/2}$, $P_{3/2}$, and $P_{5/2}$ states. The only state for which we can find an analytical solution is the $P_{1/2}$ state:

$$E(nP_{1/2}) = 1/(1+\mu)n^2, \quad n=2,3,4,... \quad (29)$$

The other equations must be solved using a numerical approach.

Reference 7 used a variational technique for solving these equations. A set of Guassian wave functions was assumed for the trial wave function:

$$f_0(r) = \sum_{i=1}^{21} A_i e^{-\alpha_i r^2} \tag{30}$$

$$g_0(r) = r \sum_{i=1}^{21} B_i e^{-\alpha_i r^2} \tag{31}$$

$$f_2(r) = r \sum_{i=1}^{21} C_i e^{-\alpha_i r^2} \tag{32}$$

$$g_2(r) = r^2 \sum_{i=1}^{21} D_i e^{-\alpha_i r^2} \tag{33}$$

The parameters A_i, B_i, C_i, and D_i were used as variational parameters in order to minimize energy. The relation

$$\alpha_{i+1} = g\alpha_i, \tag{34}$$

with g independent of α_i, was chosen so as to provide a geometrical progression to cover a wide range of expected values.

Inclusion of the discarded cubic term as a perturbation to the spherical equation was the subject of reference 8. The inclusion of the cubic term caused a splitting of the acceptor energy levels due to the degeneracy of the valence band. The $P_{5/2}$ states split into two states, the Γ_8^- and the Γ_7^- states. Solutions to the equations for GaAs are listed in Table II (8:1535).

This model has a distinctive disadvantage; however, since it uses the effective mass approximation, it ignores

Table II: Theoretical Acceptor Values for GaAs

Inputs	Value
ϵ_o	12.56
γ_1	7.65
γ_2	2.41
γ_3	3.28
μ	0.767
δ	0.114
R_0	11.3 meV
a_0	50.8 Å
Output	**Value**
$1S_{3/2}(\Gamma_8^+)$	25.67 meV
$2S_{3/2}(\Gamma_8^+)$	7.63 meV
$2P_{1/2}(\Gamma_6^-)$	1.60 meV
$2P_{3/2}(\Gamma_8^-)$	11.38 meV
$2P_{5/2}(\Gamma_8^-)$	7.20 meV
$2P_{5/2}(\Gamma_7^-)$	5.33 meV

the central cell effect (10). The central cell effect is the primary contributor to the differences observed in energy levels for different chemical species. The effect of the central cell contribution should be observable in the S-state transitions since spherically symmetric states are most affected by the central cell correction. The effect should be an alteration in the S-state energies that falls off as $1/n^3$ (10). However, research by Reynolds, et al. has shown that the central cell effects for GaAs is observable

Table III: LSS Range Statistics for Mg in GaAs

Implant Energy	Projected Range	Standard Deviation
60 keV	615 Å	308 Å
90 keV	925 Å	425 Å
120 keV	1237 Å	530 Å

for the P-states of C and Ge impurities, and that the S-states do not necessarily fall off as $1/n^3$ (46:8244).

Ion Implantation

Ion implantation in GaAs mostly produces a Gaussian concentration profile for the implanted species. The implant depth and the standard deviation for the implant depends on the implant energy and the species implanted. Calculation of the implant depth and deviation is done using the technique of Lindhard, Scharff, and Schiott (LSS). Table III contains the projected LSS range statistics for Mg in GaAs, and a plot of the profile for a 10^{13} cm^{-2} implant is shown in Figure 3. It should be noted that the actual profile may deviate from the calculation, and that diffusion of the impurity during the annealing process will occur and alter the actual profile of the implant.

Photoluminescence of GaAs

A considerable number of PL studies have been done on GaAs since it first became of interest more than two decades

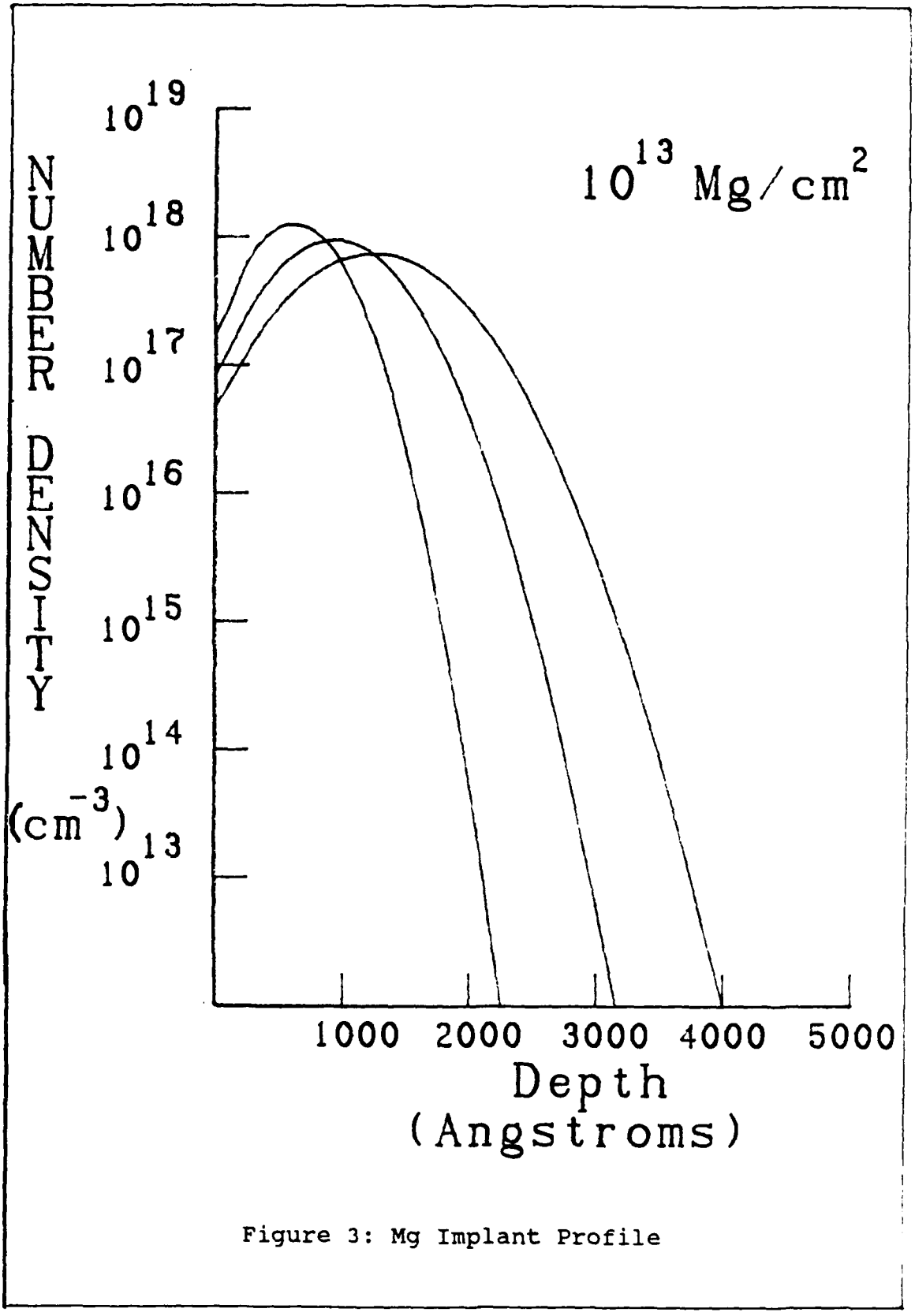

Figure 3: Mg Implant Profile

ago (4,12,14,17,19,23-25,28-31,34,35,39,41,43-45,48-57,61, 64,68,70,71,74,75). The included references represent only a small portion of the literature dealing with the PL from GaAs. Table IV represents a collection of the observed PL transitions in GaAs as compiled from the above references.

The transitions were observed at the liquid He temperature of 4.2 K. The two-electron transitions, recombination of an exciton on a neutral donor leaving the remaining electron in an excited state, are present in high purity materials in which N_A+N_D is typically less than 10^{14} cm^{-3} (38:12.5). Also, observations of the [g-v] and [g-g] transitions only occur in high purity materials (1,16,59). The [g-g] transition is a band of transitions near the g transition observed at 1.511 eV (42:2502). The [g-g] transition is only visible in high purity material implanted with acceptors to a concentration of the order of 10^{17} cm^{-3} (42). The [g-v] transitions represent a band of discrete transitions between 1.504 and 1.511 eV (1:3549). The nomenclature for numbering the individual transitions is to assign a letter between g and v sequentially from higher to lower energies (1:3549). The origin of these transitions is very much in question at this time; however, there is some evidence to support the conclusion that these transitions represent donor-acceptor pairs with pair separations between 50 and 70 Å (48:2516).

Table IV: Photoluminescence Transitions in GaAs (38:12.5)

Energy (eV)	Transition
1.5153	n=1 upper polariton of the free exciton
1.515	lower polariton of the free exciton
1.5146-1.515	excited states of neutral donor bound exciton
1.5141	exciton bound to neutral donor
1.5133	exciton bound to ionized donor and/or free to bound donor transition
1.5128	J=1/2 exciton bound to neutral acceptor
1.5124	J=3/2 exciton bound to neutral acceptor
1.5122	J=5/2 exciton bound to neutral acceptor
1.5110-1.5104	[g-v] transitions (origins currently in question).
1.5108	two-electron transition for a free exciton recombination near a neutral donor
1.5101-1.5014	two-electron transitions of excited state exciton bound to a neutral donor
1.5097	two-electron transition of a neutral donor bound exciton with donor left in n=2 state
1.5089	two-electron transition of a neutral donor bound exciton with donor left in the n=3 state
1.5080	[g-g] transition in acceptor doped high purity GaAs
1.4932	C(As) free to bound acceptor
1.4915	Be(Ga) free to bound acceptor

Table IV (cont.)

1.4911	Mg(Ga) free to bound acceptor
1.4894	Zn(Ga) free to bound acceptor
1.4892	C donor-acceptor pair
1.4880	Mg donor-acceptor pair
1.4854	Zn donor-acceptor pair
1.4850	Si(As) free to bound acceptor
1.4848	Cd(Ga) free to bound acceptor
1.4816	Si donor-acceptor pair
1.4782-1.479	Ge(As) free to bound acceptor
1.4745	Ge donor-acceptor pair
1.441	possible Ga antisite
1.406	Mn(Ga) free to bound acceptor
1.356	Cu(Ga) free to bound acceptor
1.22	donor-Ga vacancy complex

Selective Pair Luminescence of GaAs

Selective pair luminescence has been performed on GaP, ZnSe, ZnTe, InP, GaAs, and $Al_xGa_{1-x}As$ (11,18,21,22,26,40,63, 65-67). The first appearance that could be found of SPL was a 1976 paper on GaP (63). Since that time additional research has been reported, but SPL has not spread as fast as PL primarily due to the extra equipment required to perform the measurements.

The primary difference between PL and SPL in implementation is that SPL uses a tunable dye laser to pump

the material with below band gap photons while PL uses a light source which produces photons with above band gap energies. This difference in the pump energy produces dramatic differences in the luminescence results.

Donor acceptor pairs are the primary luminescence transitions studied with SPL. The intent of SPL is to create a DAP with the acceptor (or the donor) in an excited state (equation 35). That is,

$$\hbar\omega_p = E_g - (E_A^* + E_D) + e^2/\epsilon_o r + J^*(R), \qquad (35)$$

where $J^*(R)$ is the overlap wave function correction for the excited state DAP. $J^*(R)$ is a correction to the energy term which takes into account the quantum mechanical perturbations arising from overlap of the donor and acceptor wave functions for short ranges (typically less than 100 Å for GaAs).

The acceptor excited state is short lived (on the order of nanoseconds) in relation to the DAP lifetime, which varies from microseconds to seconds. The excited state acceptor will relax to the ground state before recombination of the DAP occurs (equation 36). That is,

$$\hbar\omega_l = E_g - (E_A + E_D) + e^2/\epsilon_o r + J(R), \qquad (36)$$

where $J(R)$ is the overlap wave function correction for the ground state DAP.

The result will be a luminescence transition shifted from the pump energy by the relationship in equation 37. That is,

$$\hbar\omega_p - \hbar\omega_l = E_A - E_A^* + J^*(r) - J(R). \quad (37)$$

The energy difference between the pump and the luminescence corresponds to the difference in energy between the ground and excited state of the impurity. The process involved is detailed in Figure 4. A series of sharp transitions should be observed corresponding to the excited states of the impurities in the material. The SPL related transitions should change energy as the pump energy is changed because the DAP transition energy varies with the pair separation. By tuning the pump energy, the pair separation, being selectively pumped, is changed. This is one means of distinguishing SPL related transitions from other luminescence events in the below band gap spectra. Luminescence which does not shift with the pump energy is not SPL related. This is not to say that if the transition shifts with energy it is SPL related. Some spectral features such as phonon replicas will shift with the pump energy, but are not SPL transitions (26:7452). The phonon energies for GaAs are well known and the behavior of phonons with temperature is significantly different from SPL. Therefore, distinguishing between the SPL and phonon transitions is not a problem.

The spectra from the below band gap pumping looks significantly different from what is seen in the PL. There is a singular lack of luminescence from the FB transitions. The dominant feature in the spectra arises from the DAP

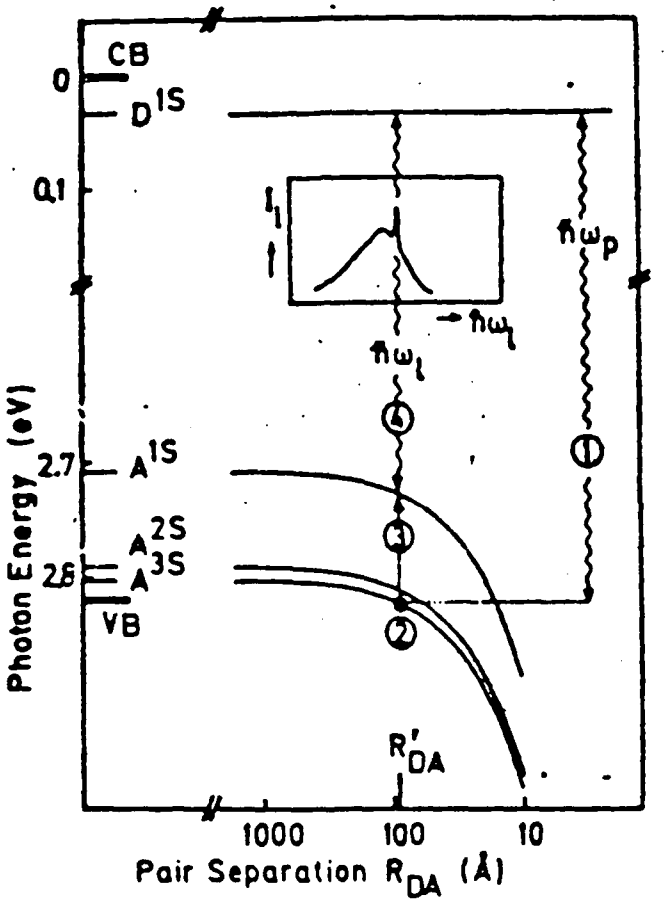

Figure 4: SPL Process (66:5179)

transitions. If the pump energy exceeds the recombination energy, exciton transitions will be observed as well. The lack of FB transitions can be explained by two mechanisms. The transition rate for the acceptor FB is dependent on the number density of free charge carriers in the conduction band. In SPL, the number of electrons is heavily restricted compared to what is available in PL. The reduced carrier population reduces the transition rate for the acceptor FB. Additionally, many of the acceptors are already tied up with the selective pumping process for the DAP. One of the primary source of free charge carriers in below band gap pumping comes from removal of electrons from ionized acceptors. If the material is n-type or compensated, then the acceptor population becomes tied up in the DAP transitions, and the FB transitions are reduced. However, the FB transitions may occur in instances where there is a substantial surplus of acceptors.

The major spectral feature in addition to the SPL transitions is the DAP ground state transition. The DAP band provides background for the SPL transitions. The source of the background comes from the pairing of the free electrons with ionized donors, and the neutral acceptors which are created when an acceptor absorbs a photon (19:131). This process produces a source of nonselectively pumped DAP which provides the observed background. The ability of pairs to migrate and change separation provides

Table V: SPL Transitions in GaAs (meV) (33:1333)

	C	Zn	Si	Ge	Mg
$1S_{3/2}$	26.0	30.7	34.5	40.4	28.4
$1S_{3/2}$-$2P_{3/2}$	15.2	19.2	23.5	26.1	17.1
$1S_{3/2}$-$2S_{3/2}$	18.4	21.7	25.1	28.3	20.0
$1S_{3/2}$-$2P_{5/2}(\Gamma_8)$	19.4	23.1	27.3	30.1	21.1
$1S_{3/2}$-$2P_{5/2}(\Gamma_7)$	21.3	25.2	29.6	31.6	23.1
$1S_{3/2}$-$3S_{3/2}$	22.4	26.2	30.8	34.0	24.3(proj)

some line broadening in the SPL spectra. Longer range pairs are more loosely bound and have longer lifetimes contributing to the process of pair migration. Therefore, SPL is confined to pairs of optimum separation. Observation reported in the literature indicate that SPL transitions will not be observed on the low energy side of the ground state DAP band peak since the lifetimes are too long and optimum conditions do not exist.

For SPL to be useful as a diagnostic tool it is necessary to build a database of known SPL transitions and the related impurities. Table V contains the previously observed SPL transitions in GaAs along with projected SPL transitions for a Mg acceptor in GaAs.

The data for Mg is contained in several sources. Kirkman, et al., performed far-infrared photoconductivity measurements on Mg doped GaAs (32:423). Far-infrared photoconductivity measurements are limited to observation of

the P transitions. The two-hole satellite transitions of Mg yields additional information for the S transitions (6:1051). Additional SPL results have been reported for more complex structures. Two states have been observed for the 78 meV double acceptor at 62.5 and 66.5 meV (27:794). The structures between 1.504 and 1.5110 eV (the [g-v] transitions) have been studied extensively using SPL. A transition at 15.8 meV has been observed, and a ground state acceptor energy of 22.9 meV was deduced. The nature of 22.9 meV acceptor is still unknown (16:814).

Chapter III

Experiment

This chapter provides the details associated with conducting this research. The discussion will include samples and their preparation, equipment and its configuration, and the procedures used in conducting the experiment.

Sample Information

Vapor phase epitaxial GaAs was selected for utilized in this experiment. The GaAs samples were from a previous dissertation by M. L. Cone in 1980 (15). The samples were Mg ion implanted with various doses and implant energies. These samples were used in this study for several reasons. First, the VPE material if it were sufficiently thick, should produce excellent results for both the PL and SPL. Second, the Mg ion implant would be of interest as SPL had not been performed on Mg in GaAs to the best of my knowledge. Third, of all the frequently used ion implants which were available, Mg has one of the largest penetration depths, which enhances the opportunity to observe the ion implant with the SPL. Fourth, a characterization study had already been done on the samples.

Growing. The epilayers were grown on chromium compensated semi-insulating GaAs substrates using a vapor phase epitaxial growth technique. The samples were grown by G. McCoy of the Air Force Avionics Laboratory. An open flow chemical vapor transport system was used with arsenic trichloride, gallium, and hydrogen as the reagents. The system is described in reference (62). The unimplanted unannealed epilayers were p-type with a room temperature carrier concentration of 7.94×10^{14} cm^{-3} and an effective mobility of 399 cm^2/V sec by Hall measurements (15:62).

Implanting. The epilayers were ion implanted with Mg by J. Ehret of the Air Force Avionics Laboratory using the ion implantation system at the Air Force Avionics Laboratory. Samples were cleaned with methanol before implantation. A hot cathode ion source of solid Mg provided the Mg source which was filtered by a magnetic separator to prevent accidental implant of other impurities. A more complete description of the implantation system is contained in reference (37).

Table VI provides a listing of the Mg ion implanted samples used for this study. A variety of doses and several implant energies were studied as well as two unimplanted samples which were studied for control purposes.

Annealing. After implantation the samples were capped with a 1000 Å film of pyrolytically grown Si_3N_4, and

Table VI: Mg Implant Data for VPE GaAs

Implant Energy (keV)	Dose (cm^{-2})	Annealing Temperature(°C)
60	$1x10^{12}$	850
	$5x10^{12}$	850
	$1x10^{12}$	850
	$5x10^{13}$	850
90	$1x10^{12}$	850
	$5x10^{12}$	850
	$1x10^{13}$	850
	$5x10^{13}$	850
120	$1x10^{13}$	900
	$1x10^{14}$	850
None	None	850
None	None	None

annealed at 850 °C for 15 minutes. One of the unimplanted control samples was also capped and annealed. Samples were placed in a spectrosil boat and annealed in flowing hydrogen gas. The caps were removed with hydrofluoric acid followed by trichloroethylene, acetone, and deionized water rinses (15:65).

Cleaning of Samples. All samples were cleaned before installation in the cryostat. Samples were cleaned by rinsing with deionized water followed by rinsing with an Alconox detergent solution then rinsed again in deionized water and blown dry with dry N_2 gas. The samples were then rinsed with trichloroethylene followed by rinses with acetone and methanol and finally blown dry again.

Experimental Systems

Overview. Figure 5 is a schematic of the experimental system. The samples were mounted on a copper cold finger in the Janis dewar. The cryostat was capable of operation down to 1.9 K by pumping the sample chamber with a 15 cfm mechanical pump and monitoring the pressure with a Wallace-Tiernan gauge. Excitation was provided by the 5145 Å line of an Argon ion laser for PL, and the output from a tunable dye box for the SPL. The laser output was conditioned using a number of filters before being transmitted into the cryostat. Luminescence from the samples were collected using two f/6 lenses and sent into a Spex 1702, 3/4 meter monochromator. Filters were added between the lenses when necessary to remove light not coming from the sample. The output from the monochromator was collected with an RCA 31034A photomultiplier tube (PMT). Photon counting was performed by sending the signal from the PMT to a EG&G/PAR Model 1112/1121A amplifier/discriminator unit and collecting

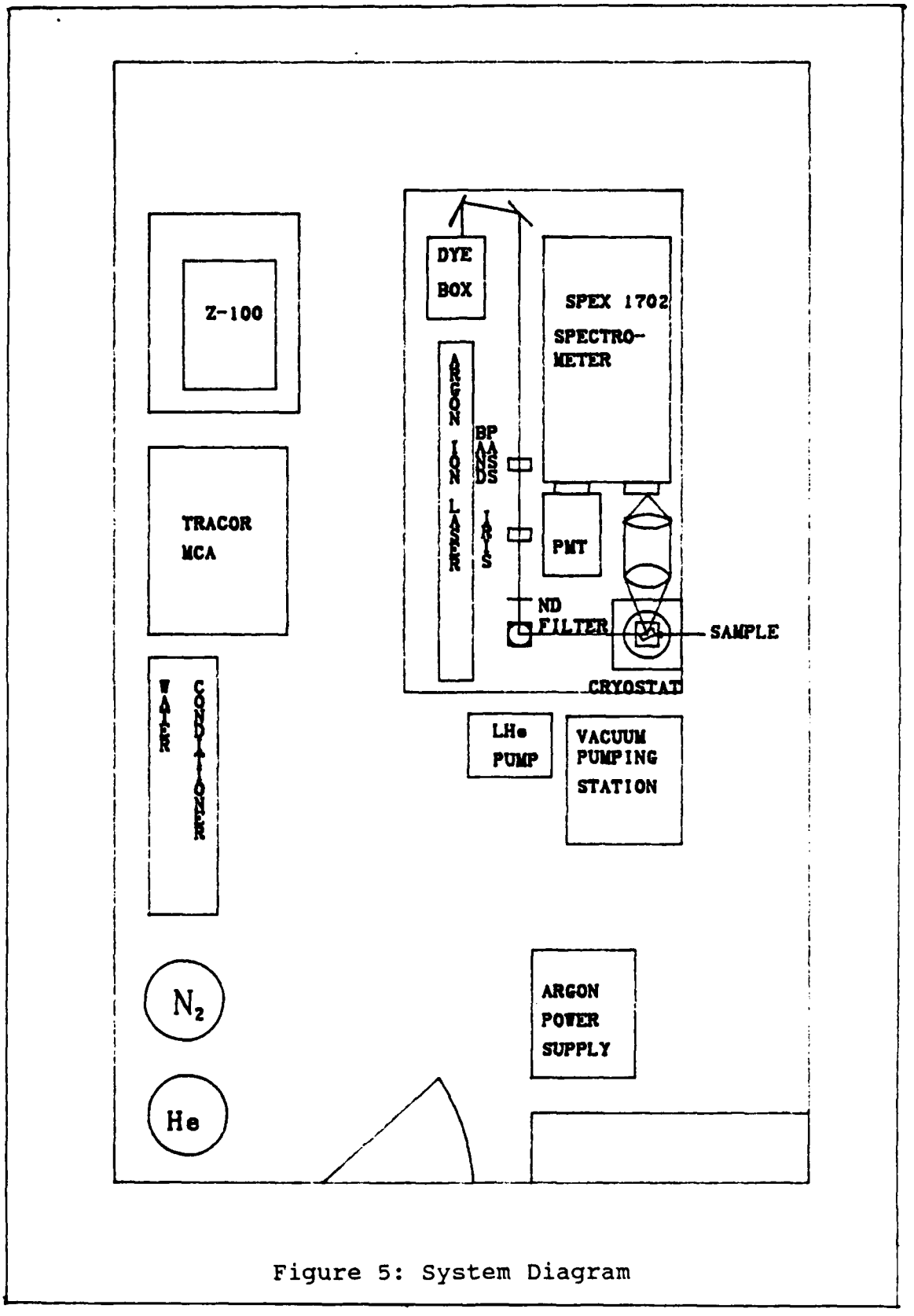

Figure 5: System Diagram

the output counts in a Tracor-Northern 1710A Optical Multichannel Analyzer (OMA) system. Data was transferred from the OMA to the Zenith Z-100 computer for data reduction and plotting.

Cryogenic System. Refrigeration was provided using a Janis DT-3 variable temperature liquid helium cryostat capable of operation from room temperature to 1.8 K. The Janis system consisted of the cryostat, the vacuum system for the insulating jacket, and the pumping system for superfluid operation. The system is shown in Figure 6 .

The Janis cryostat consists of a 3 liter liquid helium (LHe) container shielded by a 5 liter liquid nitrogen (LN_2) jacket. An insulating vacuum jacket surrounds both the LHe container and the LN_2 jacket. Vacuum is maintained using a 5 cfm mechanical fore pump and a 100 liter/sec water cooled diffusion pump. The pressure in the jacket is monitored using a Veeco ion gauge and a thermocouple gauge. On the average the jacket pressure is maintainable between 10^{-6} and 10^{-5} torr. The cold finger is inserted into the bottom of the cryostat where there are 3 fused silica windows with 3/4 inch clear apertures. The cryostat holds LHe for about 4 hours when maintaining the sample immersed at 4.2 K. Maximum optical input power is limited to 250 mW.

Cold Finger. The cold finger is a piece of machined copper as shown in Figure 7. It has room for 4

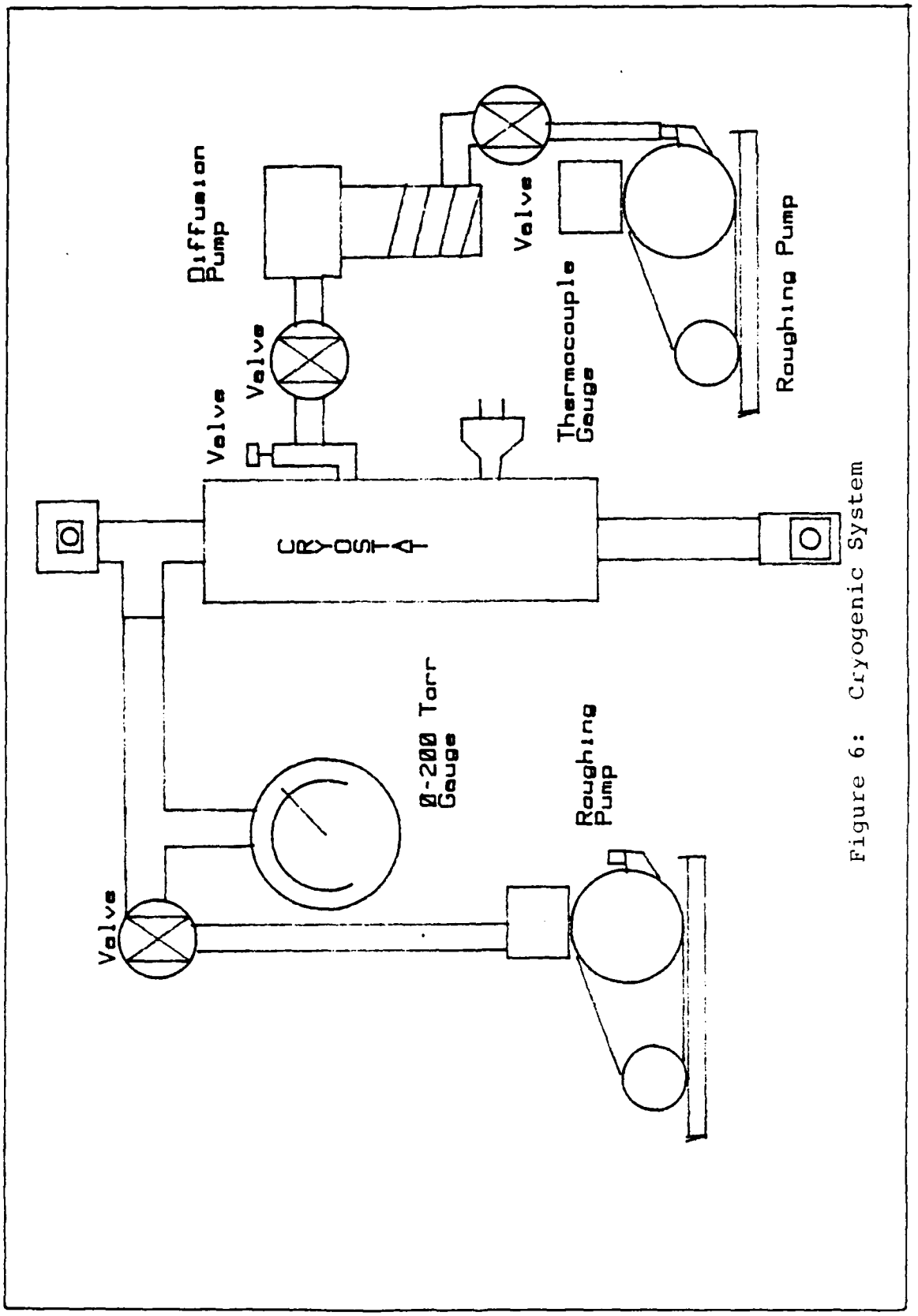

Figure 6: Cryogenic System

samples, 2 on the front and 2 on the back. The samples are mounted in a recess on the finger and secured with dab of General Electric electrical varnish in the upper left corner of the recess. A copper mask is then placed over the recess and bolted down to insure that samples do not fall out. The maximum sample size is 5mm x 5mm.

Operation of the Cryostat. Temperature of the sample is controlled using a Lakeshore Cryogenics Model DRC-80C digital temperature controller with a calibrated GaAs diode and three 3 Watt heaters imbedded in the cold finger. All 4.2 K spectra were done with the heater off and the sample immersed in LHe. The LN_2 jacket of the cryostat was filled with LN_2 and the cryostat was allowed to equilibrate over night before LHe was transferred to the system. LHe was transferred from 60 liter tanks by inserting a transfer line into the bottom of the tank and pressurizing the tank with gaseous helium.

Superfluid Operation. Operation below 4.2 K was obtained by pumping on the sample chamber of the Janis dewar with a 15 cfm Sargent-Welch mechanical roughing pump . The pump was connected through a port in the top of the sample chamber. The pumping rate was controlled by opening and closing a bellows valve located just before the sample chamber. The pressure was monitored using an 8 inch Wallace-Tiernan gauge with a 0 to 200 torr range. LHe

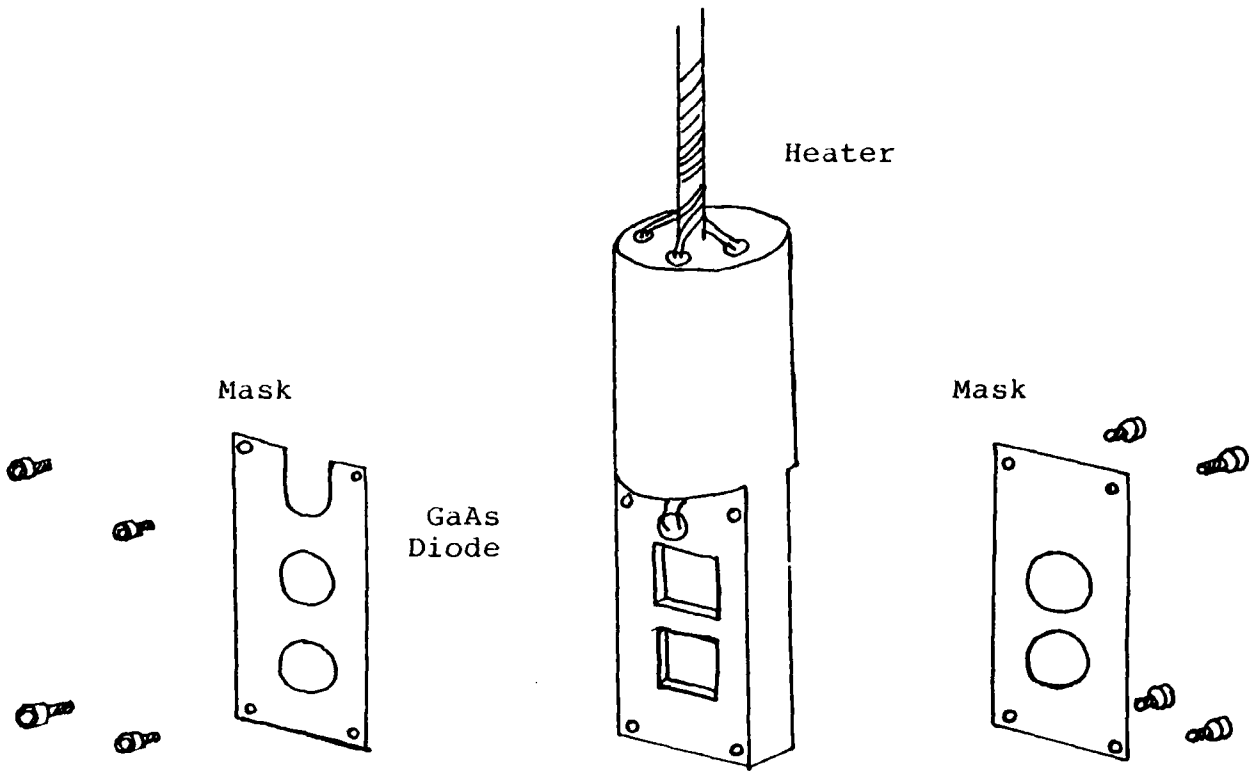

Figure 7: Cold Finger.

becomes superfluid at 38 torr. The lowest operating pressure this system could maintain and still keep the sample immersed in LHe was 28 torr. At 28 torr, the temperature of LHe is 2.0 K (72:368).

Laser Systems. The laser system used for PL differed from that used in SPL because of the need for tunability for the SPL experiments. Common to both systems was the argon ion laser.

Argon Ion Laser System. The pump laser for the photoluminescence work consisted of a Spectra Physics Model 171-17 argon ion laser capable of producing 12 W with multiline emissions, or 5 W at 5145 Å. The beam diameter in the TEM_{00} mode was 1.6 mm with a beam divergence of 0.56 mrad. Spot size at the sample was 3 mm in diameter. The argon ion laser was water cooled with a Spectra Physics Model 314 closed cycle water conditioner. Output from the laser was transmitted through an Oriel 520 nm band pass filter and the output power adjusted to maintain 100 mW on the output side of the filter. A neutral density filter was added after the band pass filter to adjust the power to the desired levels. Several of the optical filters were found to have some wedge between the surfaces. These filters produced a number of secondary beams, which it was necessary to remove by installing an adjustable iris in the system.

Dye Laser System. The dye laser system consisted of a Spectra Physics Model 376B dye box pumped by the Model 171-17 argon ion laser. The argon ion laser was operated with the multiline optics and output powers of 3.5 to 5 W were required depending on the condition of the dye. The dye used was LDS 821 from Exciton Dyes. LDS 821 is a Styryl 9 derivative with similar operating characteristics but at a significantly lower cost. The optics were Spectra Physics standard dye optics for Styryl 9 dye, a G3862-013 output coupler and two G3845-011 high reflectors. The dye was mixed in a 2 millimolar solution of 85% ethylene glycol and 15% propylene carbonate. It was necessary to pre-dissolve the dye in propylene carbonate, and place it in a heated ultrasonic bath for one half hour as LDS 821 has poor solubility in ethylene glycol. Spectra Physics recommends operating the dye circulator at 100 PSI, but the propylene carbonate adversely affects the viscosity of the dye solution and only 80 PSI was realizable from the dye circulator. Also the propylene carbonate appears to break down after about 200 W-hours of use, and the viscosity drops to as low as 65 PSI. At this point changing the dye is necessary as power output drops off and begins fluctuating. Spectra Physics claims that output powers of 800 mW at 8 W pump power are possible, but 200 mW at 5 W was the best achieved. Pump power in excess of 5 W produced no additional output power and significantly reduced dye

lifetime. The dye box was tuned using a 3 plate birefringent filter assembly specifically tuned for Styryl 9 dyes. The bandwidth of the filter ranged from 7850 Å to 8600 Å. The filter has a line width of 40 GHz (0.17 meV at 8300 Å). Output from the dye laser was transmitted through a 780 nm long pass filter to eliminate shorter wavelength light coming from the dye and the pump laser. Power was maintained at 50 mW through the filter and the adjustable iris. Neutral density filters were added as needed to adjust the power down.

Optical System. The optical system is shown in Figure 8. Luminescence from the samples was collected using a two lens system and transmitted into the Spex 1702 monochromator. The first lens in the system is an f/6 lens adjusted to provide a collimated output of the luminescence from the sample aimed at the monochromator entrance slit. The second lens was also an f/6 lens adjusted to focus the collimated light from the first lens on the entrance slit of the monochromator. The f/6 lenses provided the most optimum conditions for matching the f-number of the monochromator. In the PL research a 600 nm long pass filter was added between the two lenses to remove scattered laser light which had been contributing to the background noise.

The monochromator was a Spex 1702, 3/4 meter monochromator of the Czerny-Turner type. It is equipped with a 1200 line/mm grating blazed at 5000 Å. The

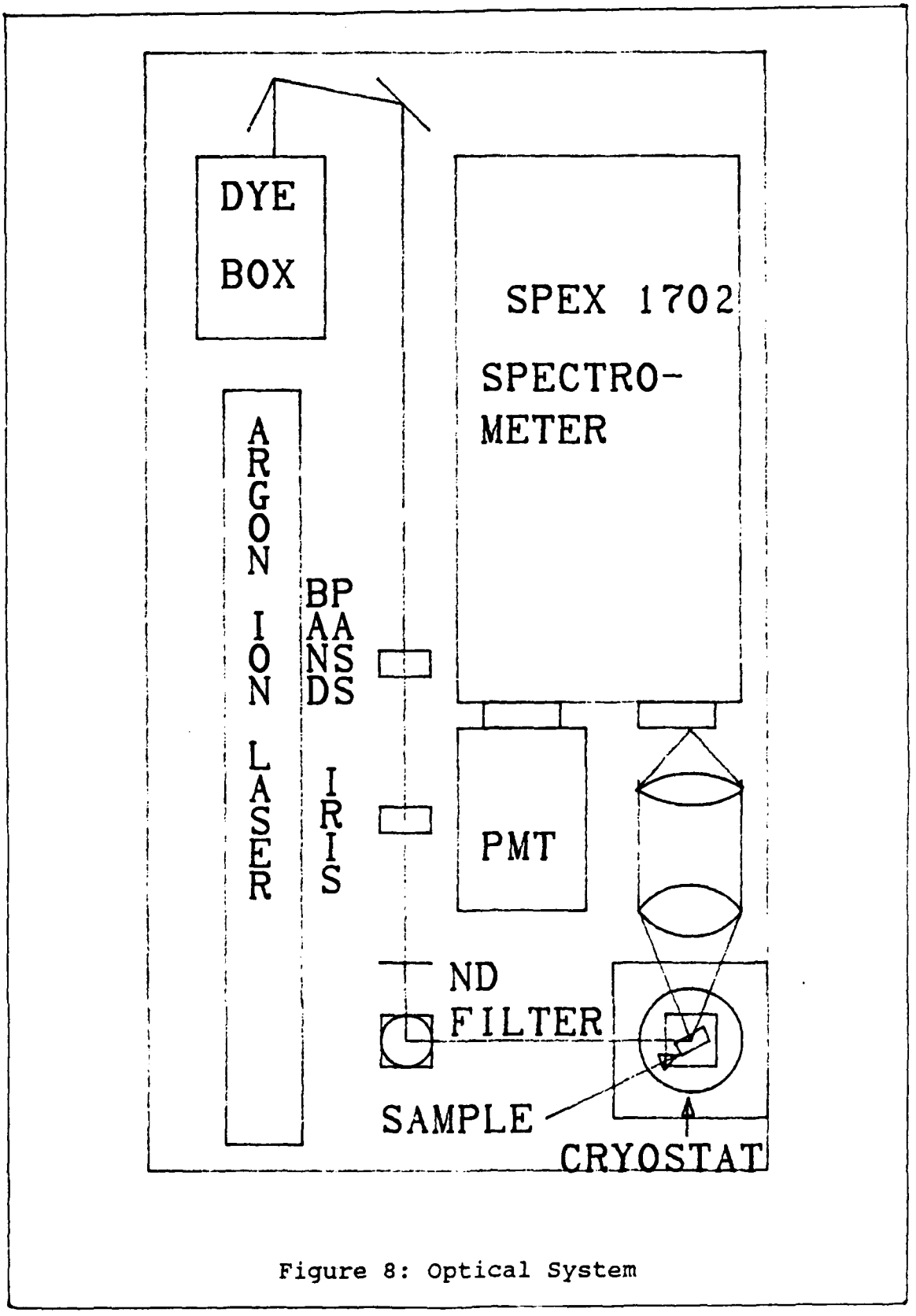

Figure 8: Optical System

monochromator has a linear dispersion of 10.2 Å/mm in the first order at 8273 Å which is the region of interest in this experiment. The entrance slit was 50 microns wide and 5 mm high, and the exit slit was set to 100 microns wide providing a resolution for the monochromator of 0.5 Å (0.09 meV).

The monochromator was controlled through an external stepping input. Application of a TTL level signal to the external input causes the monochromator drive to advance. The step size is proportional to the monochromator speed setting and is equal to 0.0868 Å/pulse with the monochromator set to the 500 Å/minute scan speed. A Wavetek square wave generator was used to drive the monochromator and a pulse divider which synchronized the advance of the monochromator with the advance of the OMA. Nominal settings of 500 Å/min on the monochromator, 10 Hz on the Wavetek, and a divide by 5 on the pulse divider would produce a 2048 channel set of data 355.5 Å long, lasting 17 minutes 4 seconds, with a dwell time of 0.5 seconds/channel,and a channel resolution of 0.1736 Å/channel. Adjusting the settings would alter the operating conditions proportionately. Calibration of the system was checked periodically to monitor changes in the electronics or monochromator using an argon spectral lamp. No measurable changes in the system were noted during the research.

Signal Detection and Processing. The signal detection system is show in Figure 9. Output from the monochromator was collected by an RCA C31034A photomultiplier tube (PMT). The PMT is a 2 inch diameter tube with a GaAs photocathode and an 11 stage copper beryllium dynode structure. Absolute responsivity of 65 mA/W for the tube is almost flat over the range of 3200 to 8600 Å with a large roll off beginning at 8600 Å and an almost complete loss of sensitivity by 9000 Å. The spectral response of the PMT is shown in Figure 10. The tube was refrigerated to -30 °C using a Products for Research LN_2 cooled PMT housing Model TE-176-RF. Operation of the tube lower than -30 °C was not recommended by RCA as thermal damage to the tube was possible around the socket-glass seal. RCA measured the dark count of the tube as 8 counts/sec; however, our measurements showed the tube had a background of 16 counts/sec under nominal operating conditions. The tube would operate with a cathode voltage of 1000 to 2200 V. The optimum operating voltage of 1300 V was obtained by providing a small signal input of light scattered from an argon spectral lamp into the monochromator and measuring the signal-to-noise ratio. The output from the tube was connected to an EG&G/PAR 1121A amplifier/discriminator unit. The amplifier/discriminator unit counts the current pulses emanating from the PMT. Adjustment of threshold voltage levels on the discriminator allow for the elimination of pulses with insufficient or too

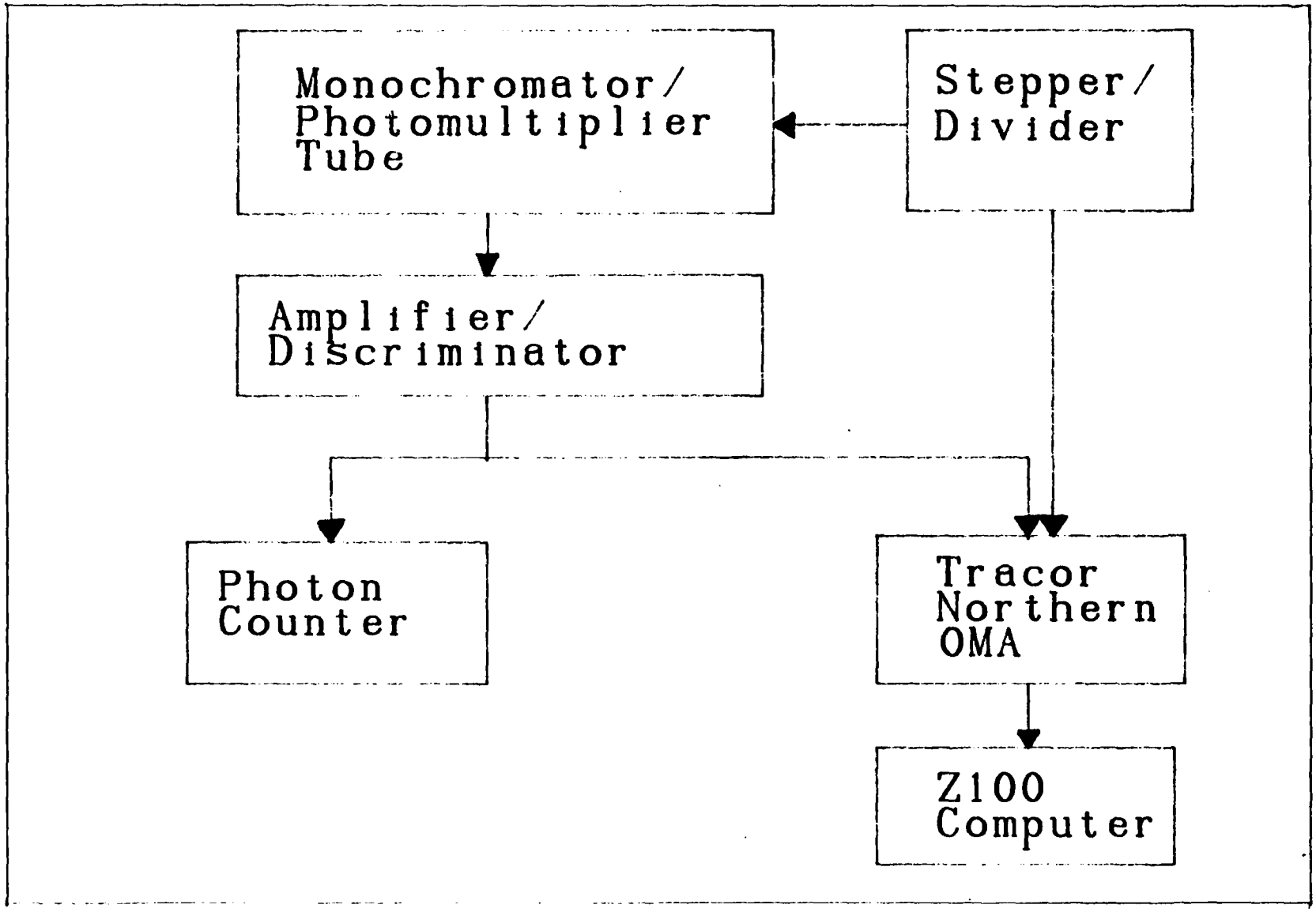
Monochromator/
Photomultiplier
Tube
Stepper/
Divider
Amplifier/
Discriminator
Photon
Counter
Tracor
Northern
OMA
Z100
Computer

RCA 31034A

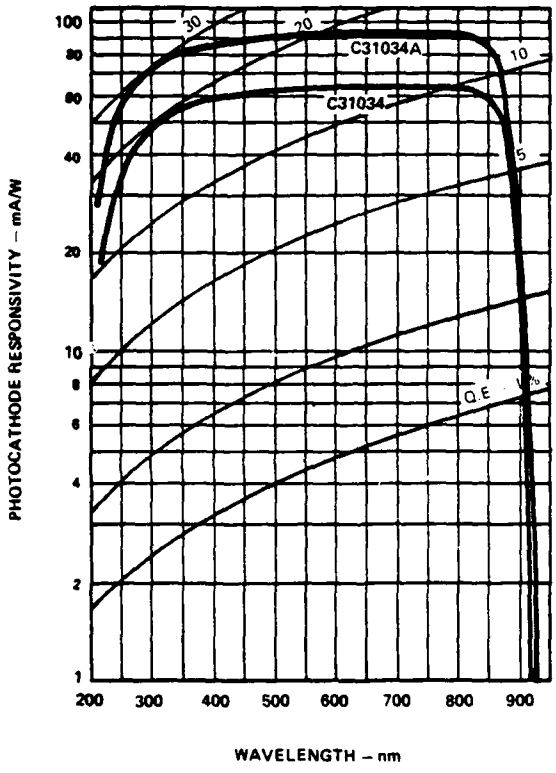

Figure 10: PMT Response
(RCA Photomultiplier Handbook)

much voltage to have originated from the photocathode. The minimum threshold of the discriminator was determined by optimizing the signal-to-noise ratio of a weak input signal. The maximum threshold setting had no observable impact on the noise level.

The amplifier/discriminator output is labeled 'fast nim' on the back of the unit. The 'fast nim' output is a very short square pulse output for each photon counted. The advantage of the 'fast nim' is that a short pulse allows a very high count rate; however, this short pulse is incompatible with the standard TTL logic levels of other digital devices, in particular the Tracor-Northern OMA. Therefore, the output of the amplifier/discriminator is sent to a box which converts the 'fast nim' pulse to a TTL level signal which is then sent to the OMA. In addition, the 'fast nim' is sent to an EG&G/PAR Model 1112 photon counter. The photon counter produces a real time digital output of the count rate coming from the PMT, and was used during alignment of the input lenses for the monochromator to maximize the input signal.

The Tracor-Northern 1710A OMA is a mainframe computer based on the PDP-11 microprocessor. It is capable of handling a variety of plug-ins for various types of detectors and can handle up to 8192 channels of data. For this research a Model 1710-30 signal averaging/multichannel analyzer module was used. The module has a maximum data

input rate of 200 kHz and care must be taken to make sure that the incoming count rate does not exceed 200 kHz. Dwell time is set to 'external' to allow channel stepping by the monochromator control circuitry, and the number of scans is set to 1.

Acquired data is sent to a Zenith Z-100 MS-DOS based microcomputer over the RS232C port on the back of the OMA. Program Tracomm.bas in the Appendix was used on the Z-100 to capture and store the data in ASCII files capable of being read by any MS-DOS machine. Before being reduced by any other program, however, it is necessary to strip off the file header of OMA settings and the channel markers sent by the Tracor-Northern to the Z-100. Program Traconv.pas was written to strip the channel markers and extraneous spaces, leaving the file as a series of numbers in ASCII format.

Chapter IV

Results and Discussion

Sequence of Presentation

The luminescence data will be presented for each sample in separate sections. Each section will consist of the photoluminescence data followed by the selective pair luminescence data. The photoluminescence information will consist of variations of temperature and pump laser intensity for the sample. The selective pair luminescence section will consist of spectra taken at several pump laser wavelengths under the same temperature and intensity conditions. In addition for the unimplanted samples, temperature and intensity dependent measurements for a preselected pump wavelength were also performed. The data will be grouped starting with the unimplanted samples, progressing to the 60 keV implants, then to the 90 and 120 keV implants. Following the individual treatment of each sample studied, a comparison will be made of the effects of implant dose and energy on the spectral properties of the samples.

Unimplanted Unannealed VPE GaAs

This sample is the virgin unimplanted material with no treatment after growth except for the standard cleaning

procedures. It was used as the control in this experiment to determine what the as grown material contained prior to implantation or annealing.

Photoluminescence The excitation intensity variations of the luminescence for this sample are shown in Figure 11. All the spectra in this figure exhibit the highly resolved exciton structures. The peak at 1.5155 eV corresponds with the previously measured position for the upper polariton branch of the free exciton. An unresolvable series of peaks exists between 1.5146 and 1.5150 eV which have been associated with excited states of the neutral donor bound exciton. The most dominant peak in the exciton structure is the 1.5141 eV neutral donor bound exciton. Slightly less intense than the neutral donor bound exciton peak is the ionized donor bound exciton and/or donor free to bound peak at 1.5133 eV. The peaks at 1.5124 and 1.5122 eV are the neutral acceptor bound exciton doublets. The 1.5124 eV peak corresponds to a total angular momentum state of J=3/2, while the 1.5122 eV peak corresponds to a J=5/2 state. Several smaller features also exist just below the exciton band. The first peak at 1.5110 eV matches fairly well with the previously observed peak for a two electron transition of a free exciton recombination near a neutral donor site, leaving the neutral donor in the first excited state (38:12.5). An alternative explanation is provided by reference 49, in which the transition is associated with a

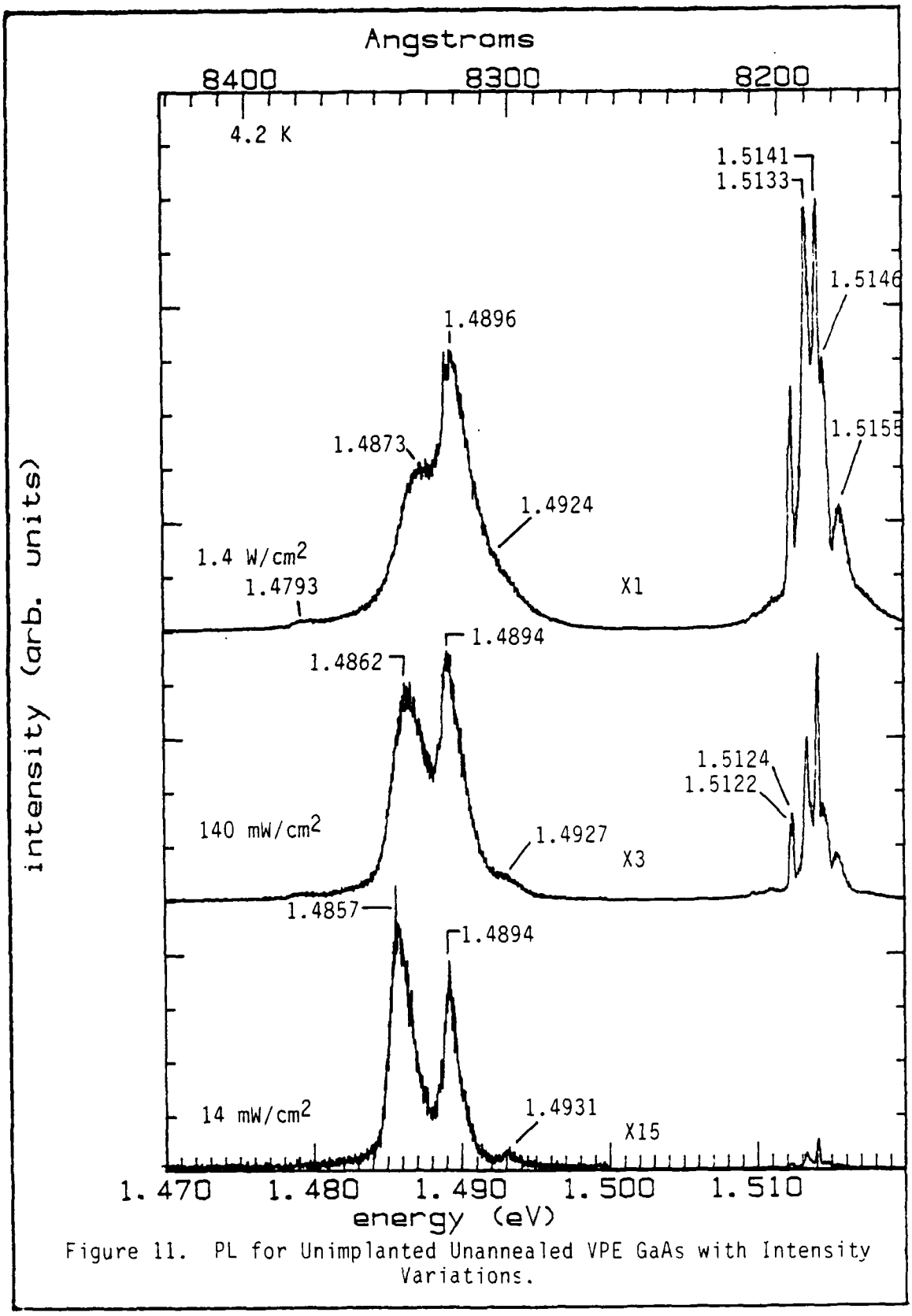

Figure 11. PL for Unimplanted Unannealed VPE GaAs with Intensity Variations.

two acceptor-one donor complex. Both acceptors are hypothesized to have excitons bound to them. Recombination of one of the neutral acceptor bound excitons would transfer the remaining exciton from the acceptor to the donor, and radiatively emit the remaining energy (49:1117). The second peak at 1.5097 eV corresponds well with the two electron transition of the neutral donor bound exciton peak, in which recombination of the exciton leaves the resultant neutral donor in the first excited state.

Four distinct peaks are observed in the energy range from 1.500 eV to 1.470 eV. The most dominant peak is a structure at 1.4894 eV. The 1.4894 eV peak maintains a constant position in the spectra during the excitation intensity variations (Figure 11). This feature and the absolute measure of peak position indicate that this peak is the Zn free to bound transition. The second most intense peak in the spectra is a peak that exists in the range from 1.4857 to 1.4873 eV, depending on the pump energy. The 1.4857 eV peak shifts to higher energies and broadens heavily with increasing pump power until at 1.4 W/cm^2, it has become a shoulder on the 1.4894 eV Zn free to bound peak at an intensity of 1.4 W/cm^2. Also there is a distinct shift in peak position to higher energies as the pump intensity is increased. These conditions indicate that the 1.4857 eV peak is the Zn DAP peak.

The third peak is a structure that shifts from 1.4931 to 1.4924 eV with increasing pump intensity. At higher pump intensities, this peak has become a shoulder on the Zn free to bound peak. The energy of this peak at lower intensities matches previous observations for the carbon free to bound transition. The fourth peak in this region exists at 1.4793 eV. This peak is only observable at higher intensities as a very small feature in the spectrum. The 1.4793 eV energy matches the high end of the previously observed range of 1.4782 to 1.479 eV for the Ge free to bound transition.

The temperature variations for the unimplanted unannealed sample are shown in Figure 12. At temperatures above 4.2 K the 1.4894 eV, Zn free to bound peak becomes the only major resolvable feature of the spectrum except the exciton related peaks. The 1.4862 eV peak falls off rapidly with increasing temperature, and is almost gone at 30 K. This is further evidence of a DAP peak. The 1.4930 eV C, free to bound peak is fully resolvable at 2.0 K, although it is only a shoulder on the Zn free to bound peak at 4.2 K. The 1.4790 eV, Ge free to bound peak is observable up to 10 K, but disappears at higher temperatures. From 2.0 to 4.2 K it shifts from 1.4790 to 1.4797 eV. Although this exceeds the 0.2 meV shift expected for a free to bound structure obeying the kT/2 energy shift, the difference may be mainly

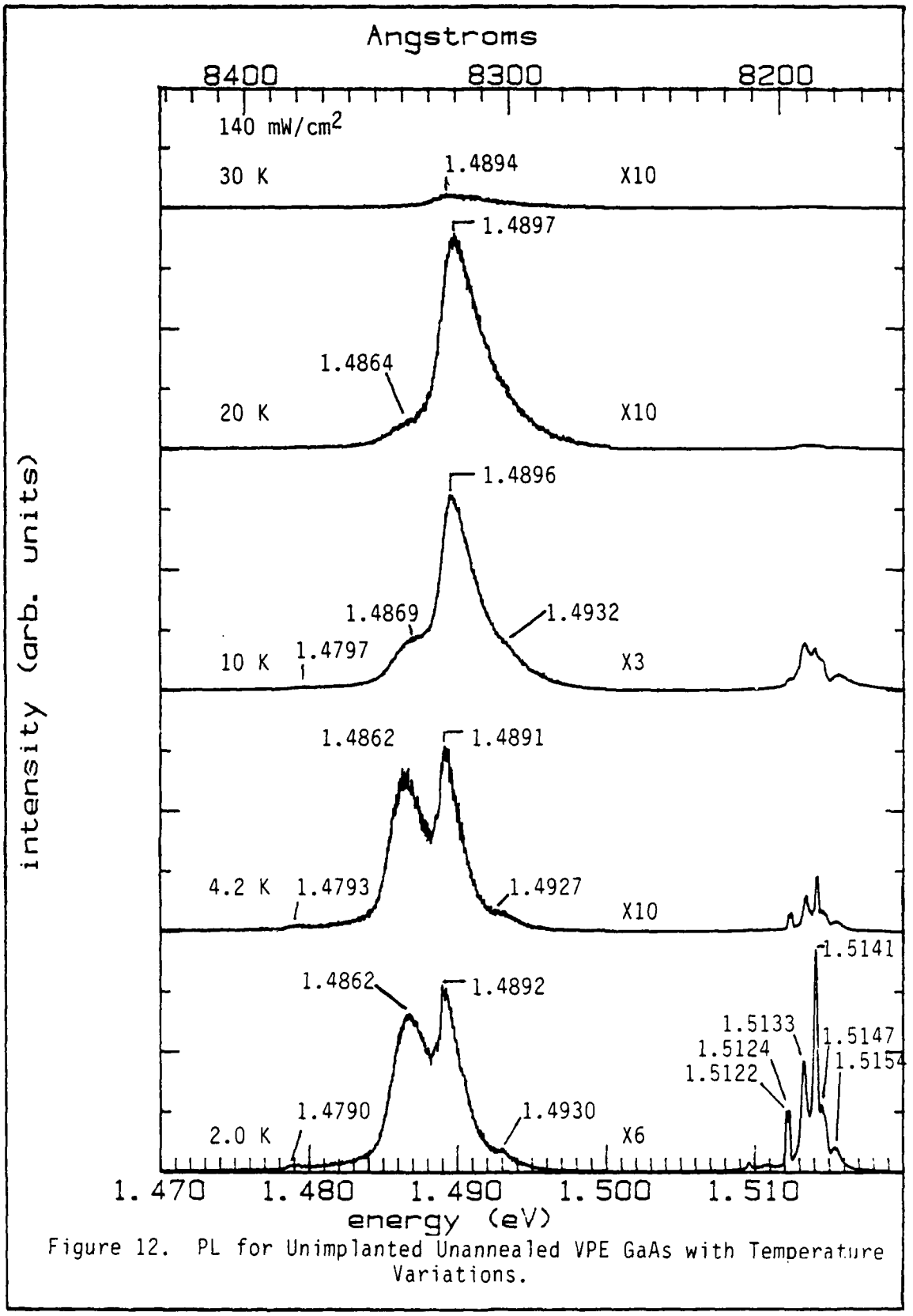

Figure 12. PL for Unimplanted Unannealed VPE GaAs with Temperature Variations.

due to the limited ability to resolve the peak, since it is a shoulder on the 1.4862 eV peak.

The photoluminescence from this sample shows that Zn is the dominant observable impurity in the material. A trace of C is also definitely observable, and the 1.479 structure indicates that Ge is also be present.

Selective Pair Luminescence of Virgin VPE GaAs

Figures 13-15 represent SPL data taken at 70 mW/cm^2 and 2.0 K. The pump energy runs from just slightly larger energy than the band gap, 1.5202 eV, to 1.5054 eV. Figure 13 shows the luminescence from just above the band gap to just below the band gap. At just above the band gap, all the standard exciton structures are observed just as in the PL. However, the FB and DAP structures have been altered significantly. At the 1.5202 eV pump energy, three structures are observed around 1.490 eV: a primary peak at 1.4876 eV with a shoulder at 1.4892 eV, and a separate peak at 1.4864 eV. The 1.4892 eV and the 1.4864 eV peaks are the Zn FB and DAP peaks, respectively. As the pump wavelength is tuned deeper into the gap, the FB peak gradually disappears. A shoulder at 1.4914 eV is also barely visible, with a 1.5181 eV pump energy, which is probably another FB transition. This energy is consistent with Mg or Be FB, although no indication of Mg or Be has been observed in the PL. On the other hand, there is no indication of the C structure which is visible in the PL. The dominant peak around 1.488 eV is

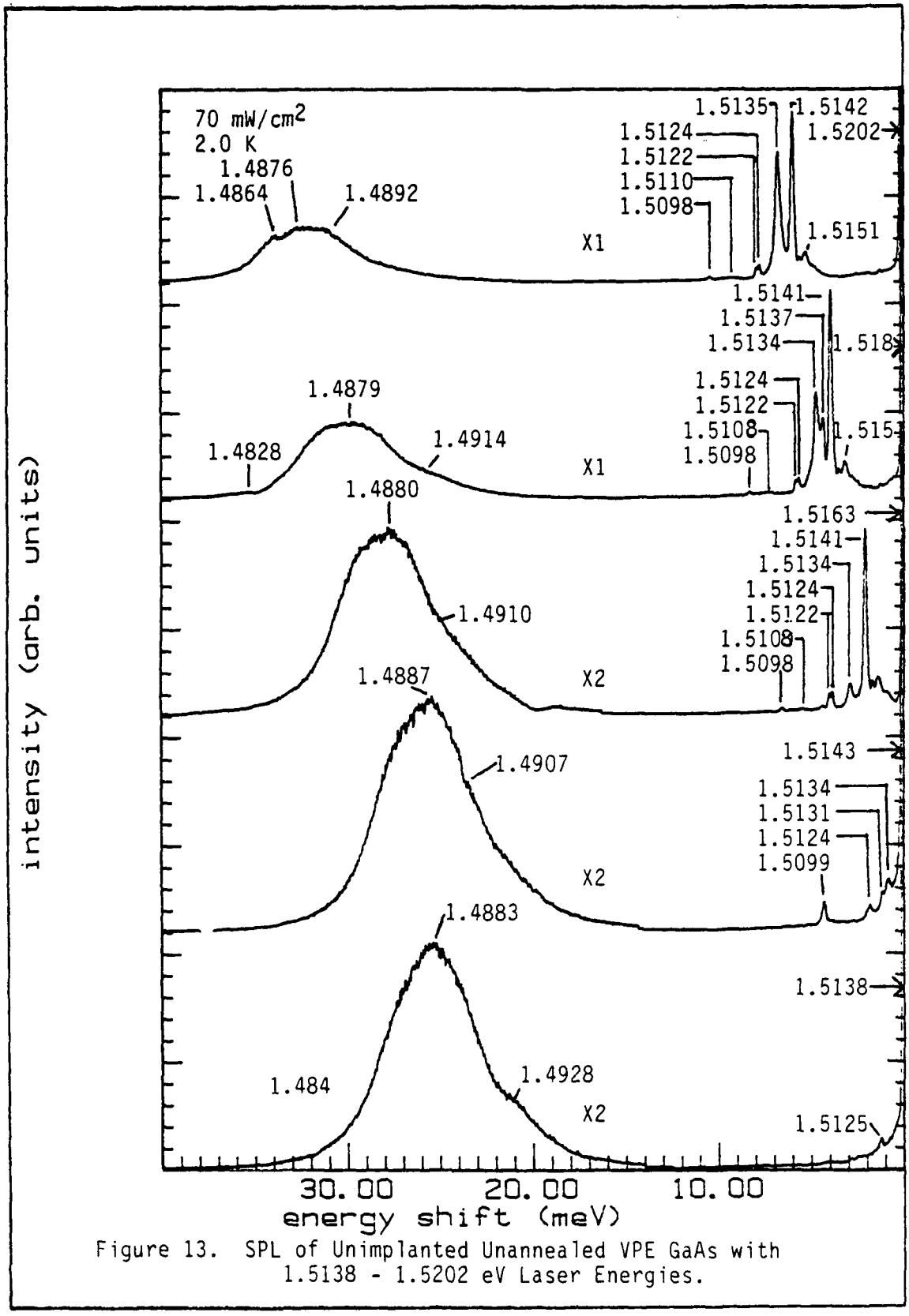

Figure 13. SPL of Unimplanted Unannealed VPE GaAs with 1.5138 - 1.5202 eV Laser Energies.

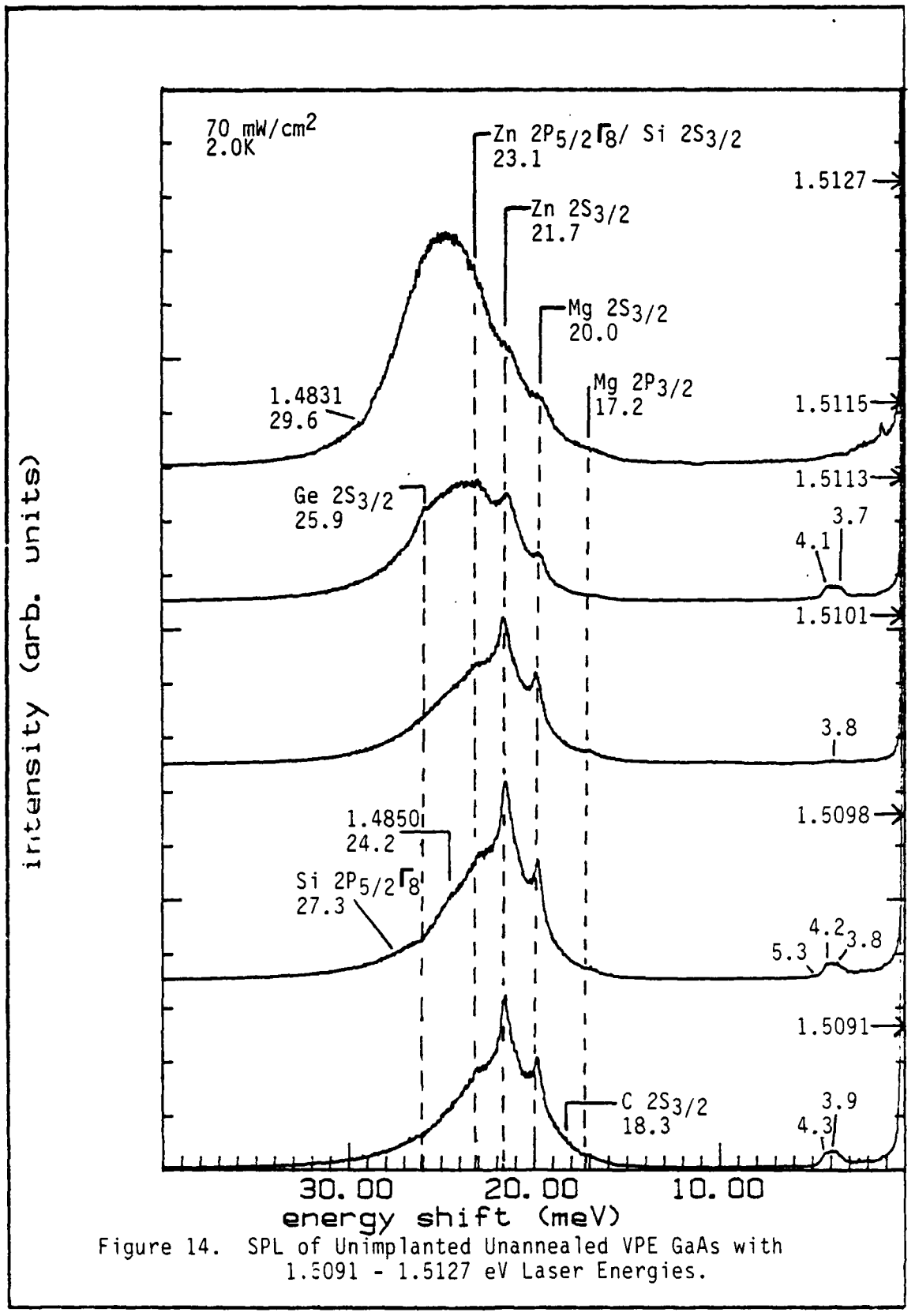

Figure 14. SPL of Unimplanted Unannealed VPE GaAs with 1.5091 - 1.5127 eV Laser Energies.

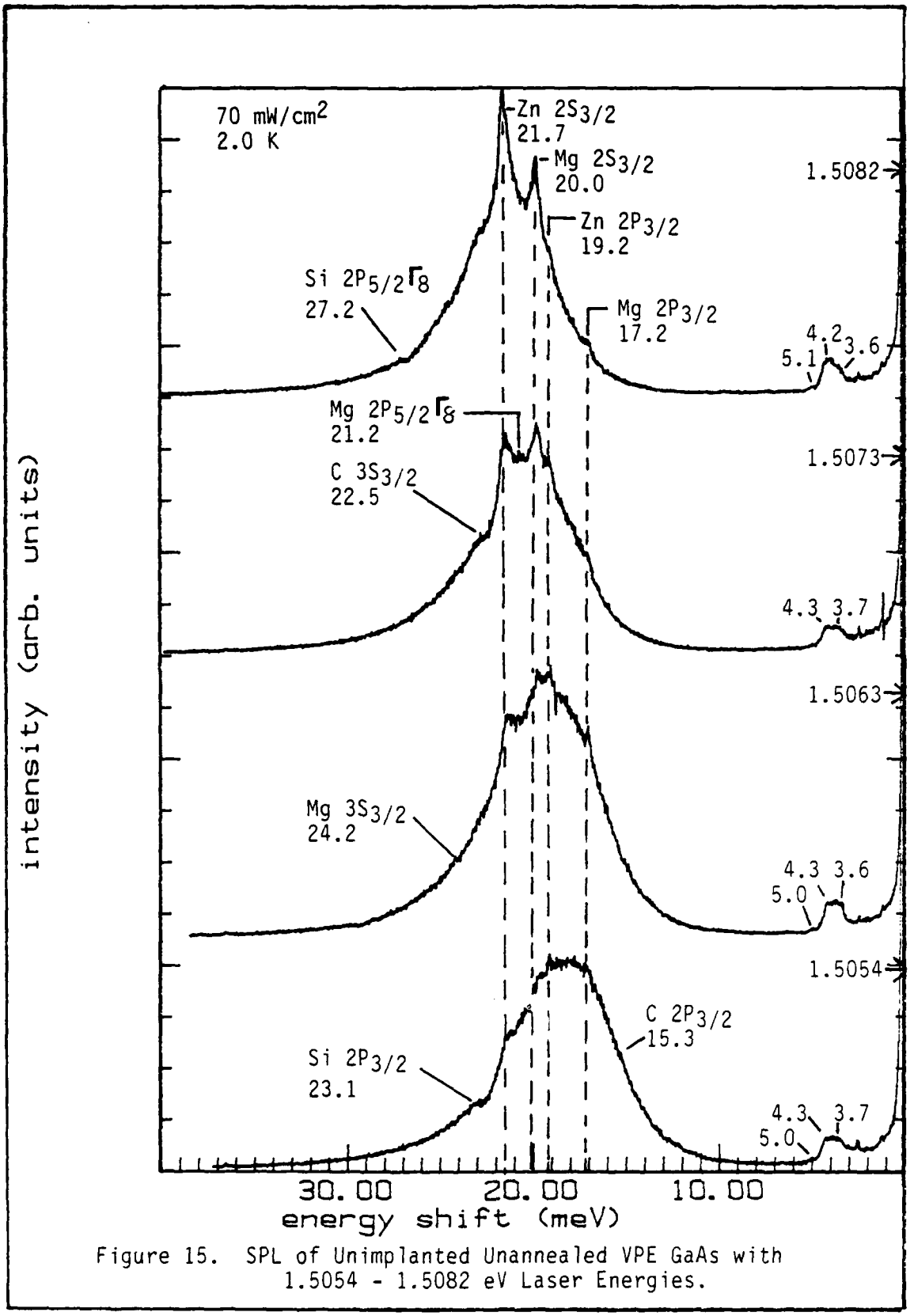

Figure 15. SPL of Unimplanted Unannealed VPE GaAs with 1.5054 - 1.5082 eV Laser Energies.

mainly due to the DAP peak associated with C and to a lesser extent the Zn DAP. With the pump energy set at 1.5143 eV, the peak at 1.5098 eV shows a significant enhancement and disappears when the pump energy drops below the neutral donor bound exciton energy of 1.5141 eV. This result further justifies the assignment of the 1.5098 eV peak to the two electron transition for the neutral donor BE. At the 1.5138 eV pump energy, a shoulder around 21.1 meV from the pump line is seen on the high energy side of the 1.4883 eV primary peak.

The onset of SPL is manifested in Figure 14. In the 1.5127 eV pump spectra, three distinct structures appear 21.7, 20.1, and 17.5 meV relative to the pump energy. The 21.7 meV peak is consistent with previous observations for the $2S_{3/2}$ to $1S_{3/2}$ transition for a Zn acceptor. The other two peaks will be the topic of further discussion in the next paragraph. A new structure shows up in the material when the pump energy drops below 1.5127 eV. This structure consists of three peaks 5.3, 4.2, and 3.8 meV below the pump energy, and these peaks do not occur at a fixed energy, but are observed to maintain a constant energy difference between the peaks and the pump energy. No explanation can be given at present for the existence of these lines. However, the lines did not show up until the pump energy was tuned below the neutral acceptor bound exciton energy of 1.5124 eV.

Table VII: SPL Transitions in Unimplanted Unannealed VPE GaAs

Energy Shift (meV)	Associated Impurity Transition
15.3	Carbon $2P_{3/2}$-$1S_{3/2}$
17.1	Magnesium $2P_{3/2}$-$1S_{3/2}$
18.5	Carbon $2S_{3/2}$-$1S_{3/2}$
19.2	Zinc $2P_{3/2}$-$1S_{3/2}$
20.0	Magnesium $2S_{3/2}$-$1S_{3/2}$
21.2	Magnesium $2P_{5/2}(\Gamma_8)$-$1S_{3/2}$
21.7	Zinc $2S_{3/2}$-$1S_{3/2}$
23.1	Zinc $2P_{5/2}(\Gamma_8)$-$1S_{3/2}$
	Silicon $2P_{3/2}$-$1S_{3/2}$
25.0	Silicon $2S_{3/2}$-$1S_{3/2}$
25.9	Germanium $2S_{3/2}$-$1S_{3/2}$
27.1	Silicon $2P_{5/2}(\Gamma_8)$-$1S_{3/2}$
29.9	Germanium $2P_{5/2}(\Gamma_8)$-$1S_{3/2}$

Figures 14 and 15 show the evolution of a variety of peaks associated with different acceptors in the material. The individual peaks are listed in Table VII. The three most dominant SPL lines are the 21.7 eV Zinc $2S_{3/2}$ line and the two lines at 20.0 and 17.2 meV. The 21.7 meV line peaks out at 1.4875 eV which is consistent with being at the high energy side of the Zn DAP peak observed in the PL. The 20.0 and 17.2 meV peaks are at a maximum when each is at 1.4892 and 1.4920 eV, respectively, indicating that the DAP band associated with it lies slightly below this region. Examination of the two hole transition data shows good

correlation between the $2S_{3/2}$-$1S_{3/2}$ two hole transition for Mg and the currently observed SPL peak at 20.0 meV. Furthermore, based on Reference 32, the $2P_{3/2}$-$1S_{3/2}$ transition for Mg would occur in the vicinity of 17.2 meV. These two transition energies agree very well with the currently observed peaks at 17.2 and 20.0 meV, respectively. The $2P_{5/2}(\Gamma_8)$-$1S_{3/2}$ transition for Mg also has an energy of 21.3 meV which is consistent with the other unknown peak at 21.2 meV (32:423). The ground state energy of Mg is 28.4 meV from the valence band with a FB transition at 1.4911 meV. Assuming the DAP peak observed in PL occurs at a pair separation of 420 Å and a donor binding energy of 5.8 meV, the DAP should appear at 1.4881 eV. This observation is consistent with that associated with the 20.0 and 17.2 meV peaks at the high energy side of the Mg DAP peak at 1.4882 eV.

Figure 16 illustrates the behavior of the SPL spectra with different excitation intensities. At 700 mW/cm^2, three distinct SPL lines are visible at 21.7, 20.0, and 17.0 meV below the pump energy of 1.5102 eV. However, the peaks have lost considerable sharpness, and the DAP background dominates the spectrum compared with spectra obtained at lower intensities. This feature is indicative of saturation of the selective pair transitions, thus leaving the pump energy only to increase the nonselectively pumped DAP background luminescence. The 70 mW/cm^2 spectra show four

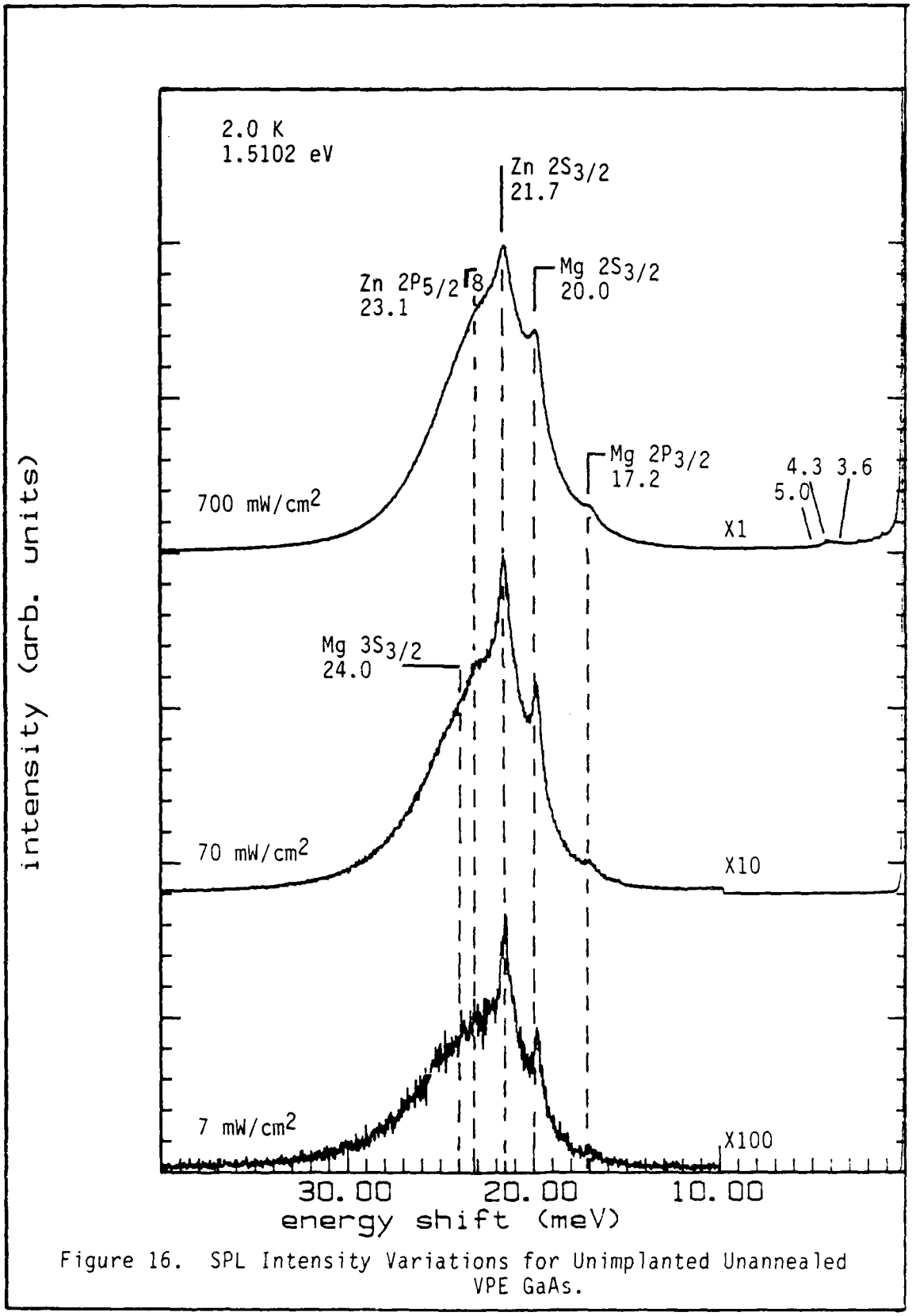

Figure 16. SPL Intensity Variations for Unimplanted Unannealed VPE GaAs.

distinct SPL lines. The linewidth has improved considerably and the ratio of the SPL lines to the background has improved as well. The 7 mW/cm^2 spectra has the narrowest linewidth but the decline in the luminescence has caused the fourth SPL line to disappear into the background noise. However, the ratio of the SPL lines to the DAP background has not changed significantly from the 70 mW/cm^2 to the 7 mW/cm^2 spectra. It is obvious from this information that the 70 mW/cm^2 range represents the optimum pumping intensity for this sample after making the trade offs between linewidth, DAP background, and signal intensity.

Figure 17 shows the behavior of the SPL data with different temperatures. At 2.0 K, four lines at 23.1, 21.7, 20.0, and 17.1 meV were clearly resolved as shown in Figure 16. As the temperature is increased to 4.2 K, there is an observable line broadening and distinct loss of resolution for the 23.1 and 17.1 meV lines. The spectrum at 10 K shows heavy line broadening, and the 20.0 meV peak is now only a shoulder in front of the 21.7 meV peak. At 20 K a significant decrease in intensity of the overall spectra has occurred, but the 21.7 and 20.0 meV peaks are still observable. By 30 K the peak around 20.0 meV is the only resolvable structure. The dramatic loss in intensity between 10 and 30 K attests to the DAP nature of the emission. The fact that the loss in intensity still occurs between 20 and 30 K indicates that the donor binding energy

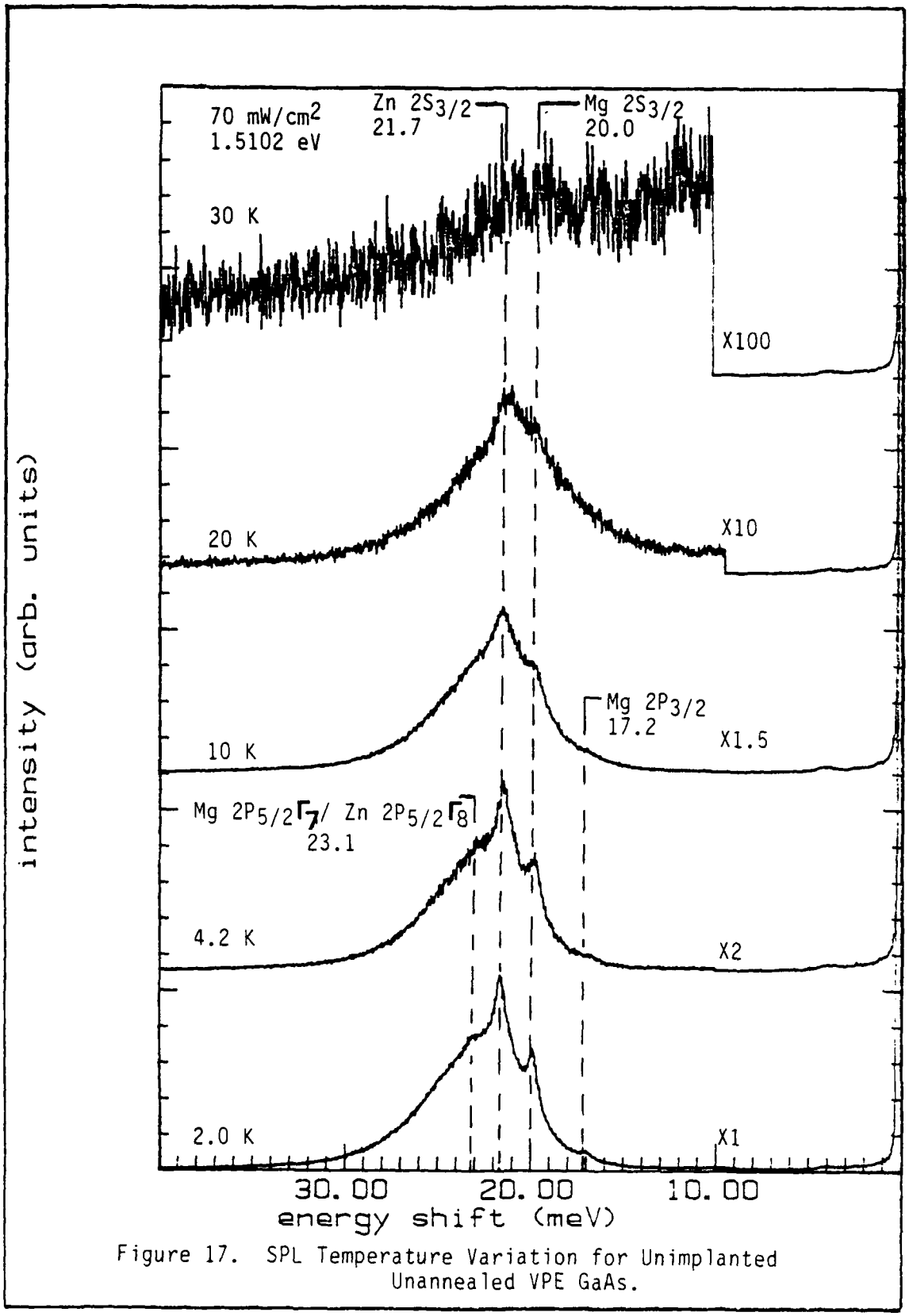

Figure 17. SPL Temperature Variation for Unimplanted Unannealed VPE GaAs.

is still the major factor controlling the temperature behavior of the DAP and SPL structure.

Observation of the SPL from the virgin unannealed sample revealed Zn as a primary acceptor impurity with the dominant 21.7 meV transition in most of the SPL. Definite traces of C and Si were also observed during the analysis. Though not conclusive, some spectra indicate the presence of Ge. The most remarkable features of this sample are two transitions at 20.0 and 17.2 meV, which match previously observed two hole and far-infrared transitions for Mg acceptors. As a result, Mg appears to be a major acceptor impurity in the virgin sample, even though the PL data did not provide any evidence of Mg in the material because of the low Mg concentration in the sample.

Figure 18 shows the SPL spectra at the higher pump intensity of 700 mW/cm^2 with different pump laser wavelengths. These spectra are included for comparison with the spectra from the implanted samples which were run at the higher pump intensity. The Zn $2P_{3/2}$ and the Mg $2S_{3/2}$ and $2P_{3/2}$ transitions are readily apparent in this data. Additionally, a peak at 21.2 meV matches the value for the $2P_{5/2}\Gamma_8$ transition for Mg observed by far infrared techniques.

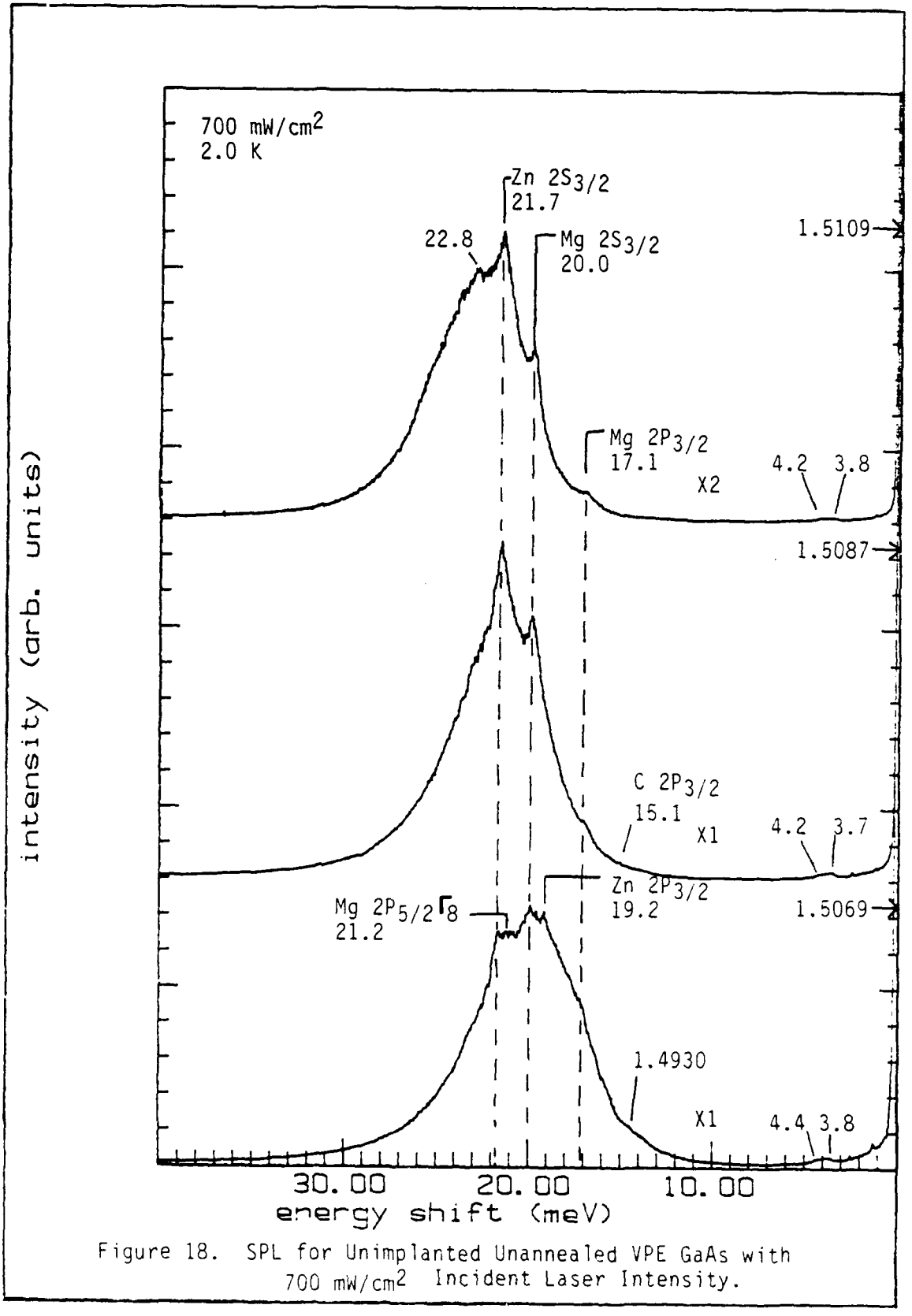

Figure 18. SPL for Unimplanted Unannealed VPE GaAs with 700 mW/cm^2 Incident Laser Intensity.

Unimplanted 850 °C Annealed VPE GaAs

This sample is identical to the previous sample except that it was encapsulated with a pyrolytically grown Si_3N_4 cap and annealed for 15 minutes at 850 °C. The effects the cap and annealing had on this sample were examined using both PL and SPL.

Photoluminescence Figures 19 and 20 show PL spectra collected using different pump intensities and different temperatures, respectively. It can be seen that the same features observed in the unannealed sample are present plus some notable differences. The exciton spectra contain the same lines as the unannealed sample. However, a substantial increase in the exciton linewidth is noted which causes a loss of resolution, especially in the region above 1.5141 eV (the neutral bound exciton line). The 1.4931 eV, C FB peak is evident at lower temperature and smaller pumping intensity conditions. The 1.4893 eV grows faster with increasing pumping intensity compared to other nonexciton features, and at 30 K, it is one of two remaining resolvable peaks as shown in Figure 20. This behavior represents the characteristic features of a FB transition, and from the energy of the peak, this transition appears to be the Zn FB. The 1.4857 eV peak shifts to higher energies as the pump intensity increases; also, the PL intensity also decreases with increasing temperature (Figure 20). This behavior

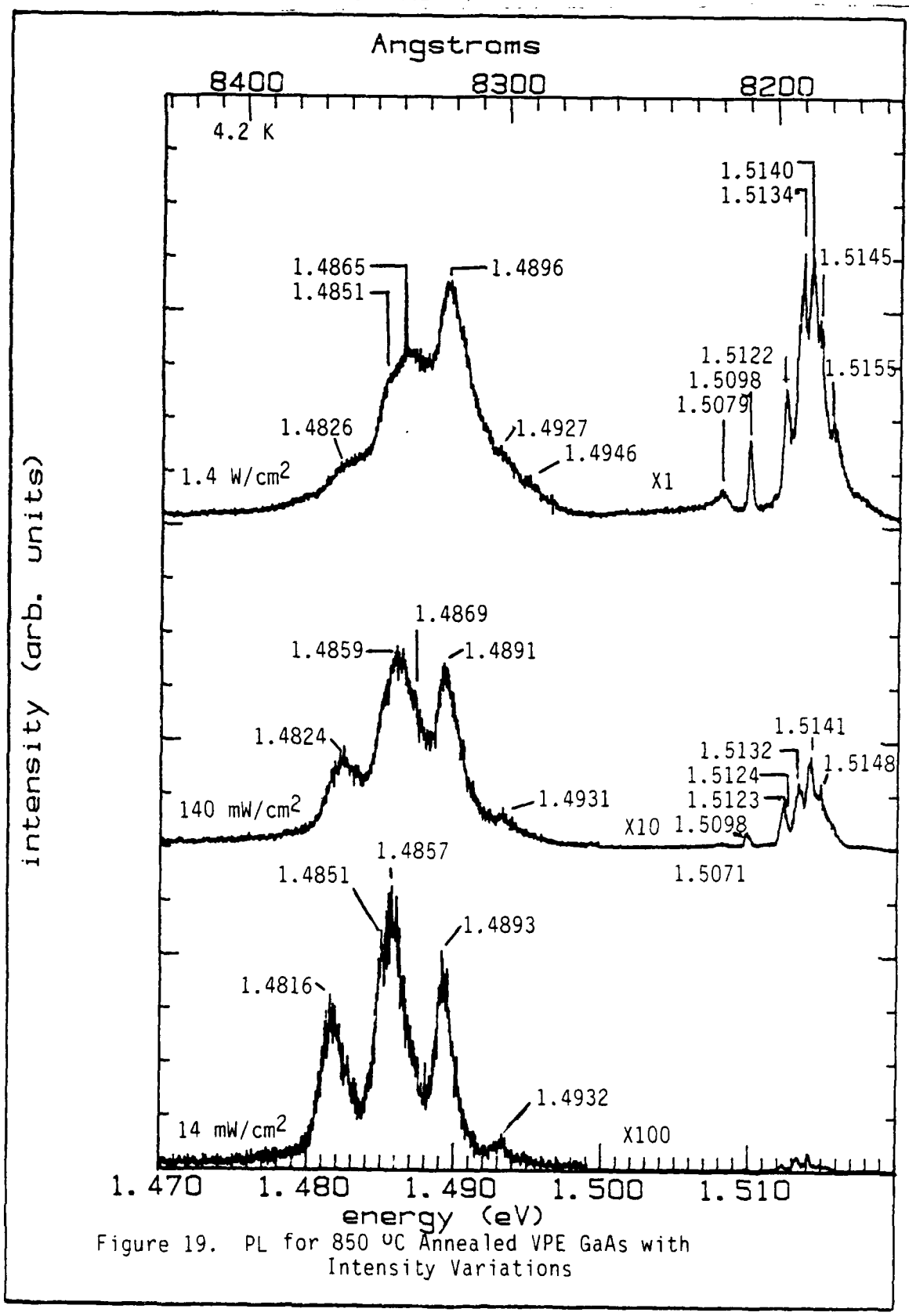

Figure 19. PL for 850 °C Annealed VPE GaAs with Intensity Variations

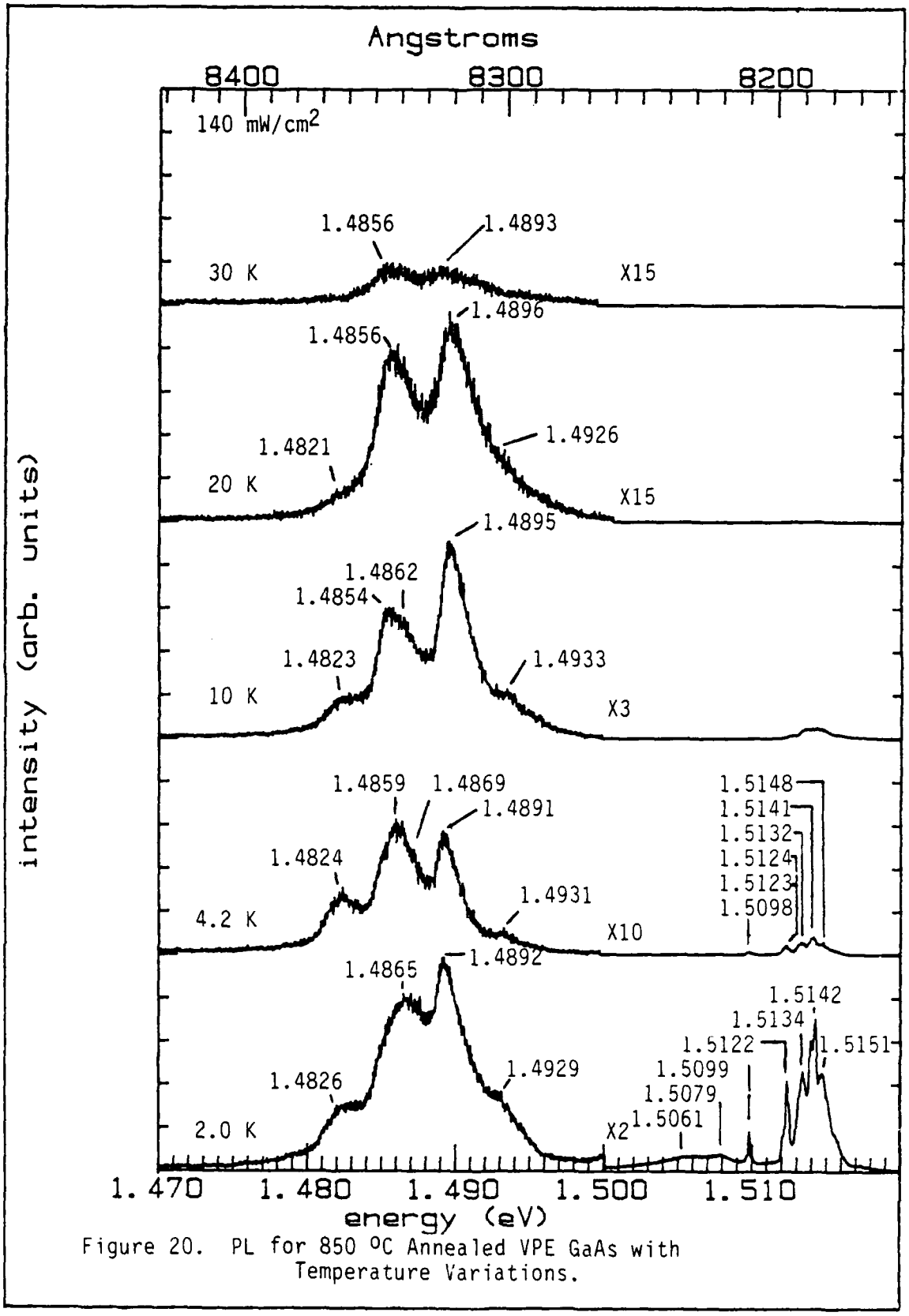

Figure 20. PL for 850 °C Annealed VPE GaAs with Temperature Variations.

indicates that the 1.4857 eV peak is a DAP transition. The energy level indicates this peak is the Zn DAP transition. At 30 K, the peak has shifted to about 1.4856 eV, and it is the only distinguishable feature besides the Zn FB. This peak matches previously reported energies for the Si FB. An additional new feature not observed in the unannealed sample is the peak at 1.4824 eV. The 1.4824 eV peak at 140 mW/cm^2 shifts to 1.4815 eV at lower intensities, and to 1.4826 eV at higher intensities. The peak decreases in intensity with increasing temperature and is almost completely unobservable at 20 K. This behavior indicates the 1.4824 eV peak is a Si DAP transition.

Several additional structures are visible just below the exciton region. The first peak at 1.5098 eV is exciton-like in appearance and matches the expected values for the two electron transition for a neutral donor bound exciton. The other two feature are only apparent at 4.2 K or less and at higher pump intensities. The peak at 1.5079 eV is visible at 4.2 K, and 2.0 K (Figure 20). The peak at 1.5060 eV is clearly visible in the 2.0 K spectra, but barely discernible in the 1.4 W/cm^2, 4.2 K spectra. Appearance of the peaks indicates that the 1.5079 eV peak may be a FB transition, and the 1.5060 eV peak may be associated with the DAP band. The state would have to be very shallow in order to explain the extreme sensitivity to temperature. Possible explanations include defect

structures such as interstitials and defect-vacancy complexes. The other alternative is that this transition may be the [g-g] band. The possibility of it being the excited state of one of the already observed impurities can be eliminated by comparing the difference in energy between this peak and the ground state FB transitions observed in the PL with the energy differences for various impurities as determined by SPL measurements.

The photoluminescence measurements for the unimplanted annealed sample show that Zn is the dominant acceptor impurity and C and Si are present to a lesser degree. The addition of Si as a major observable impurity after annealing may result from many sources; migration from the substrate into the epilayer, and/or in-diffusion from the cap into the epilayer. The addition of the structure at 1.5079 and 1.5060 eV may be explained as an annealing induced defect structure possibly related to a vacancy complex or a localized surplus acceptor population forming more complex centers.

Selectiv' Pair Luminescence. SPL spectra were taken on this sample starting with a pump energy of 1.5143 eV to 1.5071 eV as shown in Figures 21 and 22. The pumping energy of 1.5143 eV is slightly above the energy that SPL can be first observed, but below the band gap energy. At this energy, several exciton lines are observed and a strong transition at 1.5099 eV is seen. As the laser is tuned to

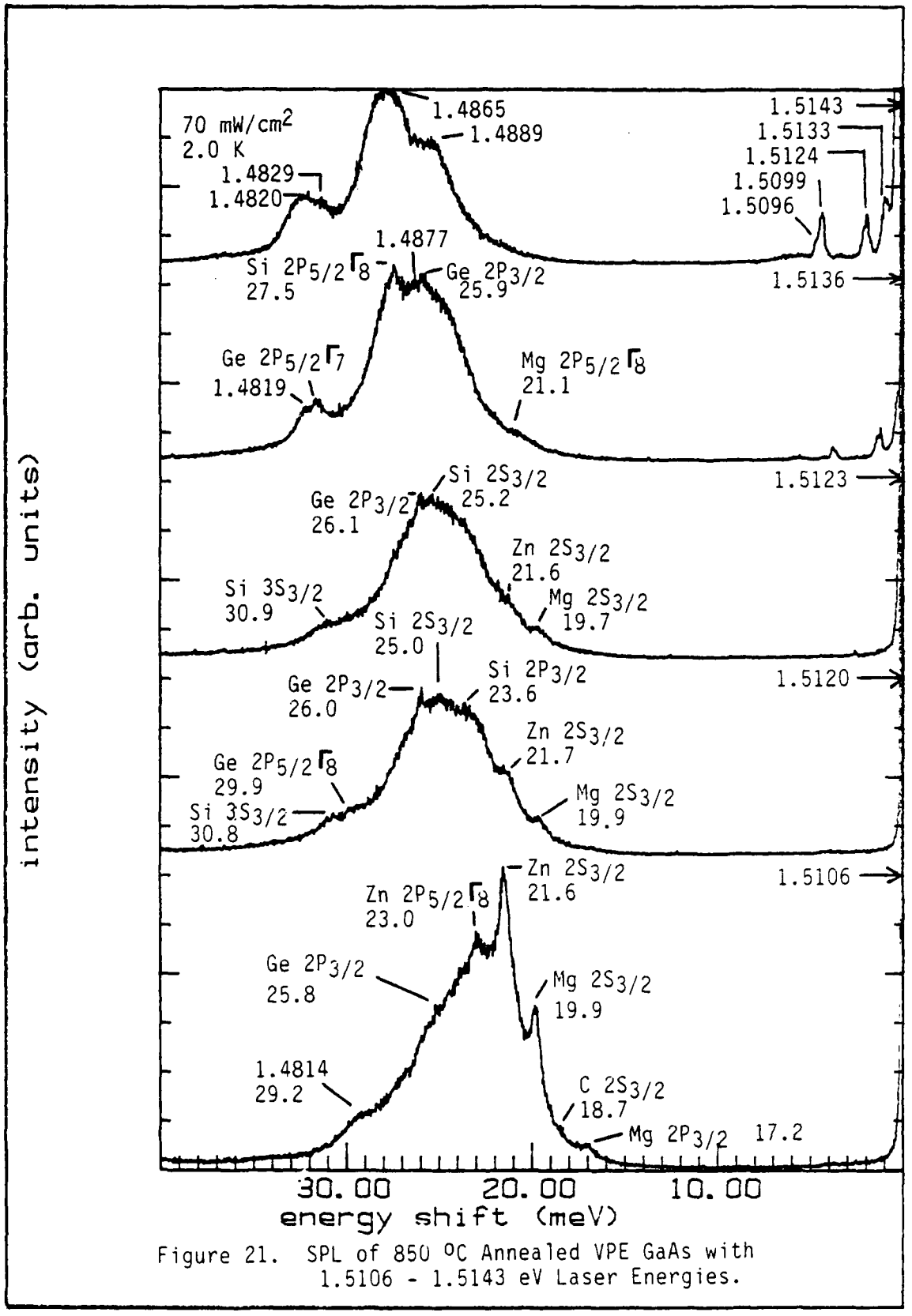

Figure 21. SPL of 850 °C Annealed VPE GaAs with 1.5106 - 1.5143 eV Laser Energies.

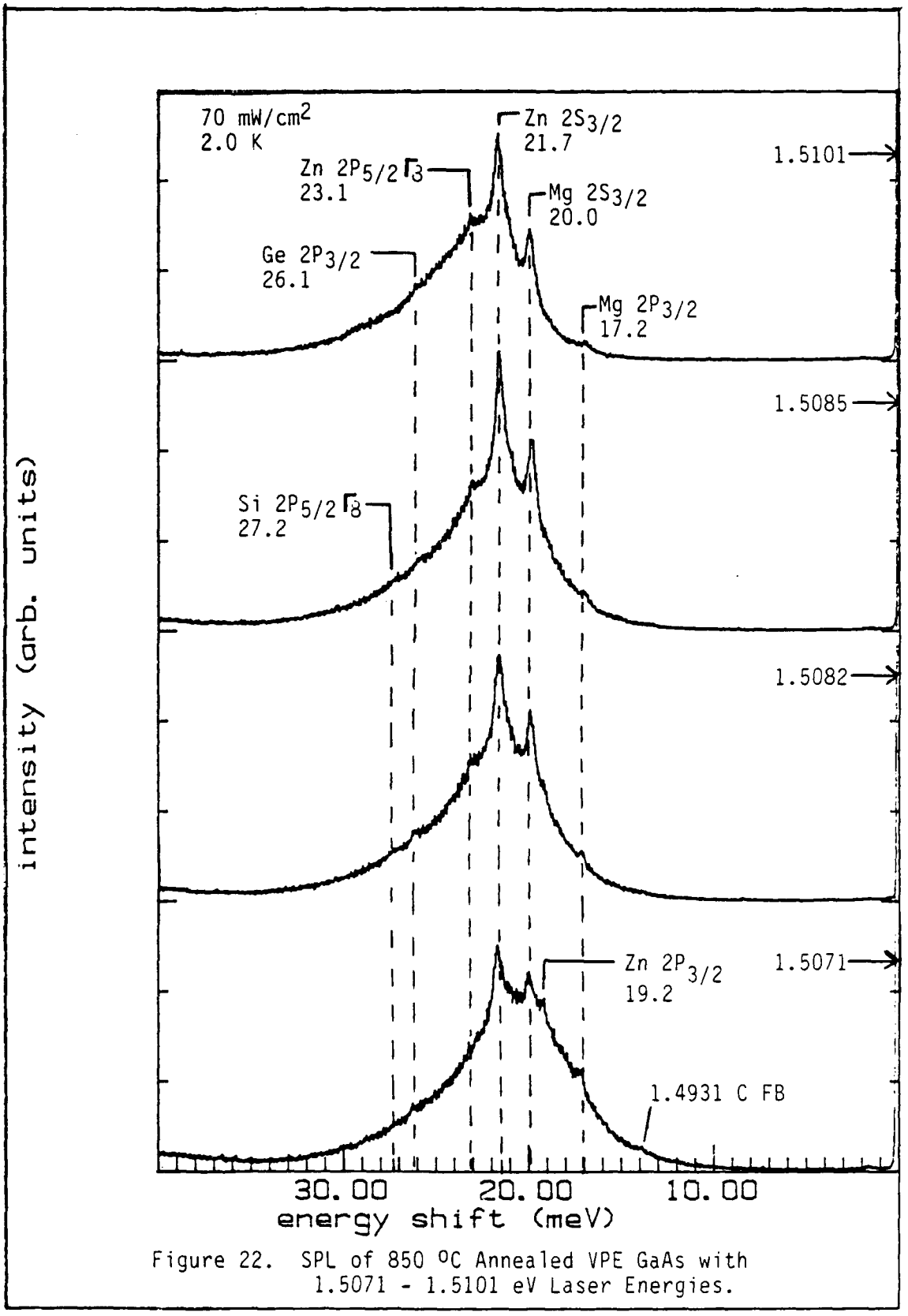

Figure 22. SPL of 850 °C Annealed VPE GaAs with 1.5071 - 1.5101 eV Laser Energies.

lower energies, this peak becomes less intense and has disappeared at pump energies of 1.5120 eV or lower, indicating this peak is related to the exciton st ucture. Strong enhancement when the pump is tuned to the neutral donor bound exciton line indicates that this peak is the two electron transition for the neutral donor bound exciton. Other distinctive features of this first spectrum at 1.5143 eV pump energy are the three peaks at 1.4889, 1.4865, and 1.4820 eV. Since pumping is occurring below gap DAP are expected to dominate in this region. The peaks at 1.4865 and 1.4820 have already been identified as the Zn and Si DAP transitions, respectively. The new peak at 1.4889 eV is unidentified and could be a C DAP or the remnants of the Zn FB.

At a pump energy of 1.5136 eV, the first signs of SPL begin to manifest themselves with a peak at 21.1 meV which is the $2P_{5/2}\Gamma_8$ to $1S_{3/2}$ transition of Mg. In addition, two major DAP pair bands are now visible at 1.4877 and 1.4819 eV. The 1.5123 eV pump energy matches closely the neutral acceptor bound exciton energy, and thus, an enhancement in the spectra from the two hole transitions is expected. Seven SPL lines are observed at the 1.5120 eV pump energy. The first peak at 19.9 meV closely matches the $2S_{3/2}$ transition for Mg. The second at 21.7 meV matches exactly the $2S_{3/2}$ transition for Zn. The third line at 23.6 meV is close to the 23.5 meV peak for the Si $2P_{3/2}$ transition. The

Table VIII: SPL Transitions for Virgin Annealed VPE GaAs

Energy Shift (meV)	Associated Impurity State
17.2	Mg $2P_{3/2}$-$1S_{3/2}$
18.7	C $2S_{3/2}$-$1S_{3/2}$
19.2	Zn $2P_{3/2}$-$1S_{3/2}$
20.0	Mg $2S_{3/2}$-$1S_{3/2}$
21.7	Zn $2S_{3/2}$-$1S_{3/2}$
23.1	Zn $2P_{5/2}(\Gamma_8)$-$1S_{3/2}$
23.5	Si $2P_{3/2}$-$1S_{3/2}$
25.2	Si $2S_{3/2}$-$1S_{3/2}$
26.1	Ge $2S_{3/2}$-$1S_{3/2}$
27.3	Si $2P_{5/2}(\Gamma_8)$-$1S_{3/2}$
30.8	Si $3S_{3/2}$-$1S_{3/2}$

fourth line at 25.0 matches the $2S_{3/2}$ transition for Si. The fifth line at 26.0 meV matches the Zn $3S_{3/2}$ transition or possibly the Ge ($2P_{3/2}$) transition. The sixth line at 29.9 meV matches the Ge $2P_{5/2}\Gamma_8$ transition, and the seventh line at 30.8 meV matches the Si $3S_{3/2}$ transition. Tuning lower pump energies causes additional peaks to emerge. All the SPL transitions observed from the unimplanted, 850 °C annealed VPE GaAs are listed in Table VIII.

Figure 22 shows the SPL in much sharper detail. Optimum pump energies for the SPL have been reached, and the DAP background is greatly reduced. A new transition for this sample is the Si $2P_{5/2}\Gamma_8$ peak.

The Zn and Mg $2S_{3/2}$ transitions peak at, 1.4890 and 1.4907, respectively are consistent with the DAP peaks observed for Zn and Mg.

The laser pump intensity dependence on SPL spectra from this sample (Figure 23) varies in the same manner as that associated with the unannealed sample, and confirms the conclusion that 70 mW/cm^2 is the optimum pump intensity for the unimplanted samples.

The variations in the spectra with temperature (Figure 24) also match those of the unannealed sample. The 21.6 meV, Zn $2S_{3/2}$, and the 19.9 meV, Mg $2S_{3/2}$, peaks are visible even up to 20 K. However, a distinct loss in resolution due to line broadening is visible beginning at 10 K.

Figure 25 is the SPL spectra for the highest pump power of 700 mW/cm^2, and is included for comparison with the implanted samples.

60 keV Mg Ion Implant

The 60 keV ion implanted samples were implanted with doses of 10^{12}, $5X10^{12}$, 10^{13}, and $5X10^{13}$ cm^{-2} of Mg. Samples were capped with Si_3N_4 and annealed for 15 minutes at 850 °C.

$1x10^{12}$ Implant. Figures 26 and 27 show the spectra for this sample at various excitation intensities and temperatures, respectively. The photoluminescence data

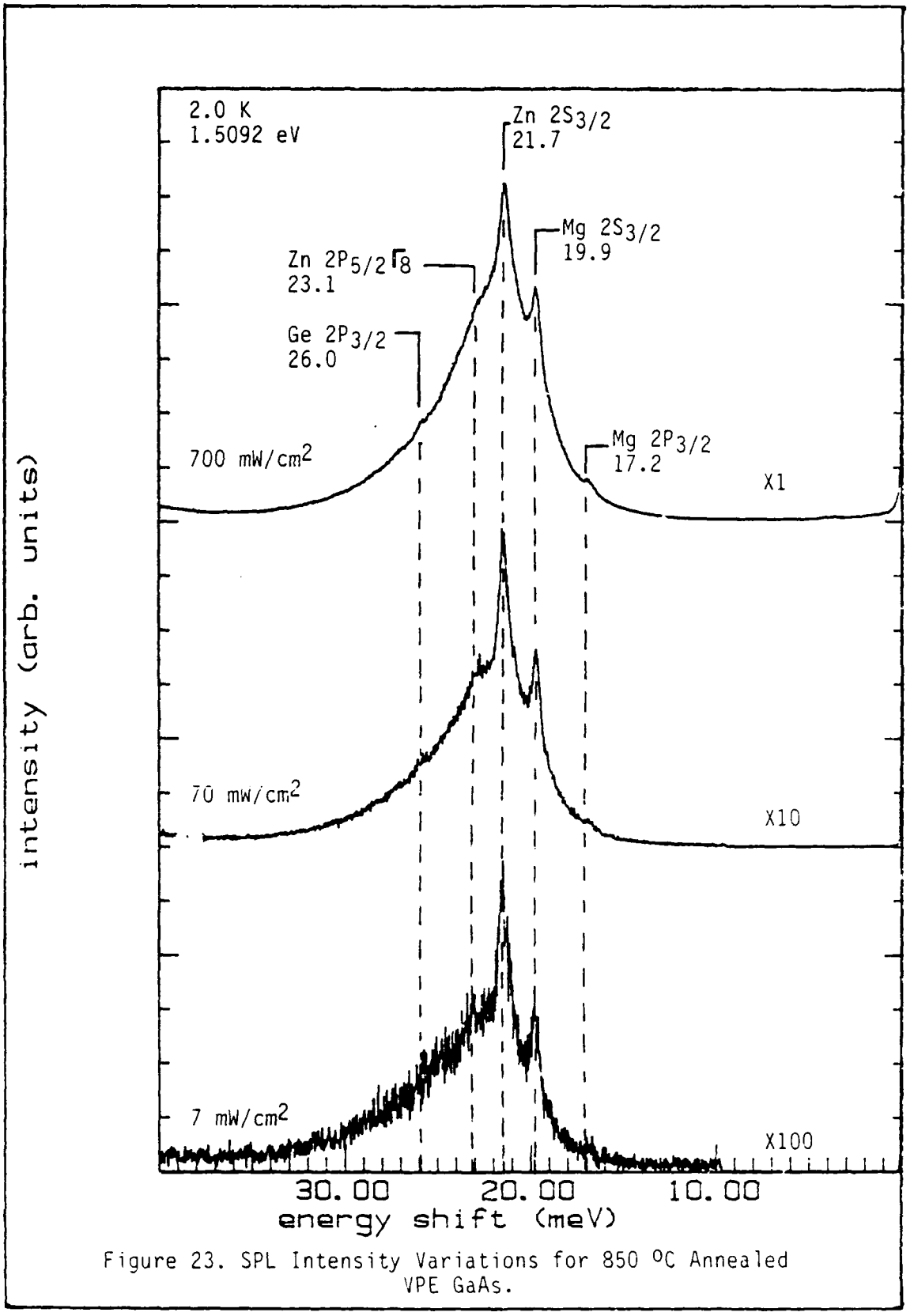

Figure 23. SPL Intensity Variations for 850 °C Annealed VPE GaAs.

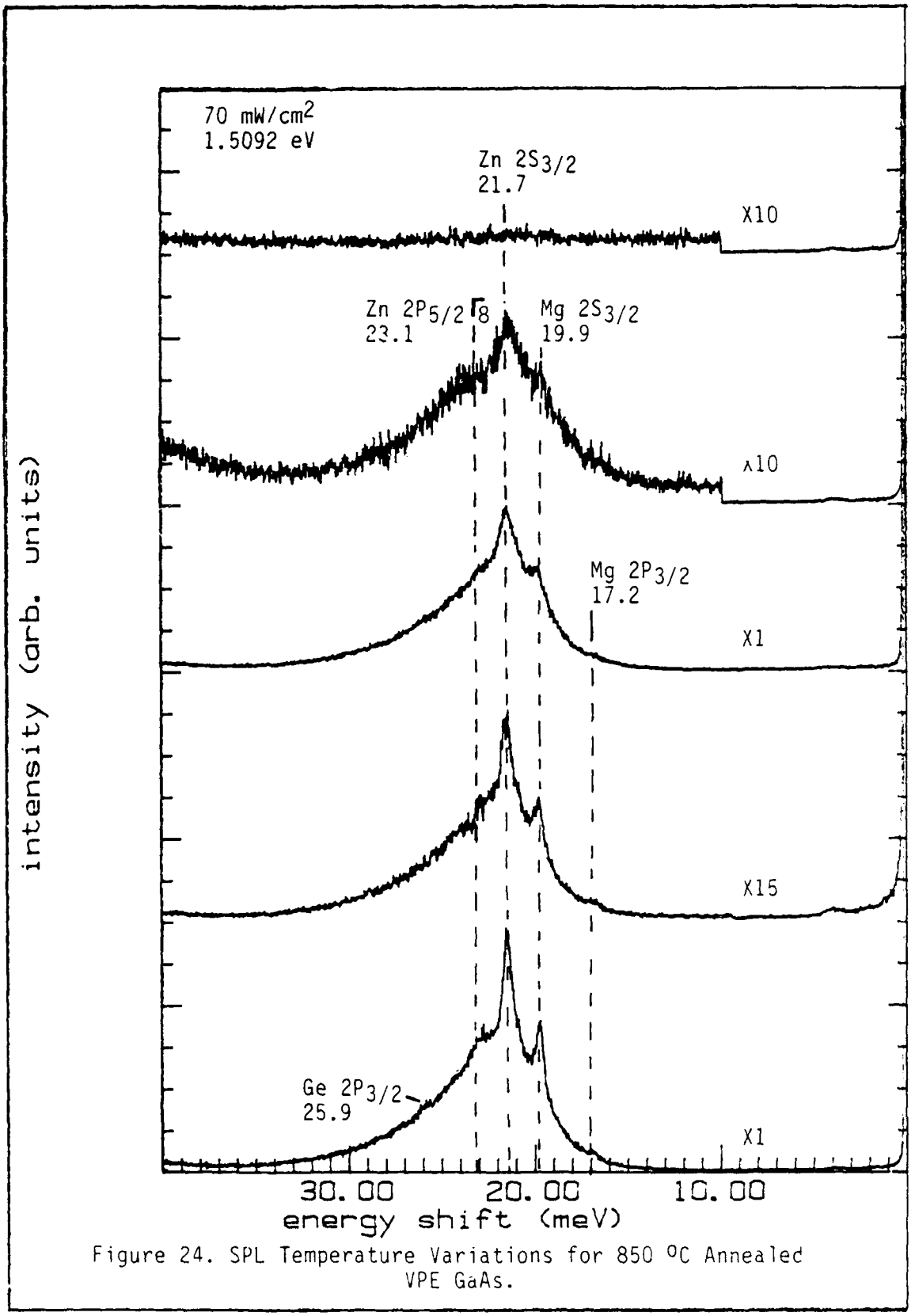

Figure 24. SPL Temperature Variations for 850 °C Annealed VPE GaAs.

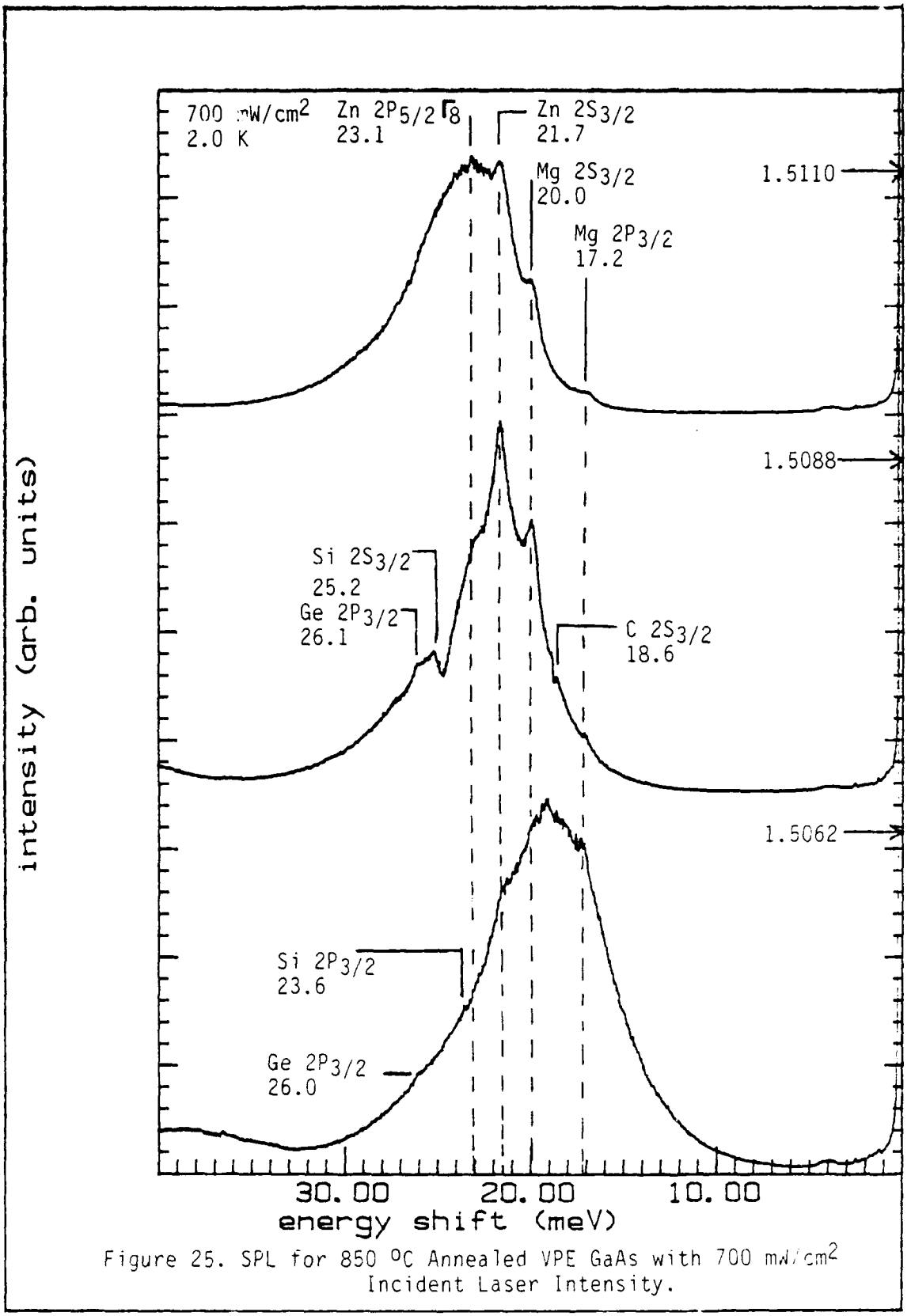

Figure 25. SPL for 850 °C Annealed VPE GaAs with 700 mW/cm^2 Incident Laser Intensity.

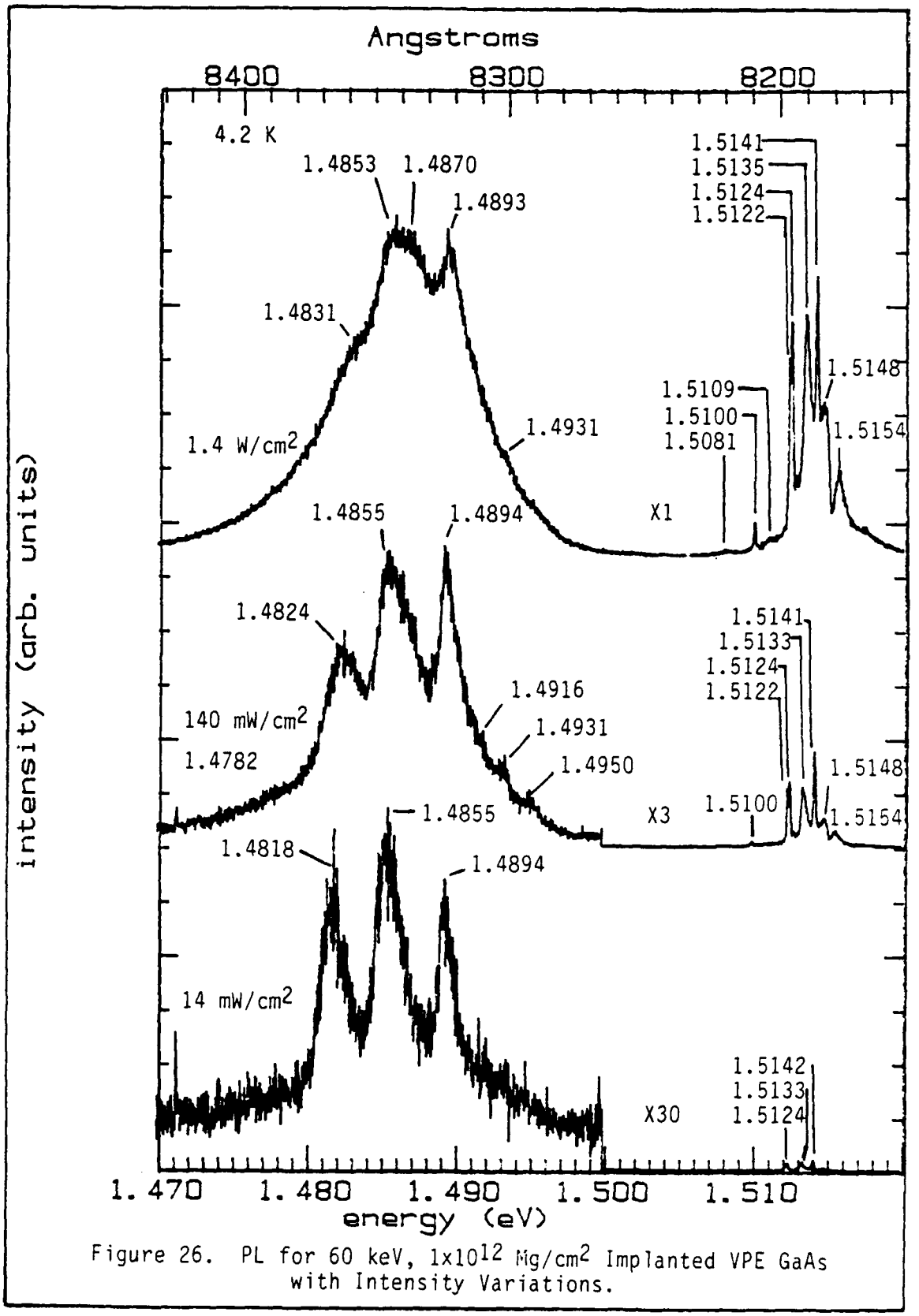

Figure 26. PL for 60 keV, $1x10^{12}$ Mg/cm^2 Implanted VPE GaAs with Intensity Variations.

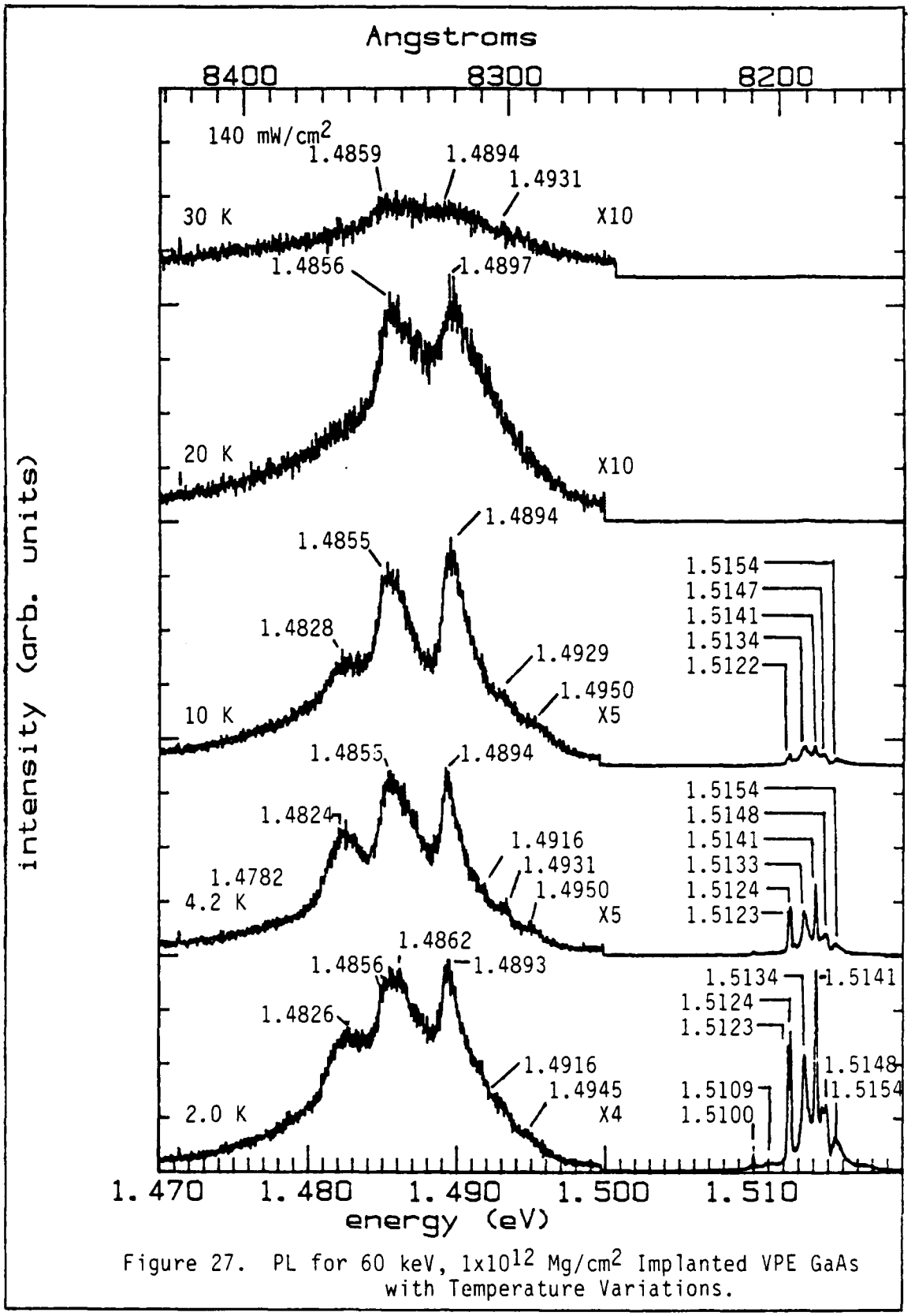

Figure 27. PL for 60 keV, $1x10^{12}$ Mg/cm^2 Implanted VPE GaAs with Temperature Variations.

closely resembles the spectra from the undoped annealed sample. The exciton structure is present and is clearly resolvable at 4.2 and 2.0 K. Additionally, three peaks are noted just below the exciton band at 1.5109, 1.5100, and 1.5081 eV. The 1.5109 eV peak could be the two electron transition for a free exciton near a donor. The 1.5100 eV peak is the two electron transition for the neutral donor bound exciton. The 1.5081 eV is barely visible in one of the spectra. Its source is unknown, but it is possibly the [g-g] transition.

The most notable feature in the PL spectra for the $1X10^{12}$ implanted sample is the absence of the structure associated with the Mg implant. The C FB is observed at 1.4931 eV, the Zn FB is observed at 1.4894 eV, and the combination of the Zn DAP and Si FB at 1.4855 eV are also seen. The Zn DAP peak is observed in the 1.4 W/cm^2 , 4.2 K spectrum, and the 1.4824 eV Si DAP peak is visible in all spectra for which the temperature is less than 20 K. The 4.2 K spectrum with 140 mW/cm^2 pump intensity only suggests that the presence of Mg as a shoulder at 1.4916 eV could be the Mg FB.

This sample optically bears great similarity to the undoped samples. The Mg-ion implant is almost undetectable in the PL spectra, indicating that the Zn and Si acceptors are more numerous than Mg, or that the Mg implant has not been effectively incorporated into the crystal.

The SPL spectra, as shown in Figure 28, are also very similar to those of the unimplanted samples. The only difference is a slight decrease in the overall spectral intensity for this sample relative to the unimplanted samples. The visible features are the 19.2, 21.6, and 22.9 meV peaks associated with the Zn acceptor, the 23.6 and 25.0 meV peaks for Si, the 26.0 meV peak which may be the $2S_{3/2}$ transition for Ge, and the 17.1 and 19.9 meV peaks which are tentatively associated with the Mg $2P_{3/2}$ and $2S_{3/2}$ transitions, respectively. A peak 4.3 meV from the pump energy is seen in all the spectra at low intensity. The origin of this peak is presently unknown. It may be speculated that this 4.3 meV peak is the 2S transition for an excited donor state DAP. If this is the case, it would be the first observation of its kind by SPL.

Overall, this sample is almost identical to the unimplanted annealed crystal, and the implant appears to have had little impact on the PL or the SPL.

<u>$5X10^{12}$ Implant.</u> Photoluminescence of this sample is different from the first three samples in that the Mg acceptor is now clearly visible in the spectra (Figures 29 and 30). A peak observed at 1.4912 eV exhibits the behavior of a FB transition and closely matches previously reported energy peaks for the Mg FB (38:12.5). Further, the peak dominates the spectrum at higher pump intensities and temperatures. At intensities below 1.4 W/cm^2 and

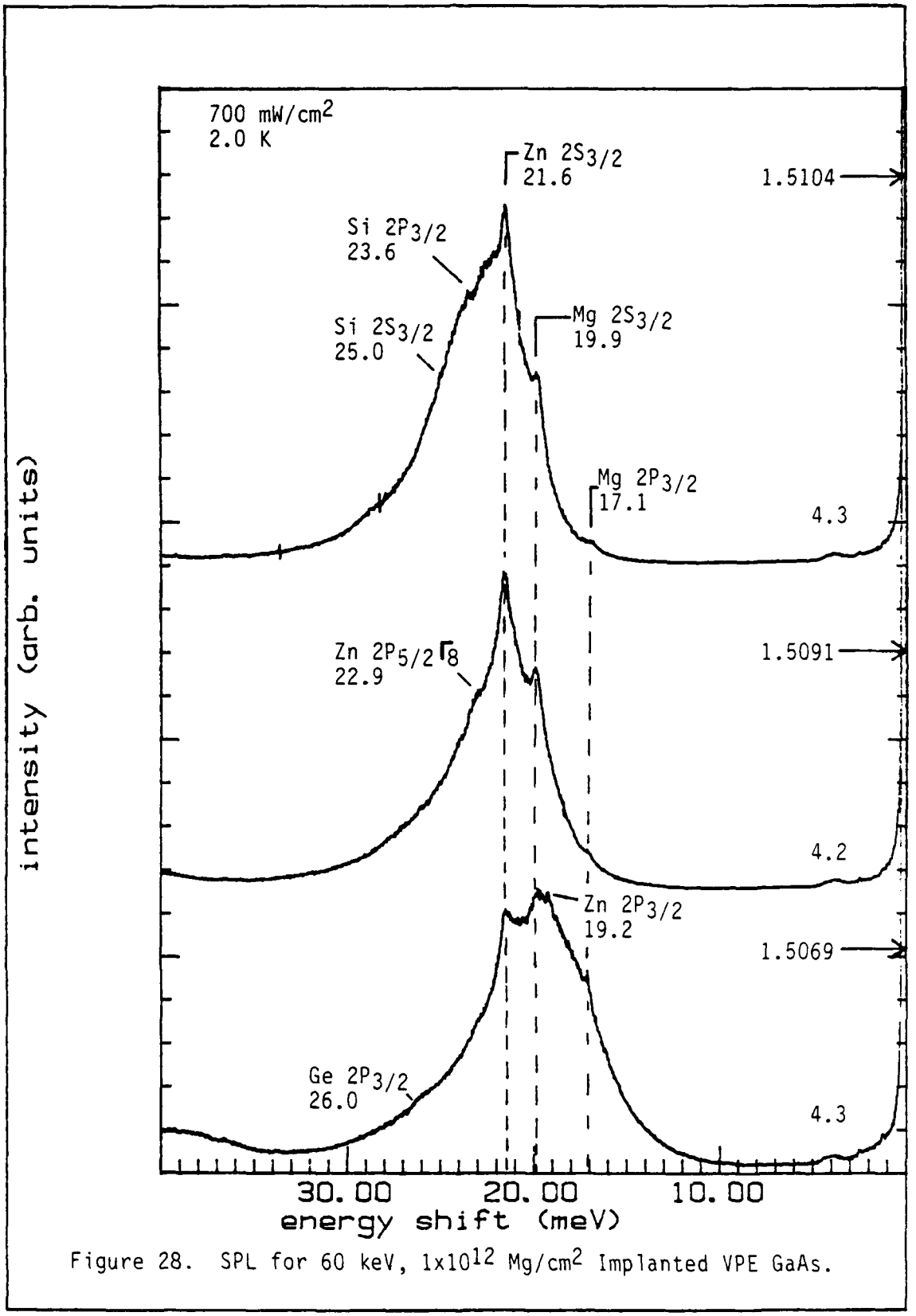

Figure 28. SPL for 60 keV, $1x10^{12}$ Mg/cm^2 Implanted VPE GaAs.

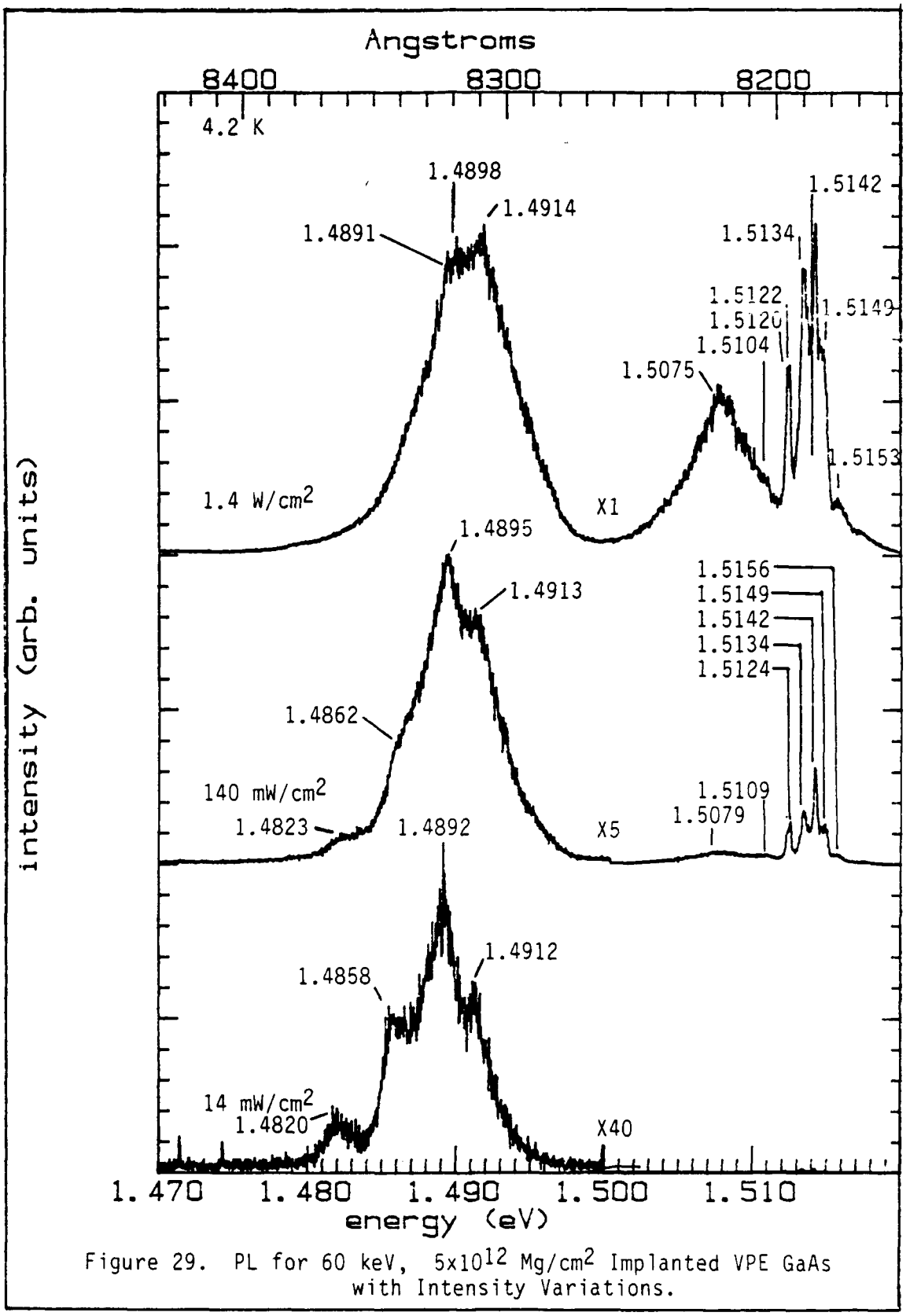

Figure 29. PL for 60 keV, 5×10^{12} Mg/cm^2 Implanted VPE GaAs with Intensity Variations.

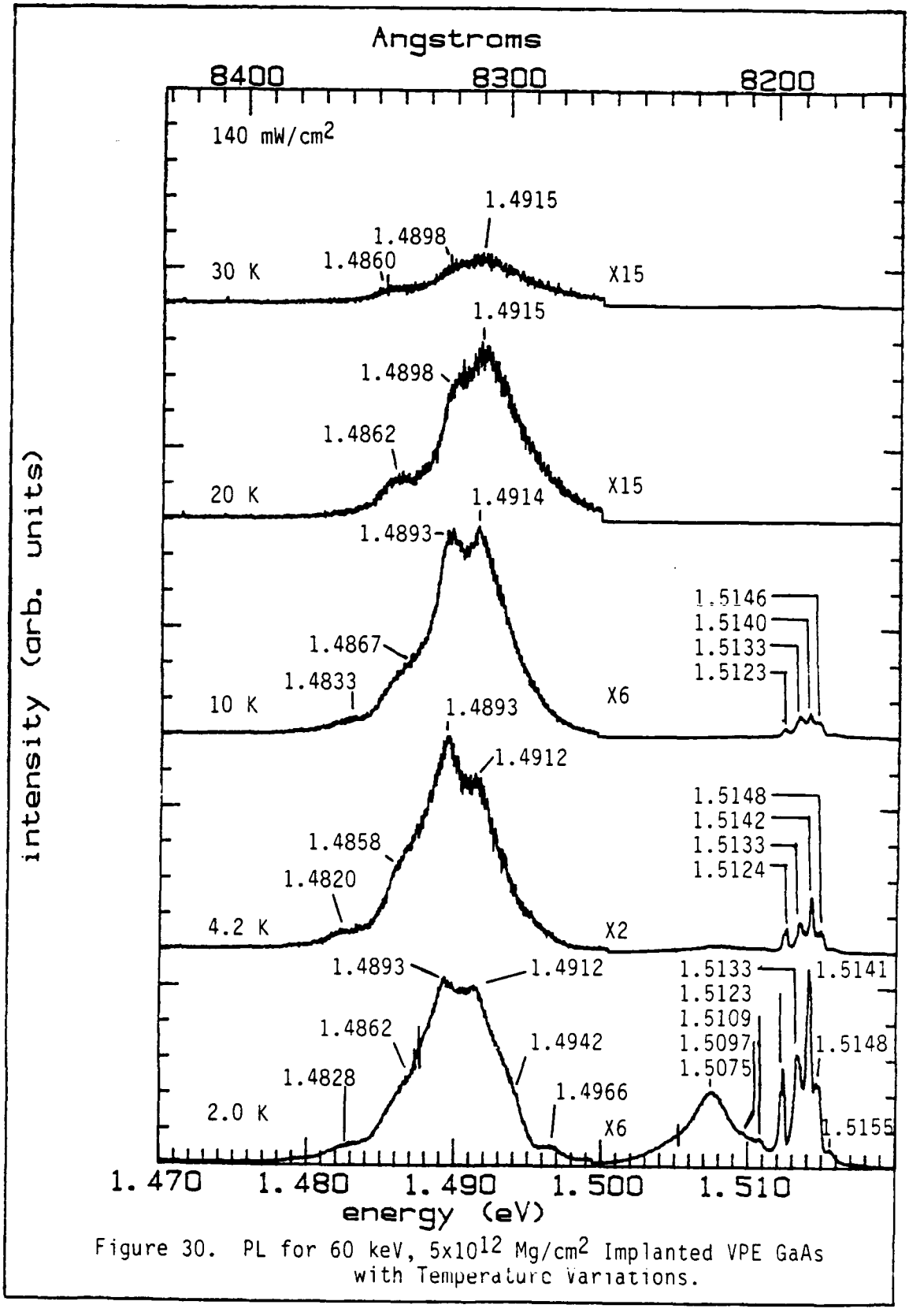

Figure 30. PL for 60 keV, 5×10^{12} Mg/cm^2 Implanted VPE GaAs with Temperature Variations.

temperatures less than 10 K, the spectra are dominated by a peak at 1.4892 eV. This peak at first appears to be the Zn FB transition, but it shifts to slightly higher energies with increasing laser energies. Also, the Mg FB grows faster than the 1.4892 eV peak with increasing temperature and intensity. From this behavior it appears that the 1.4892 eV peak is a superposition of the Zn FB and the Mg DAP peaks. Peaks at 1.4862 and 1.4823 eV are associated with the Zn and Si DAP transitions, respectively. Another highly visible part of the spectra from this sample are the three peaks at 1.5109, 1.5097, and 1.5075 eV. The 1.5109 and 1.5097 eV peaks have already been associated with two electron transitions in the previous samples. The 1.5075 eV peak is an anomalous feature in this sample. The peak is very intense in the 4.2 and 2.0 K spectra but nonexistent above 4.2 K. Also, a shoulder is visible in the 2.0 K spectra in the vicinity of 1.505 eV. Behavior of this peak with pump intensity is similar to that of FB transitions, while the temperature behavior is inconsistent with a FB transition. This peak is further from the band edge than the exciton structure and should be less sensitive to temperature. The tentative assumption is that this is the [g-g] transition, and that the extreme sensitivity to temperature is consistent with the acceptor-acceptor pair theory.

The SPL from this sample as shown in Figure 31 has fewer visible peaks compared to previous samples. The most distinct features in the SPL are the 21.7 meV transition from the Zn, and the 17.1 and 20.0 meV transitions from Mg. The 19.3 and 21.7 meV peaks for Zn are observed at the 1.5071 eV pump energy. A feature 4.3 meV from the laser line appears in these spectra and moves with the laser energy. This feature may be related to the 1.5075 eV peak observed in the PL. The fact that this feature tunes with the laser implies that it may be DAP related. Noticeably missing from the SPL for this sample are the transitions associated with Si. Both Si and C were seen to be present in the PL, but no evidence of the transitions are observed in the SPL. It is possible that the C and Si transitions are lost in the stronger DAP background from the Mg and Zn DAP bands.

The $5X10^{12}$ implant showed distinct signs of C, Mg, Zn, and Si in the PL but only the Zn and Mg peaks were observed in the SPL. The Mg is now strongly observed in the samples, and the Zn structure is comparable to that of Mg.

<u>$1X10^{13}$ Implant.</u> The PL from this sample shows a dominance of the Mg FB transition at 1.4914 eV for most conditions (Figures 32 and 33). The 1.4900 eV Zn FB peak is also almost as prominent as the Mg peak. However, this Zn FB peak overlaps heavily with the Mg DAP peak under most conditions. The Mg DAP band becomes visible at 1.4881 eV

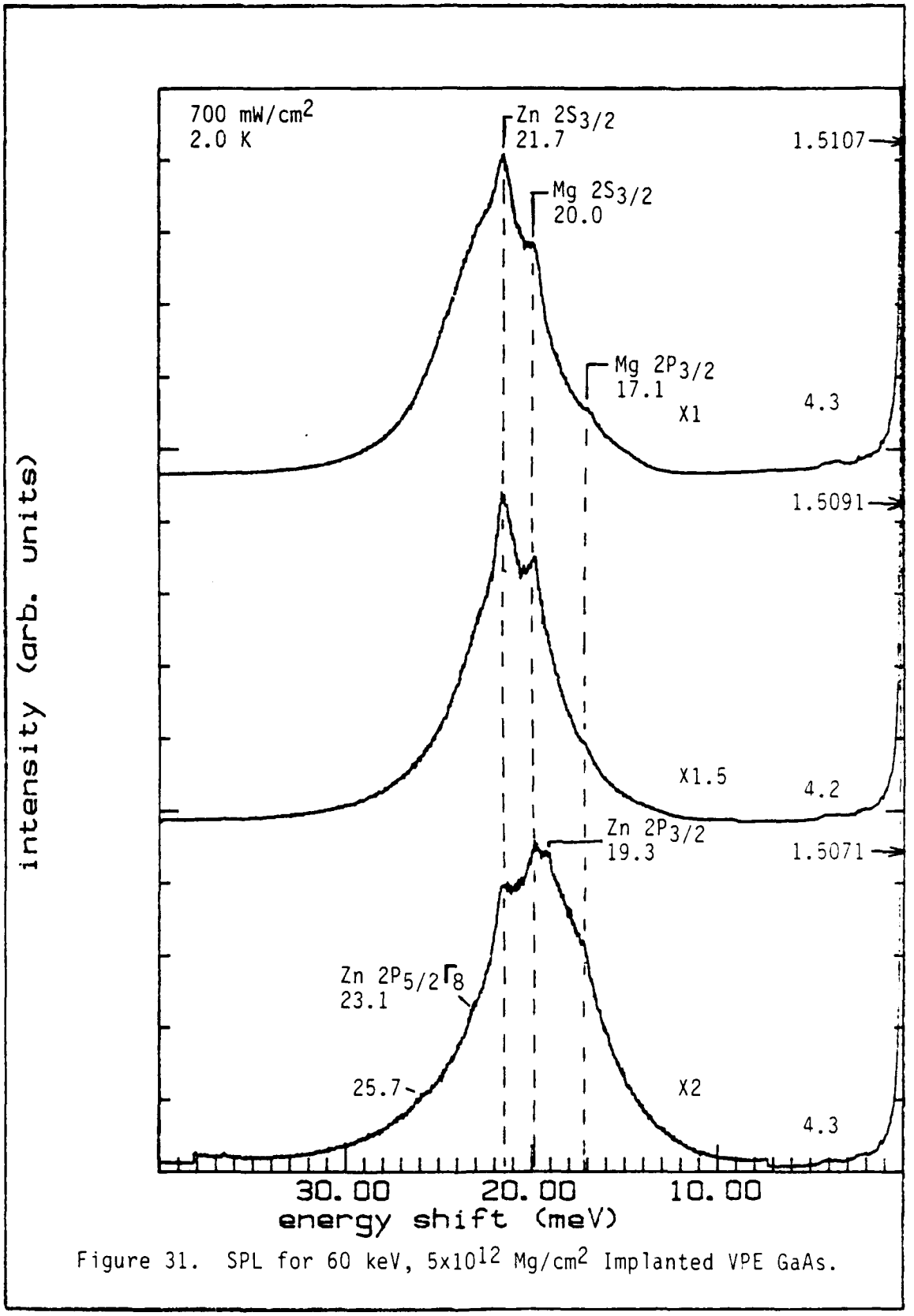

Figure 31. SPL for 60 keV, 5×10^{12} Mg/cm^2 Implanted VPE GaAs.

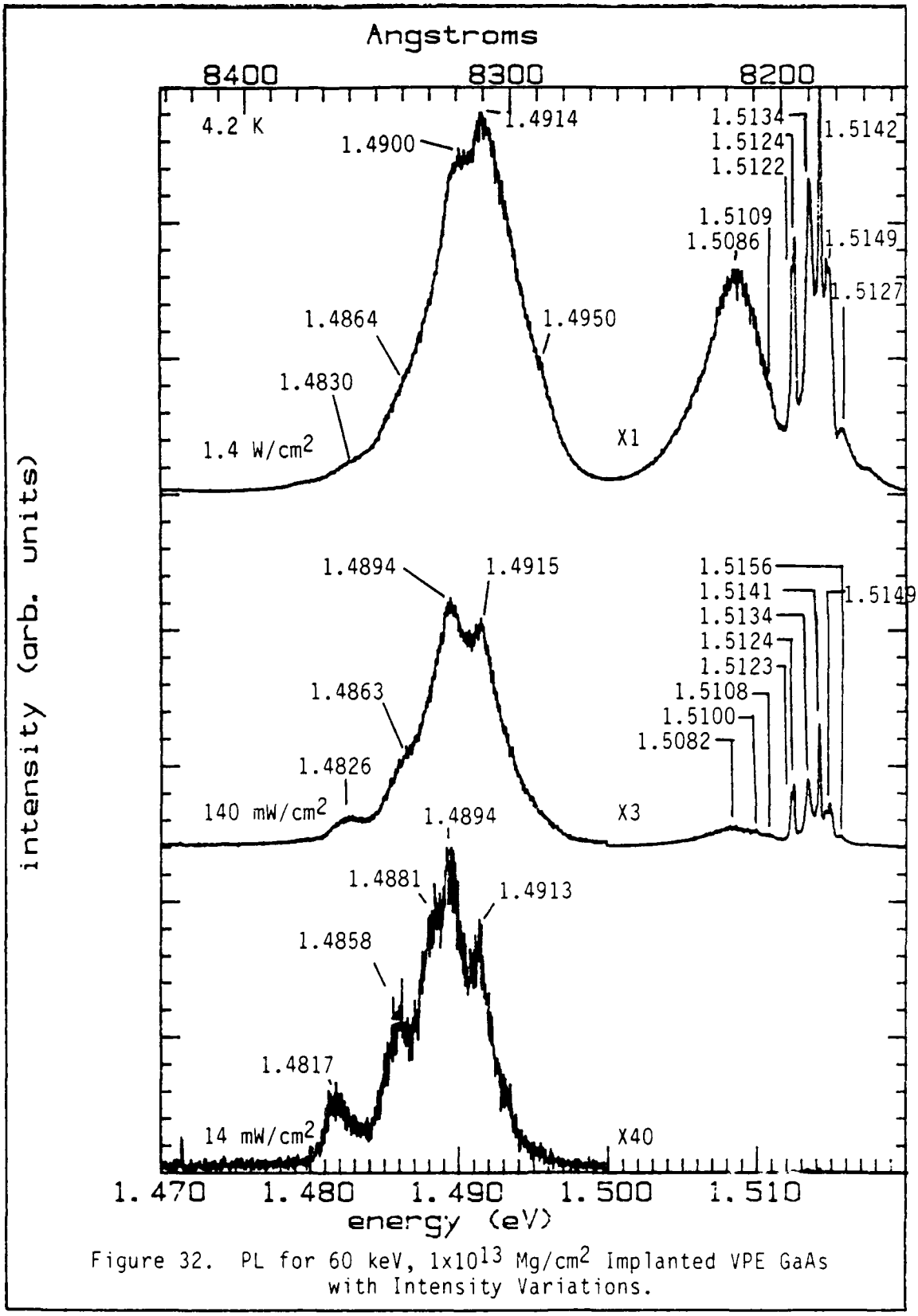

Figure 32. PL for 60 keV, $1x10^{13}$ Mg/cm^2 Implanted VPE GaAs with Intensity Variations.

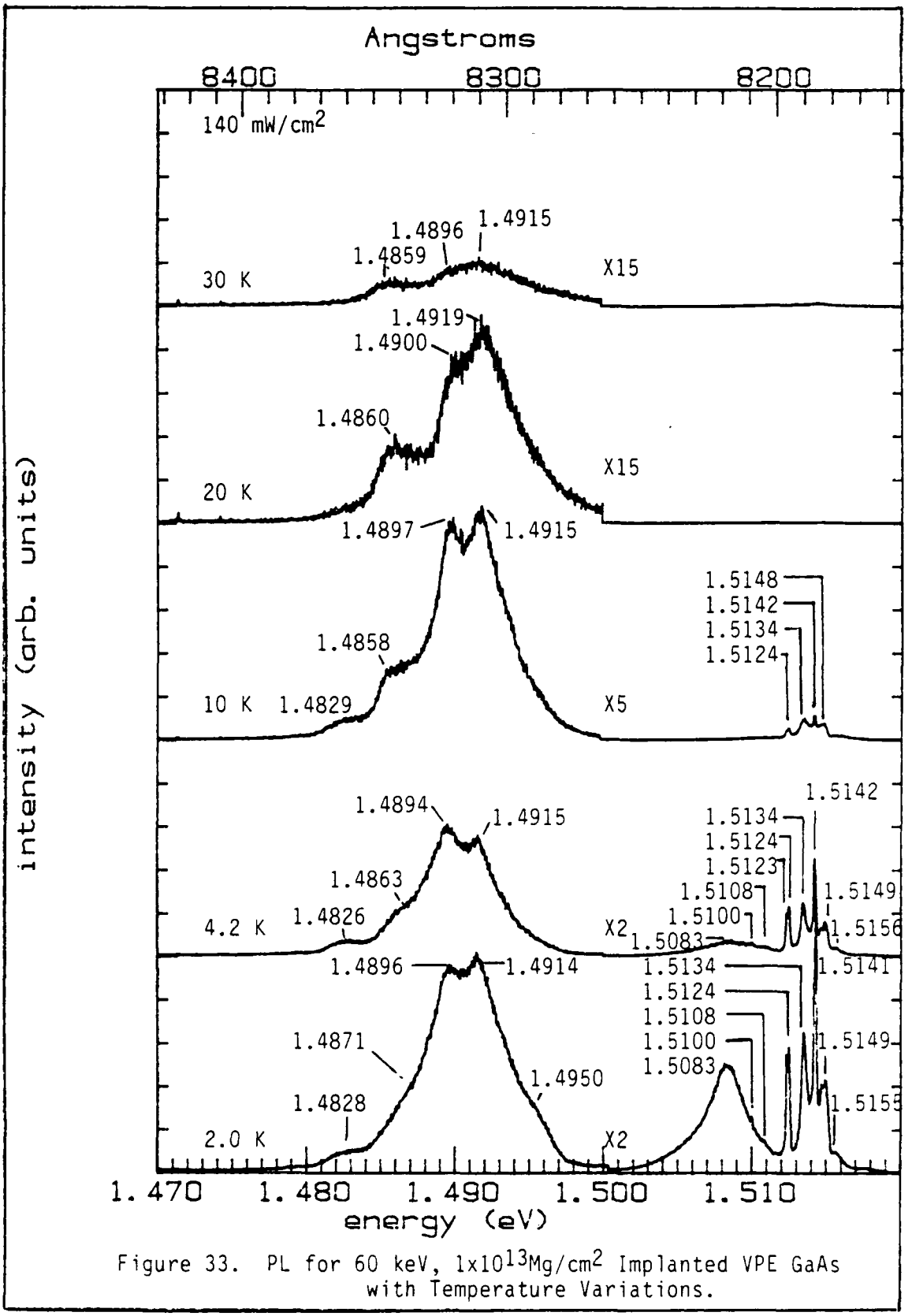

Figure 33. PL for 60 keV, $1x10^{13}$Mg/cm^2 Implanted VPE GaAs with Temperature Variations.

when the pump intensity is 14 mW/cm^2. A shoulder is observed around 1.4950 eV. This may be related to the C FB transition at 1.4932 eV. Another shoulder at 1.4863 eV is comprised of the Zn DAP and the Si FB peak. At higher temperatures this peak is resolved into the Si FB structure at 1.4858 eV. A peak at 1.4826 eV which disappears at 30 K is the Si DAP band. Other very prominent features of the PL are the three peaks at 1.5108, 1.5100, and 1.5083 eV. The peaks at 1.5108 and 1.5100 eV are the previously observed two electron transitions. The peak at 1.5083 eV is a peak similar to the 1.5079 eV peak observed in the $5X10^{12}$ Mg/cm^2 implanted sample. This behavior implies that the peak intensity has been increased with a higher dosage. This behavior is consistent with the characteristics of the DAP process, and indicates a relationship to the impurity concentration.

The SPL data shown in Figure 34 is basically the same as those from the previous $5x10^{12}$ Mg/cm^2 implanted sample. A slight increase may exist for the Mg peaks relative to the Zn peaks at this higher dose. The peaks seen from this sample are at 17.2, 20.0, and 21.1 meV, which were previously assigned to the Mg $2P_{3/2}$, $2S_{3/2}$, and the $2P_{5/2}(\Gamma_8)$ peaks, respectively. The Zn $2P_{3/2}$ and $2S_{3/2}$ peaks are observed at 19.3 and 21.6 meV. Anomalous peaks at 3.8 and 4.0 meV also appeared in the spectra for this sample. It is

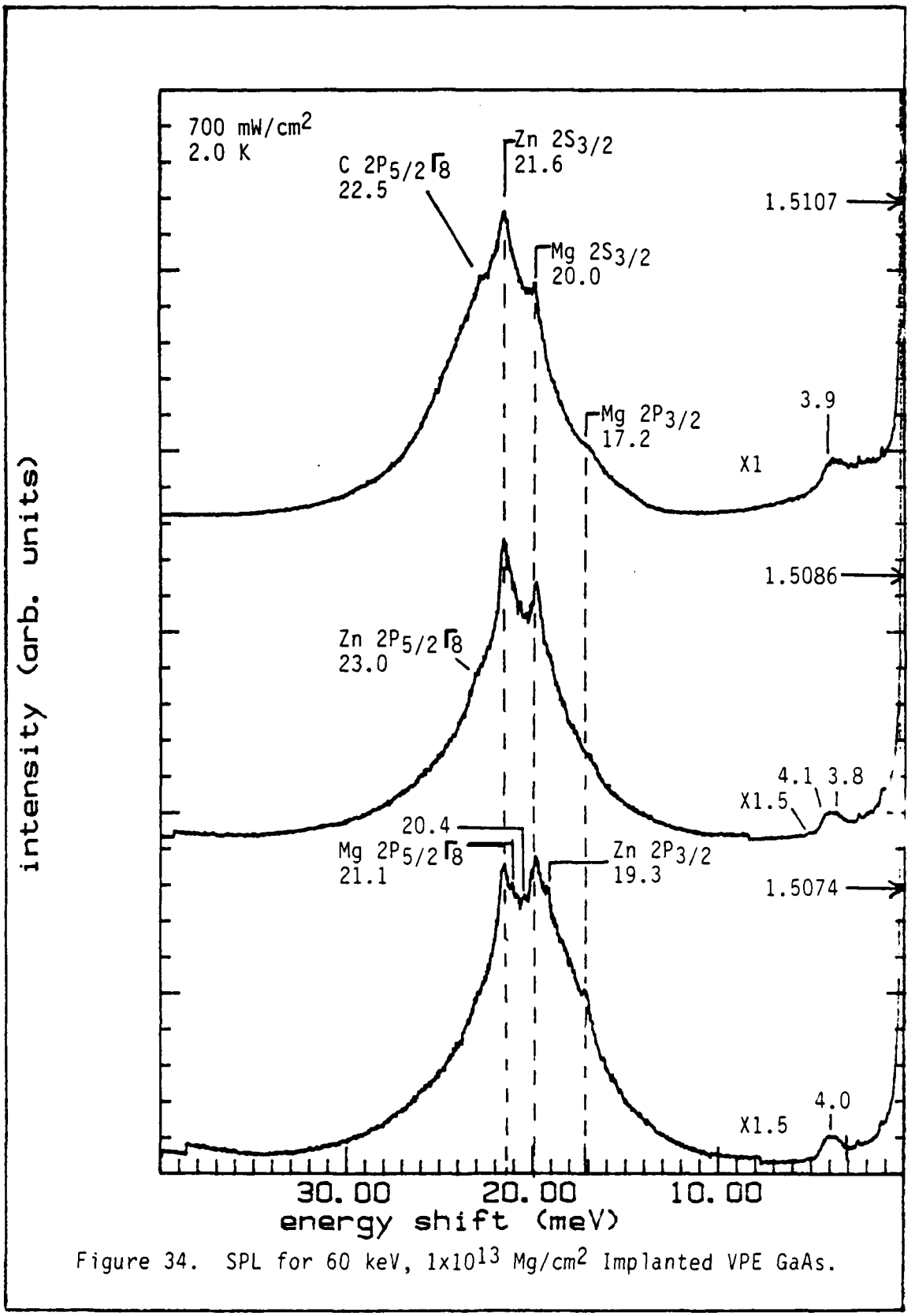

Figure 34. SPL for 60 keV, $1x10^{13}$ Mg/cm^2 Implanted VPE GaAs.

believed that these transitions are linked to the [g-g] structure observed in the PL.

5X10^{13} Implant. The spectra from this sample is significantly different from that observed in the lower dose implanted samples. The PL spectra from this sample exhibits heavy line broadening, and the sharp spectral features observed in other samples are not seen in this sample. Figures 35 and 36 reveal that the spectra are dominated by a broad peak around 1.49 eV. Various shoulders and other small peaks appear as the sample conditions are changed. A major change is the decrease in the intensity of the exciton structure relative to the other spectral features. The exciton peaks are still present, but at a substantially reduced intensity. The FB/DAP structure is the dominant feature of this sample. A new set of features are present on the high energy side of the FB/DAP structure. A shoulder at 1.4972 eV is observed at 2K, but not at higher temperatures. Present in all the spectra is a peak at 1.502 to 1.503 eV which shifts to higher energies with increasing temperature. These structures did not show up at lower implant doses and do not correlate with any previous transitions attributed to the Mg impurities. It appears that these new transitions may be defect related structures that result from the high implant dose and low implant energy.

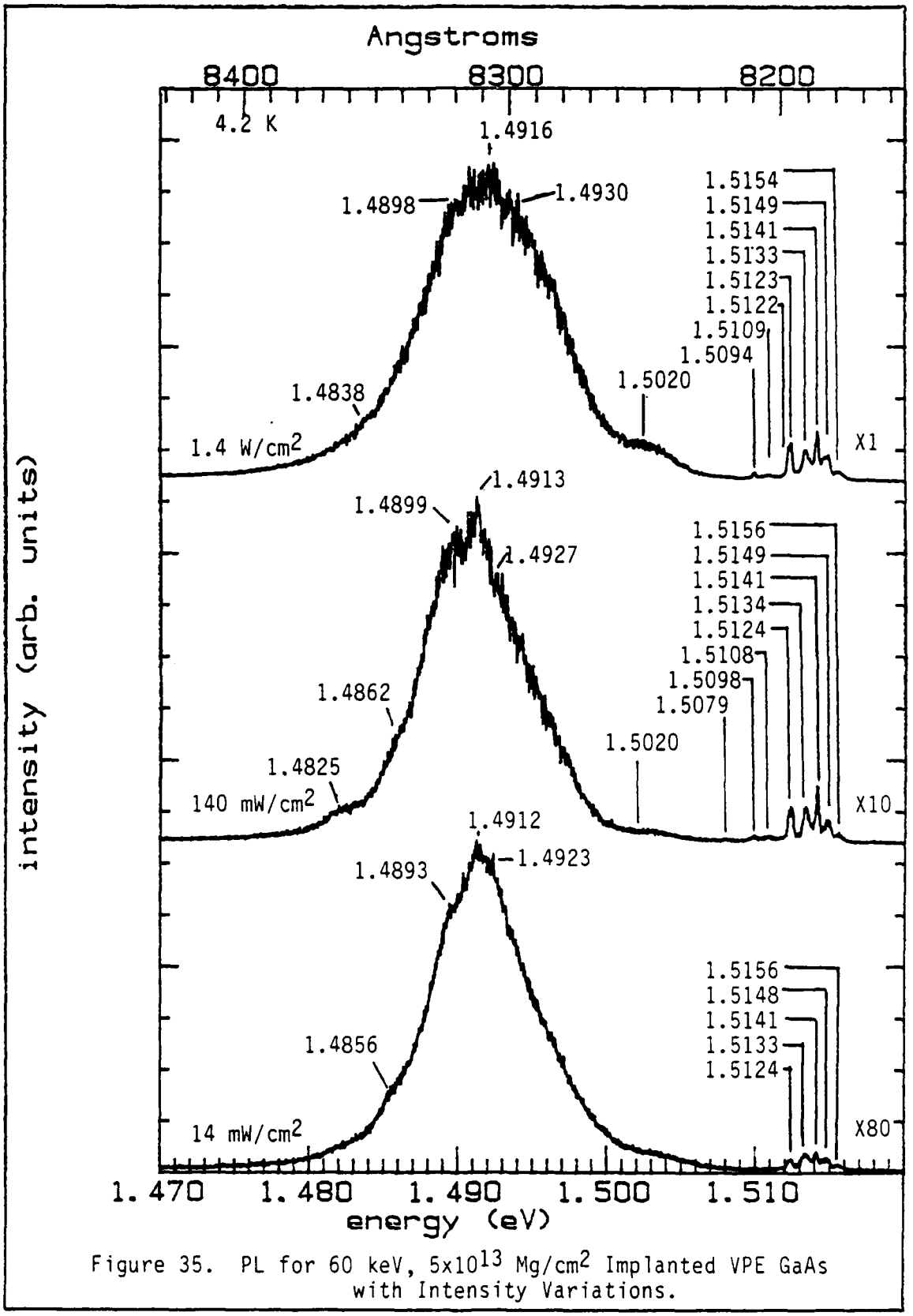

Figure 35. PL for 60 keV, 5×10^{13} Mg/cm^2 Implanted VPE GaAs with Intensity Variations.

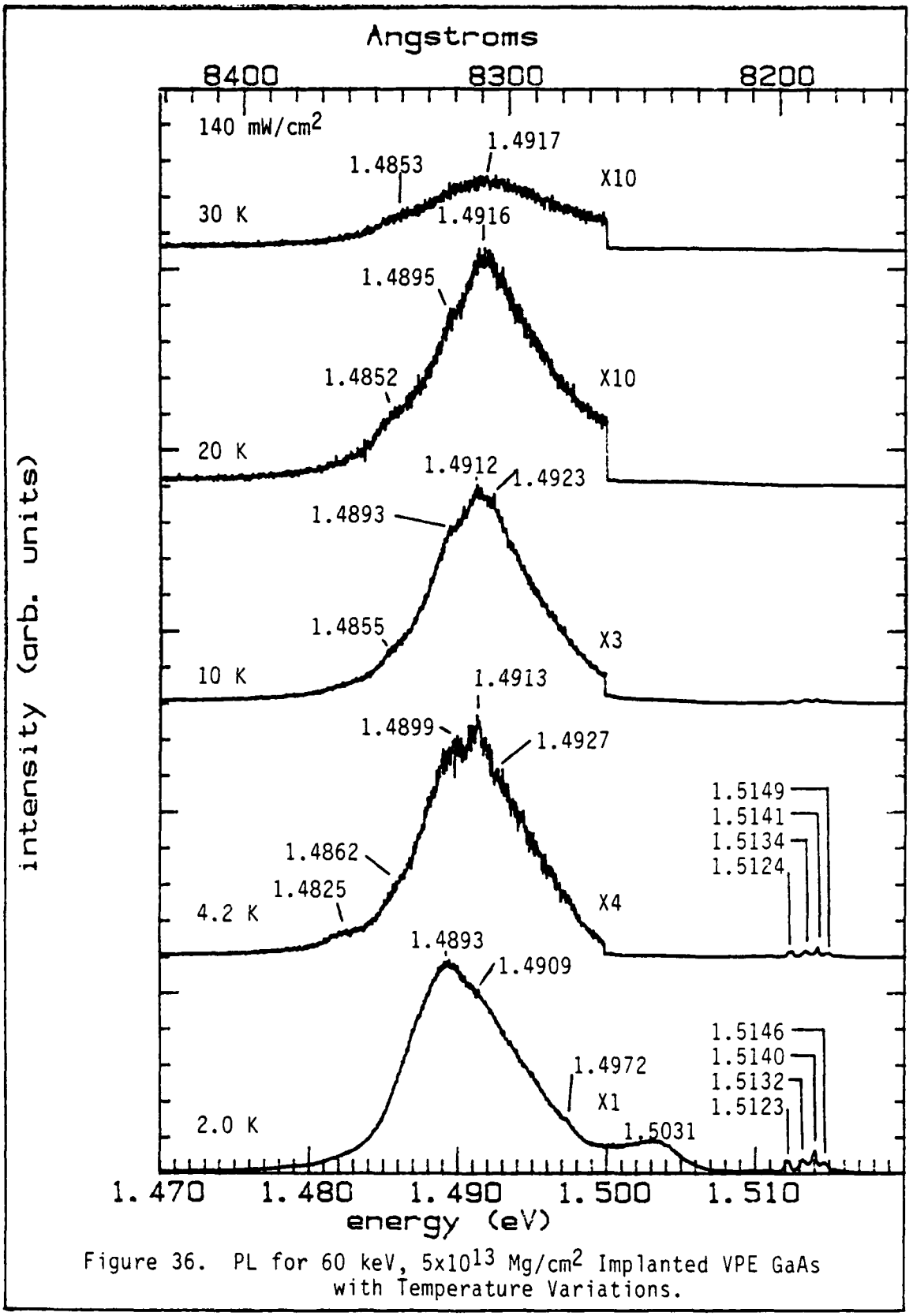

Figure 36. PL for 60 keV, $5x10^{13}$ Mg/cm^2 Implanted VPE GaAs with Temperature Variations.

The broad peak in the region of 1.49 eV may be considered as a conglomeration of several FB and DAP transitions. Visible in all the spectra is the Mg FB transition near 1.4913 eV which dominates the structures. A peak at 1.4899 eV is observed, which appears to be the Zn FB. The Mg FB peak near 1.4912 eV appears in the 14 mW/cm^2 spectrum. The 14 mW/cm^2 spectrum contains the most detail of all the spectra collected for this sample. Visible at 1.4856 to 1.4862 eV is a shoulder which consists of the Si FB and the Zn DAP. The presence of Si is confirmed by the appearance of the Si DAP peak at 1.4825 to 1.4838 eV. A very weak peak at 1.4930 eV is probably the C FB transition. Carbon has been present in trace amounts in the unimplanted samples, but has not been readily observable in the implanted samples.

In general, the quality of the spectra from the $5X10^{13}$ cm^{-2} implant has been heavily degraded compared to the lower implant doses, and the ability to resolve the individual impurity transitions has been greatly impaired by peak broadening. The growth of what may be defect related structures is apparent on the high energy side of the FB transitions. Despite the implantation of a considerable amount of Mg in the sample, the Zn impurity still appears to dominate the spectra.

The broadening of the luminescence features visible in the PL is also visible in the SPL, as shown in Figure 37.

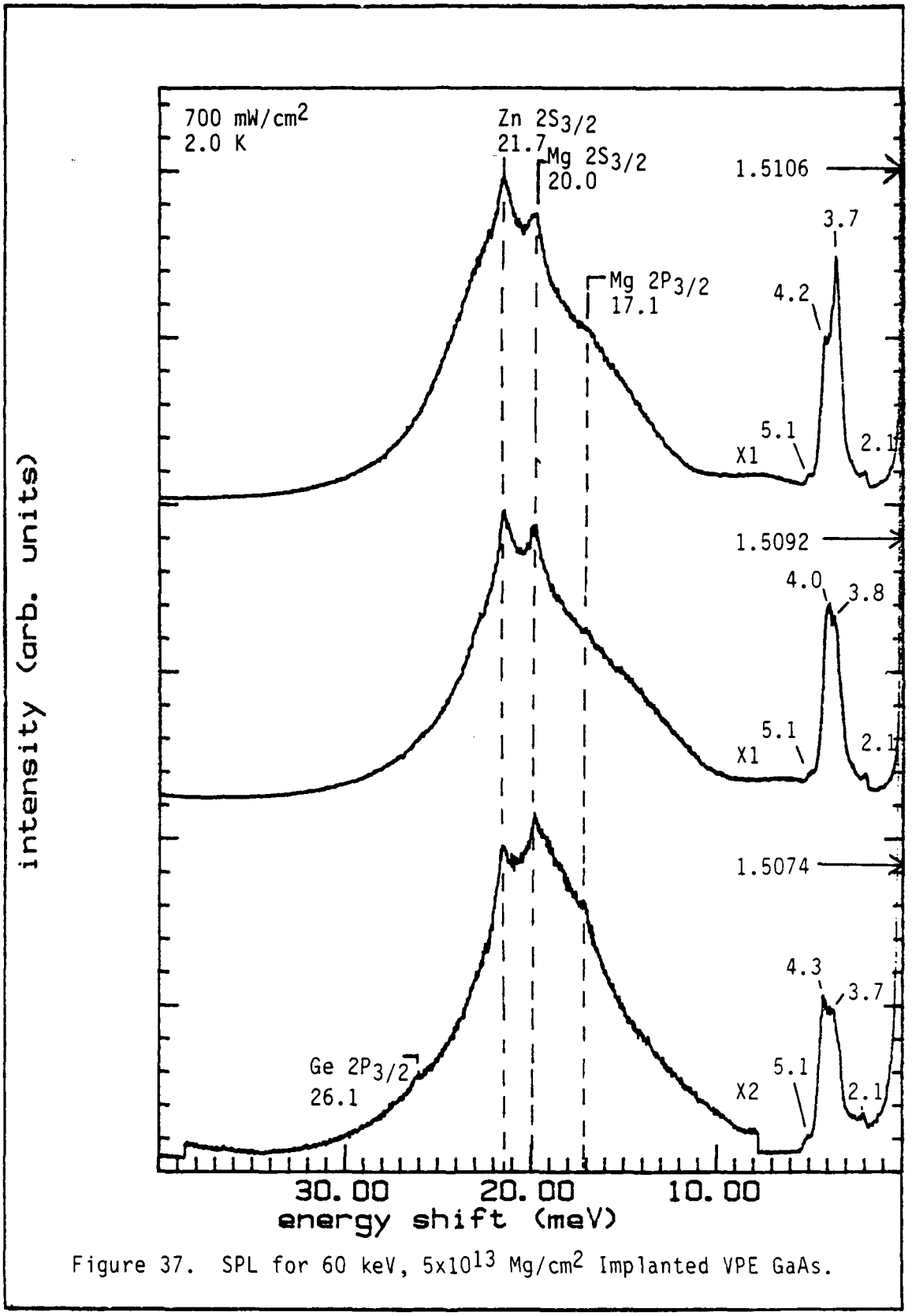

Figure 37. SPL for 60 keV, 5×10^{13} Mg/cm^2 Implanted VPE GaAs.

Four distinct SPL transitions are visible in the spectra. The $2P_{3/2}$ and $2S_{3/2}$ peaks at the 17.1 and 20.0 meV transitions for Mg, respectively, are observed in all three spectra. The $2S_{3/2}$ transition for Zn is also observed in the SPL spectra. In the spectra at 1.5074 eV pump energy, an additional peak was observed at 26.1 meV (1.4813 eV absolute) from the pump energy. The possible source of this peak could be either the $2P_{3/2}$ state of Ge or the $3S_{3/2}$ state of Zn. However, the peak occurred at 1.4813 eV, and appears on the low energy side of the Zn DAP peak where DAP recombination rates are relatively low, thus decreasing the probability that the peak is the Zn $3S_{3/2}$ transition. Therefore, this peak is most likely the Ge $2P_{3/2}$ transition.

A set of peaks with magnitude equivalent to the SPL structure is observed close to the pump energies. The peaks at 2.1, 3.7, 4.2, and 5.1 meV associated with the pump energy shift, change relative intensity when compared to each other. These peaks appear in regions where defect structures were observed in the PL. The peaks could result from the selective pumping of excited states associated with the [g-g] band. However, it should be noted that the expected values for the first two excited donor states are 4.4 and 5.2 meV, which fall very close to two of the four peaks observed.

90 keV Mg Ion Implanted Samples

The 90 keV ion implanted samples were produced under identical conditions characteristic of those associated with the previous samples. The only change in these samples is the higher implant energy. Growth and annealing conditions for the samples are the same as for the other samples.

1X10^{12} Implant. Photoluminescence from the 1x10^{12} Mg/cm^2, 90 keV sample is shown in Figures 38 and 39. The usual exciton lines are observed between 1.512 and 1.516 eV. A considerable amount of structure is visible in the exciton region for a temperature of 4.2 K or less. The exciton structure is dominated by the 1.5142 eV neutral donor bound exciton. The other two major exciton peaks are the 1.5135 eV ionized donor bound exciton and/or the donor free to bound transition and the 1.5125 eV neutral acceptor bound exciton doublet. Three additional peaks were observed at a slightly lower energy compared to the exciton band, 1.5108, 1.5100, and 1.5082 eV. The 1.5108 eV transition was previously reported in Reference 38 and attributed to the two electron transition for a free exciton near a neutral donor. The 1.5100 eV is a sharp peak much like the exciton transitions in appearance. The 1.5100 eV peak closely matches the previous observations for the two electron transition for the n=2 neutral donor bound exciton transition. The 1.5082 eV peak is barely resolvable as a

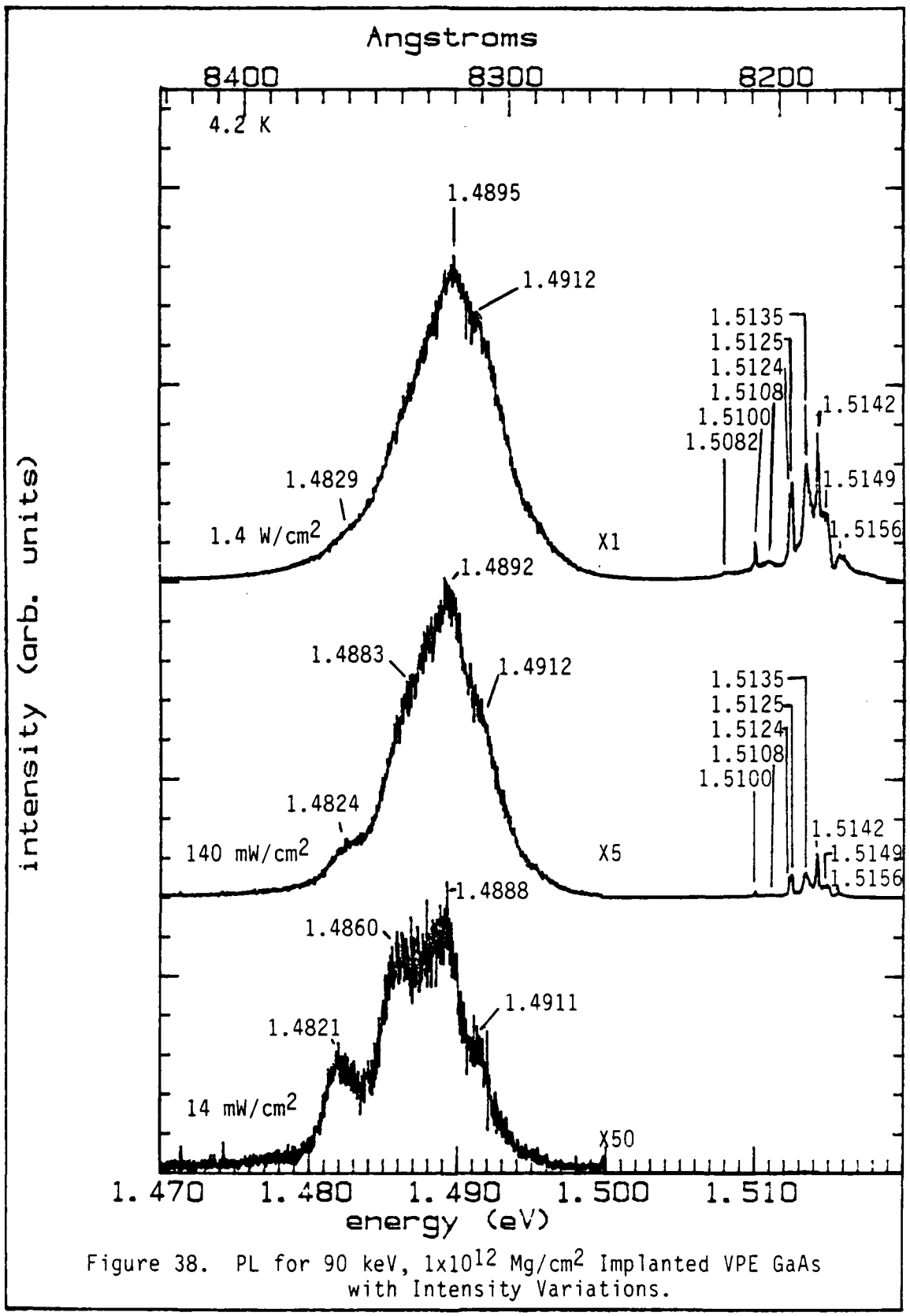

Figure 38. PL for 90 keV, $1x10^{12}$ Mg/cm^2 Implanted VPE GaAs with Intensity Variations.

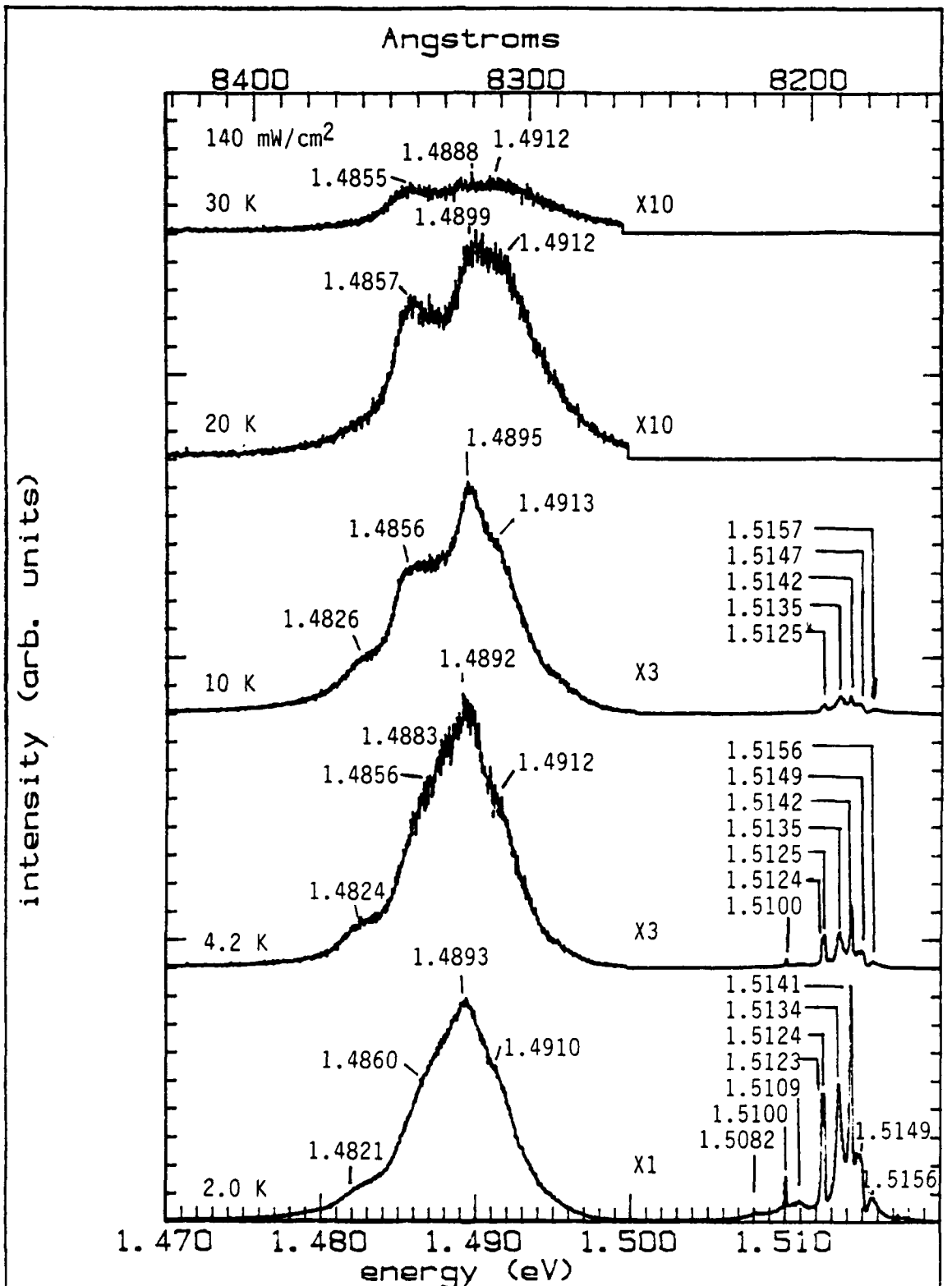

Figure 39. PL for 90 keV, $1x10^{12}$ Mg/cm^2 Implanted VPE GaAs with Temperature Variations.

peak. Reference 5 noted a transition at 1.5089 eV which they attributed to the n=3, two electron transition of the neutral donor bound exciton.

Figure 38 shows a broadening of the spectrum in the 1.48 to 1.50 eV region at higher intensities so that it becomes a broad featureless peak. The results of the lowest intensity (14 mW/cm^2) reveal the most detail of all the spectra. Four distinct peaks are visible at 1.4911, 1.4888, 1.4860, and 1.4821 eV. The 1.4911 eV peak is the Mg FB peak, while the 1.4888 eV peak appears to be a superposition of the Mg DAP and the Zn FB transitions. The temperature dependent data reveal that the 1.4860 eV peak moves slightly to lower energy with increasing temperature, which is not the usual behavior for FB and DAP transitions. This can be explained if the 1.4860 eV peak is a superposition of the Zn DAP and Si FB peaks. The shift to lower energy is then explained by the faster decline in the Zn DAP intensity as temperature increases. The interpretation that the 1.4860 eV peak is at least partially attributed to Si is also supported by the existence of the 1.4821 eV peak, which exhibits characteristics of a DAP peak, and matches the Si DAP transition.

The SPL spectra from the 90 keV, 10^{12} Mg/cm^2 implanted sample shown in (Figure 40) exhibits a number of lines already observed in the other samples. As with the 60 keV, the spectra for the 10^{12} Mg/cm^2 implanted sample does not

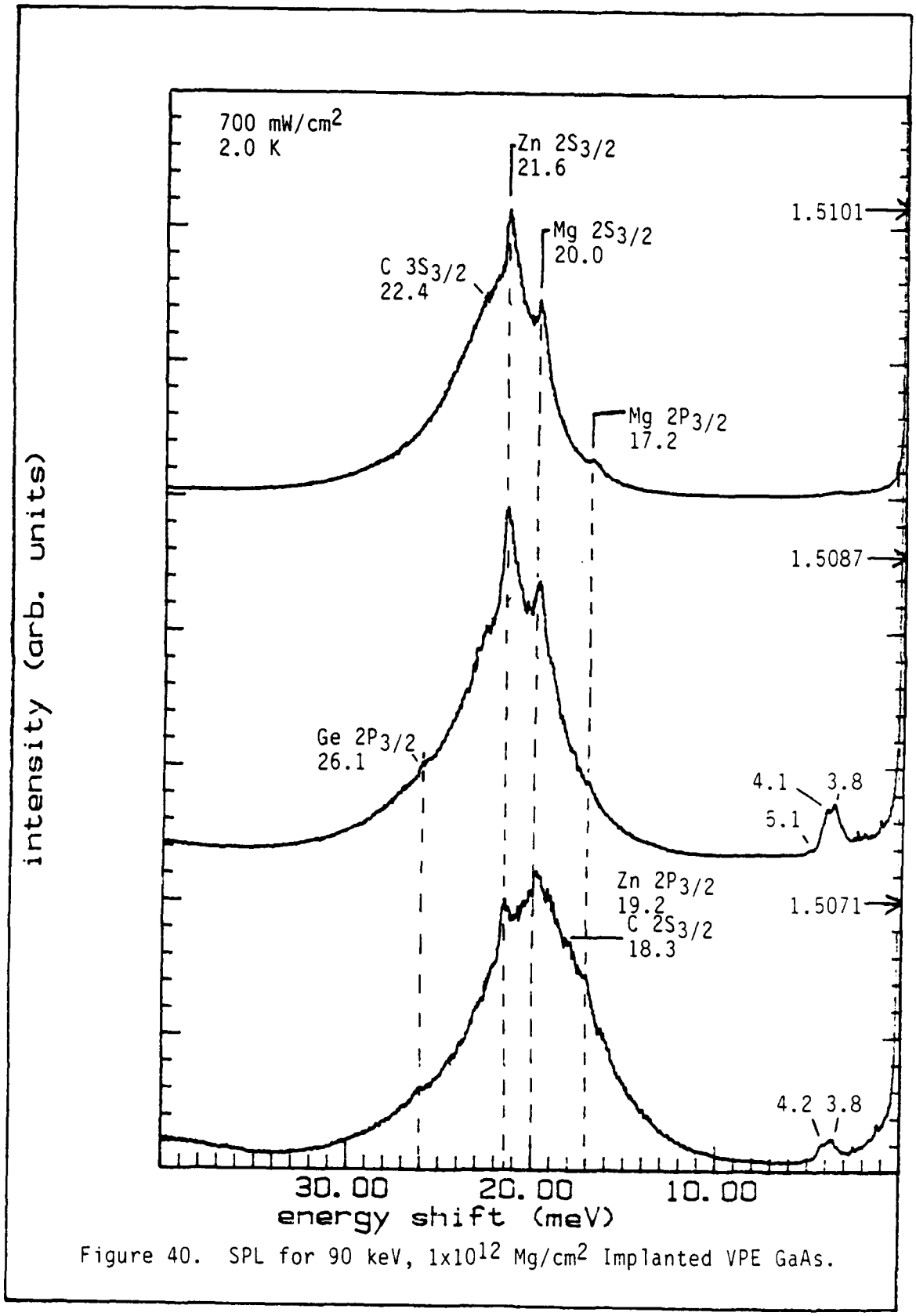

Figure 40. SPL for 90 keV, $1x10^{12}$ Mg/cm^2 Implanted VPE GaAs.

significantly deviate from those associated with the unimplanted samples. Line widths are very similar for a given excitation energy, and relative peak intensities are nearly the same. Two peaks at 17.2 and 20.0 meV match the peaks observed in the other samples, and they were attributed to the $2P_{3/2}$ and the $2S_{3/2}$ states of Mg. Peaks at 19.2 and 21.6 meV match the $2P_{3/2}$ and $2S_{3/2}$ transitions for Zn, respectively. In addition, two other peaks were observed at 18.3 meV and 26.1 meV. The peak at 18.3 meV is probably the $2S_{3/2}$ transition for C. The peak at 26.1 meV is on the low energy side of the overall DAP band, and it is probably the $2P_{3/2}$ Ge transition. It should be noted that there is no clear transition that can be associated with Si SPL, even though the existence of Si is indicated in the PL. This may be a result of the Si spectra being lost in the tail of the Zn DAP background or a restriction of the Si material to a thin layer near the surface of the sample. Also, three structures at 3.8, 4.2, and 5.1 meV were observed in this sample. The maximum of these peaks is near 1.505 eV. If these transitions are related to SPL from an unknown acceptor it would indicate that the DAP band for the transition is centered around 1.505 eV. Assuming a 5.8 meV donor binding energy, and a mean pair separation of 420 Å, the unknown acceptor binding energy would be approximately about 11.3 meV. Another possibility is that these peaks represent SPL transitions for donor excited states.

5X10^{12} Implant. The PL structure for the 5X10^{12} Mg/cm^2 implant is shown in Figures 41 and 42. Strong exciton luminescence is observed with the standard exciton features as in previous samples. In addition, a peak at 1.5107 is observed. This peak could possibly be the g-transition that has been previously reported (58:4694). Another peak at 1.5053 eV is clearly seen in the spectra at temperatures of 4.2 K or lower, and is very intense at an excitation intensity of 1.4 W/cm^2. This transition is fairly broad and bears some resemblance to the merged FB/DAP bands which appear at lower energies. The 1.5053 eV peak is located in a region of the spectra for which the v-transition was reported in reference 58. However, the 1.5053 eV transition lacks the sharp structure observed for the v-transition, but instead exhibits a shoulder near 1.504 eV.

The spectra for this sample reveals that the Mg implant is the dominant feature in the FB/DAP region of the spectrum under all conditions. At the low intensity excitation of 14 mW/cm^2, the Mg FB transition is visible at 1.4914 eV. The peak at 1.4892 eV is the superposition of the Zn FB and the Mg DAP. The shoulder at 1.4860 eV appears to be the Zn DAP. No strong evidence of Si transitions is present in this sample, although in some of the spectra a slight shoulder at 1.4819 eV hints at the presence of Si.

The SPL spectra shown in Fig. 43 has relatively few transitions. The two peaks at 17.0 and 20.0 meV closely

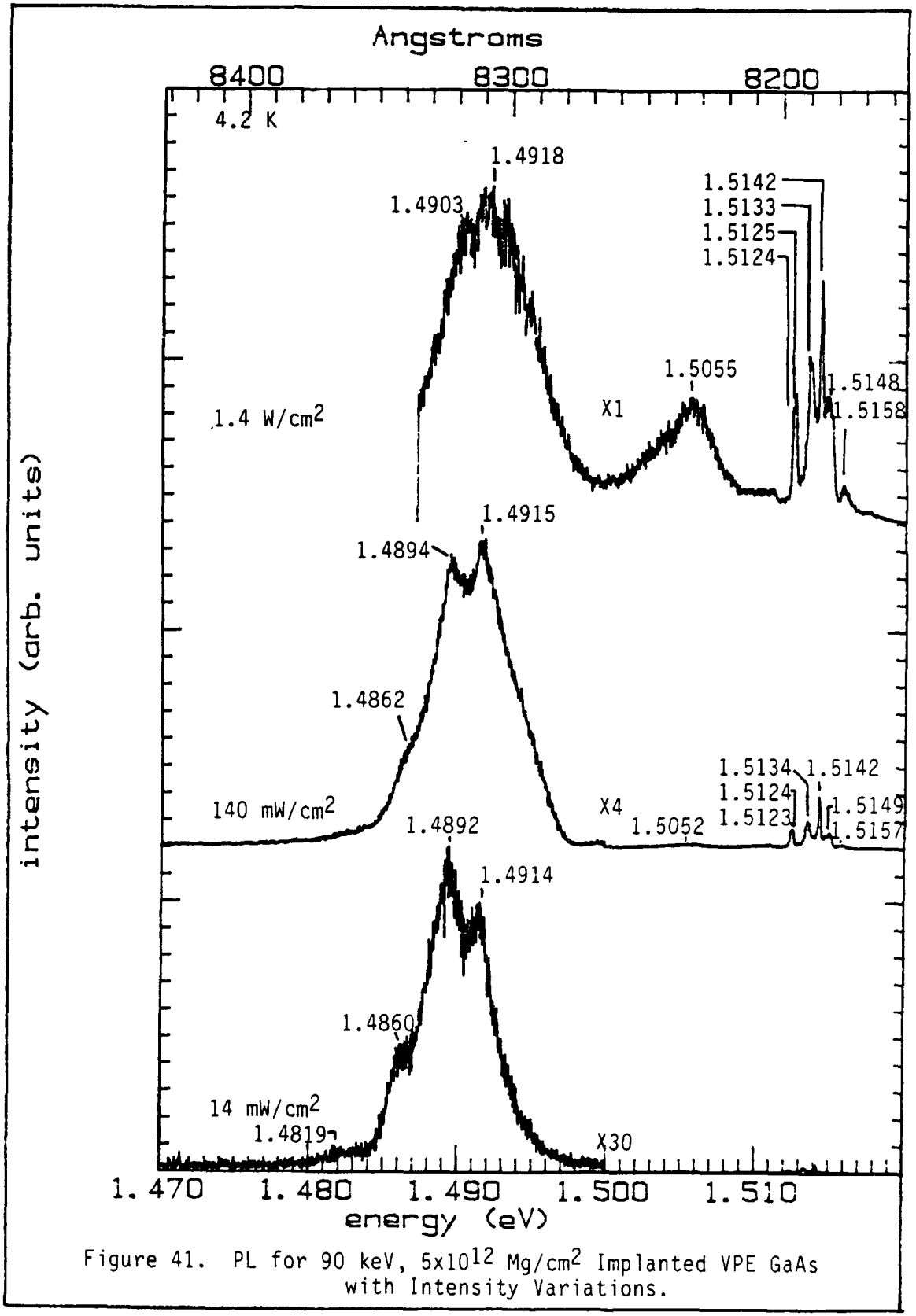

Figure 41. PL for 90 keV, 5×10^{12} Mg/cm^2 Implanted VPE GaAs with Intensity Variations.

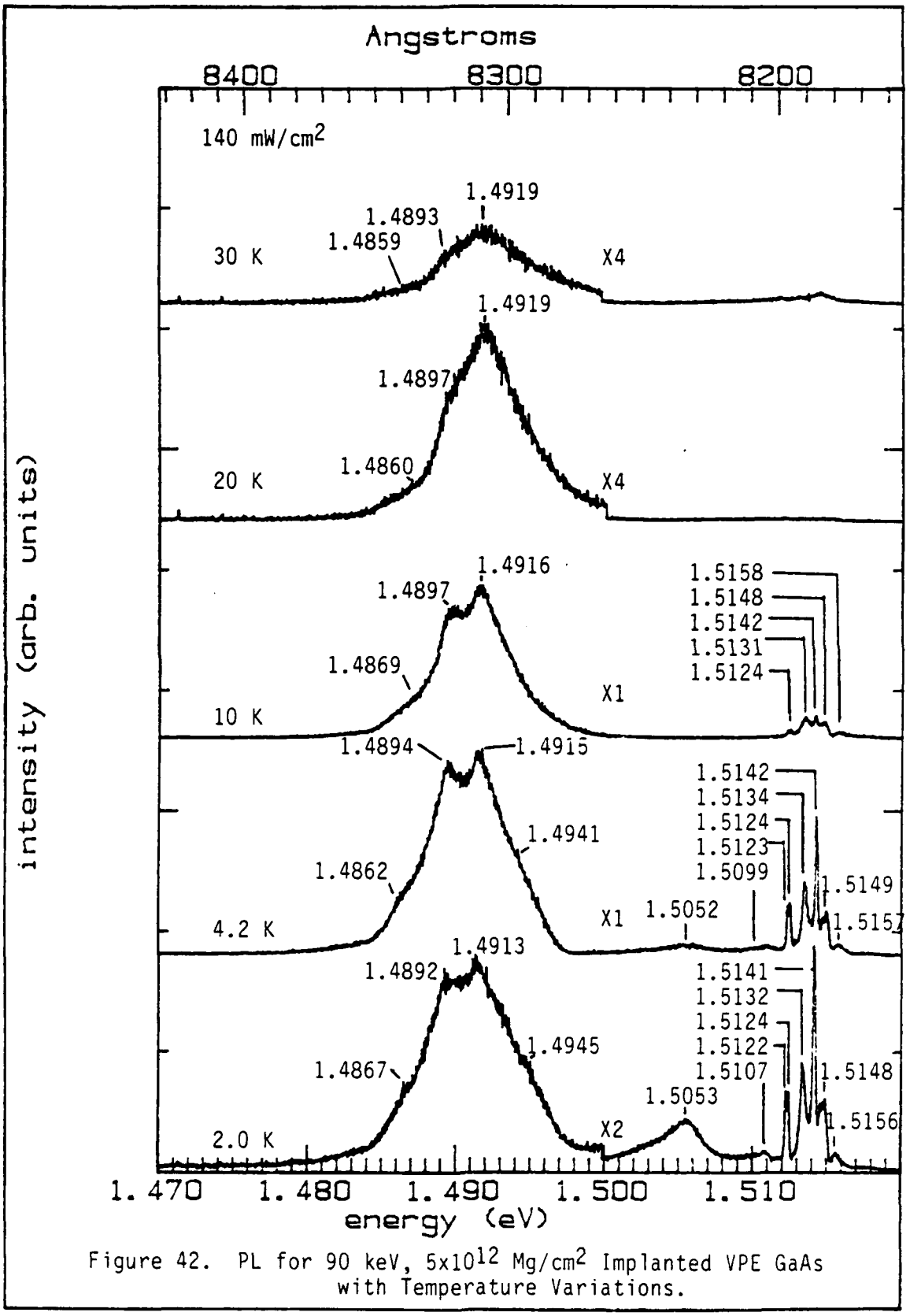

Figure 42. PL for 90 keV, 5×10^{12} Mg/cm^2 Implanted VPE GaAs with Temperature Variations.

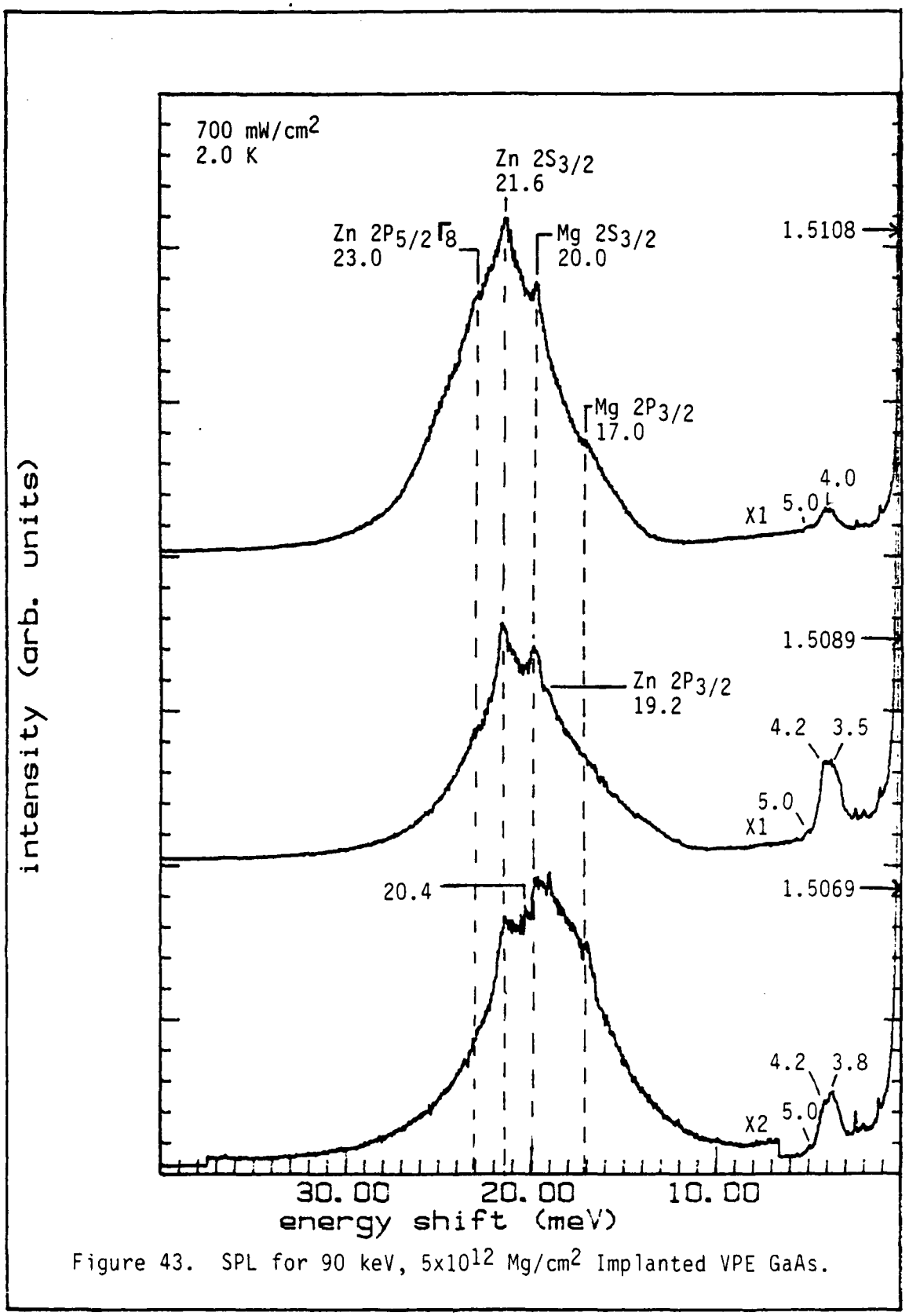

Figure 43. SPL for 90 keV, 5×10^{12} Mg/cm^2 Implanted VPE GaAs.

match the peaks associated with the $2P_{3/2}$ and $2S_{3/2}$ transitions for Mg, respectively. The Zn $2P_{3/2}$, $2S_{3/2}$, and $2P_{5/2}(\Gamma_8)$ transitions were observed at 19.2, 21.6, and 23.0 meV, respectively. The three transitions at 3.8, 4.2, and 5.0 meV are quite strong in the SPL spectra. It appears that these transitions are associated with the defect related emission bands observed by other studies. However, the exact relationship is not clear.

1X10^{13} Implant. The PL spectra for the 10^{13} cm^{-2} implanted sample are shown in Figures 44 and 45. At 2.0 K, the exciton transitions are quite strong, and the major exciton lines are easily resolvable. The defect related structure between 1.504 and 1.5110 eV now becomes a major feature of the spectra with magnitude almost equal to the luminescence from the FB/DAP transitions. The FB/DAP structure degenerates to a featureless peak as the temperature or pump intensity increases. The strong Mg FB is visible at 1.4913 eV, while the Zn structure is a barely resolvable shoulder in all but the 14 mW/cm^2 spectrum. The most detailed structures for the FB/DAP transitions are visible in the 14 mW/cm^2 spectrum. In this spectrum, the Zn FB is visible at 1.4883 eV, followed by the Mg DAP transition as a shoulder at 1.4870 eV. A shoulder around 1.4850 eV is probably due to both the Zn DAP and the Si FB. A peak at 1.4819 eV disappears above 20 K and is probably the Si DAP.

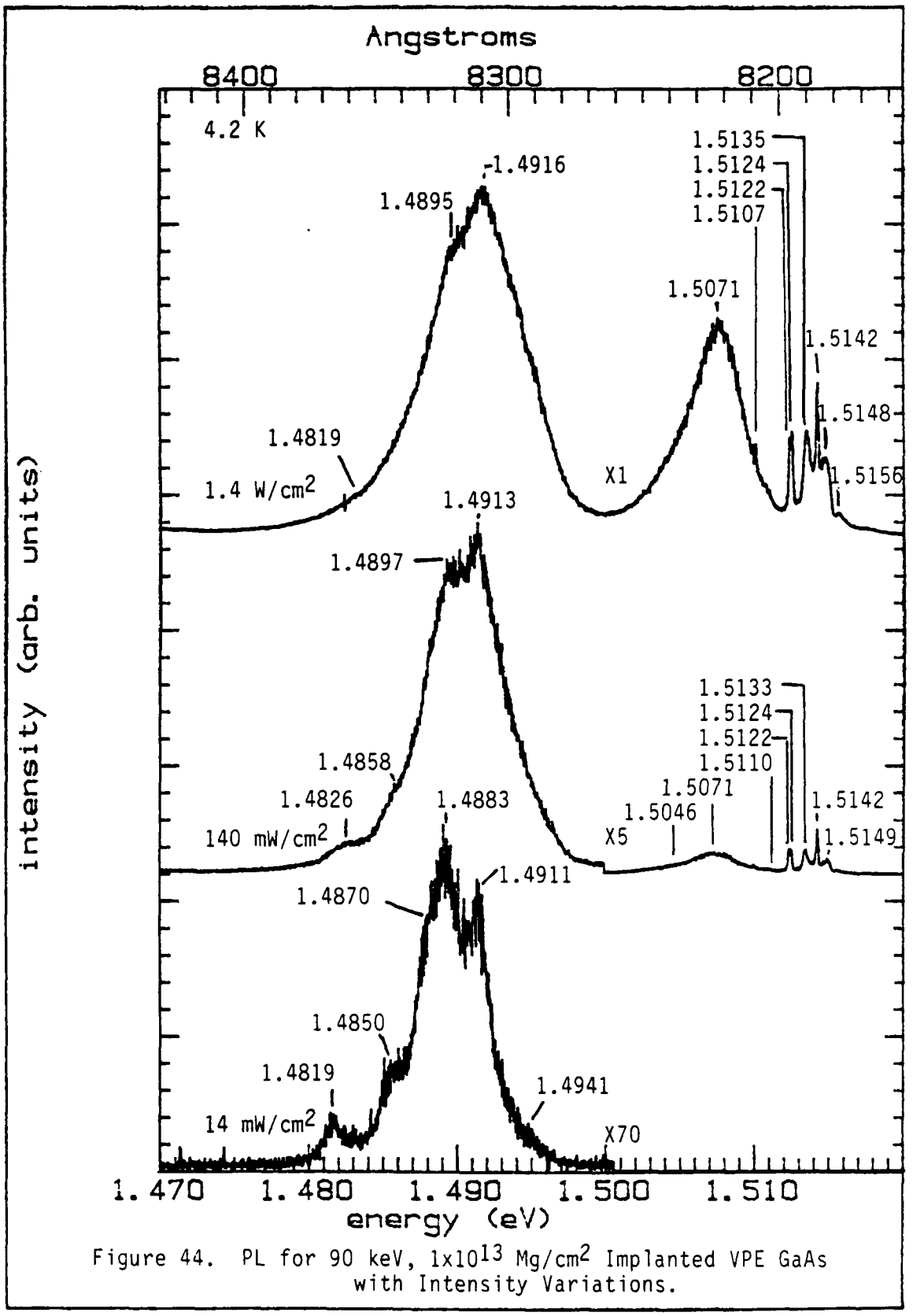

Figure 44. PL for 90 keV, $1x10^{13}$ Mg/cm^2 Implanted VPE GaAs with Intensity Variations.

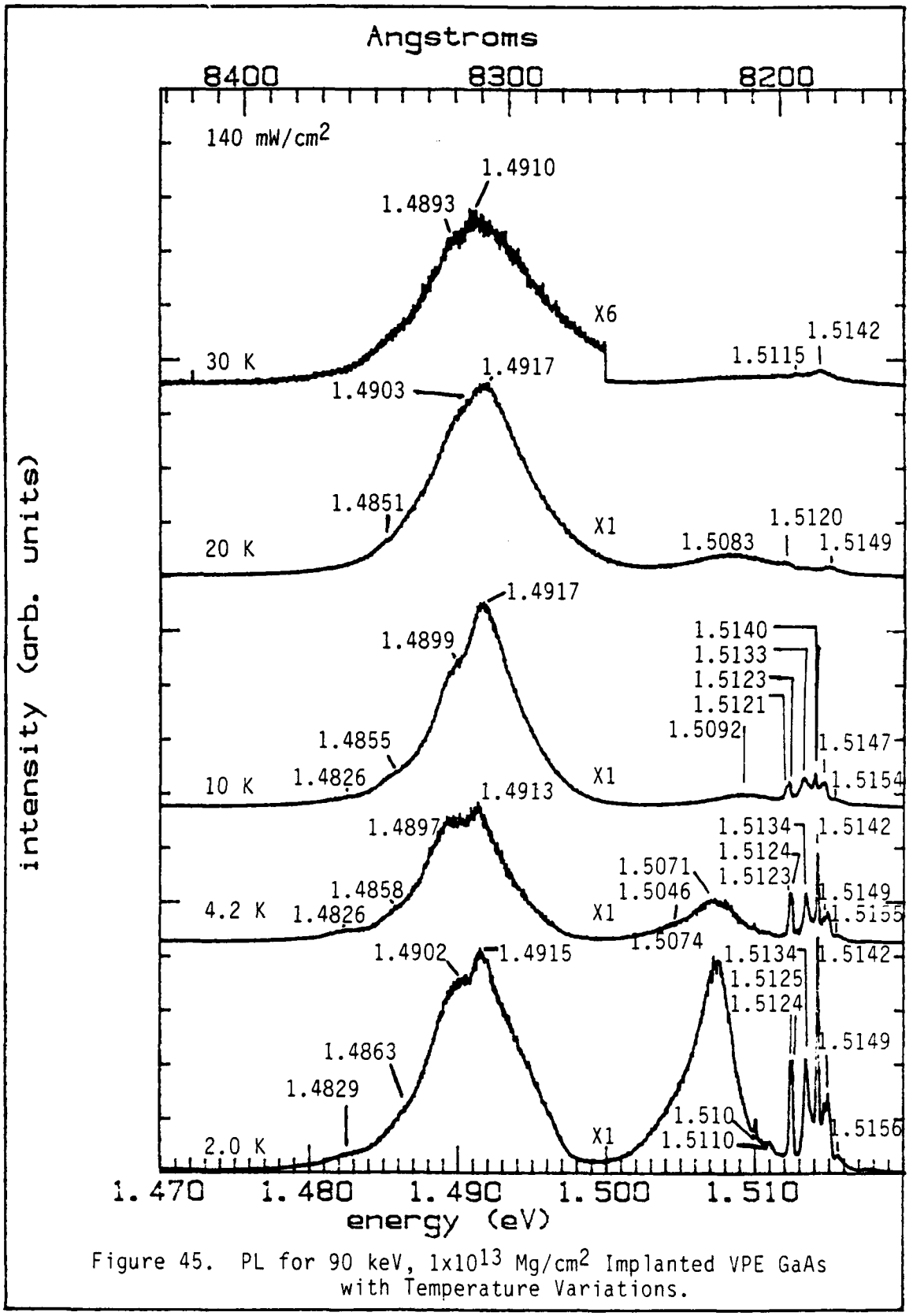

Figure 45. PL for 90 keV, $1x10^{13}$ Mg/cm^2 Implanted VPE GaAs with Temperature Variations.

The SPL spectra in Fig. 46 is very similar to those observed in the previous sample, with some exceptions. The $2P_{3/2}$, $2S_{3/2}$, and $2P_{5/2}(\Gamma_8)$ transitions of the Mg are seen at 17.2, 19.9, and 21.1 meV, respectively. Transitions seen at 19.2 and 21.7 meV correspond to the $2P_{3/2}$ and $2S_{3/2}$ Zn states, respectively. An interesting feature is the 1.5074 eV peak visible in the SPL. This peak is the same one that is visible in the PL. There are no SPL transitions superimposed on it. However, its appearance is very similar to other spectra that were collected in which the pump energy was very close if not in the DAP band. When the pump energy drops below the formation energies for the first acceptor excited state of the DAP, all that appears in the spectrum is the DAP ground state energy. When the pump energy enters the high energy side of the DAP band, what appears is a truncated version of the DAP band, minus the part higher in energy than the pump.

<u>$5X10^{13}$ Implant.</u> The PL from this sample is shown in Figures 47 and 48. The most obvious feature in this sample is the exciton band which is strong and well resolved. Barely visible next to the exciton structure are two peaks at 1.5112 and 1.5100 eV. The 1.5112 eV transition appears to be the g transition, while the 1.5100 eV transition is the n=2 two electron transition for the neutral donor bound exciton. The major change in the PL spectra, compared to the previous samples, is a distinct decrease in the

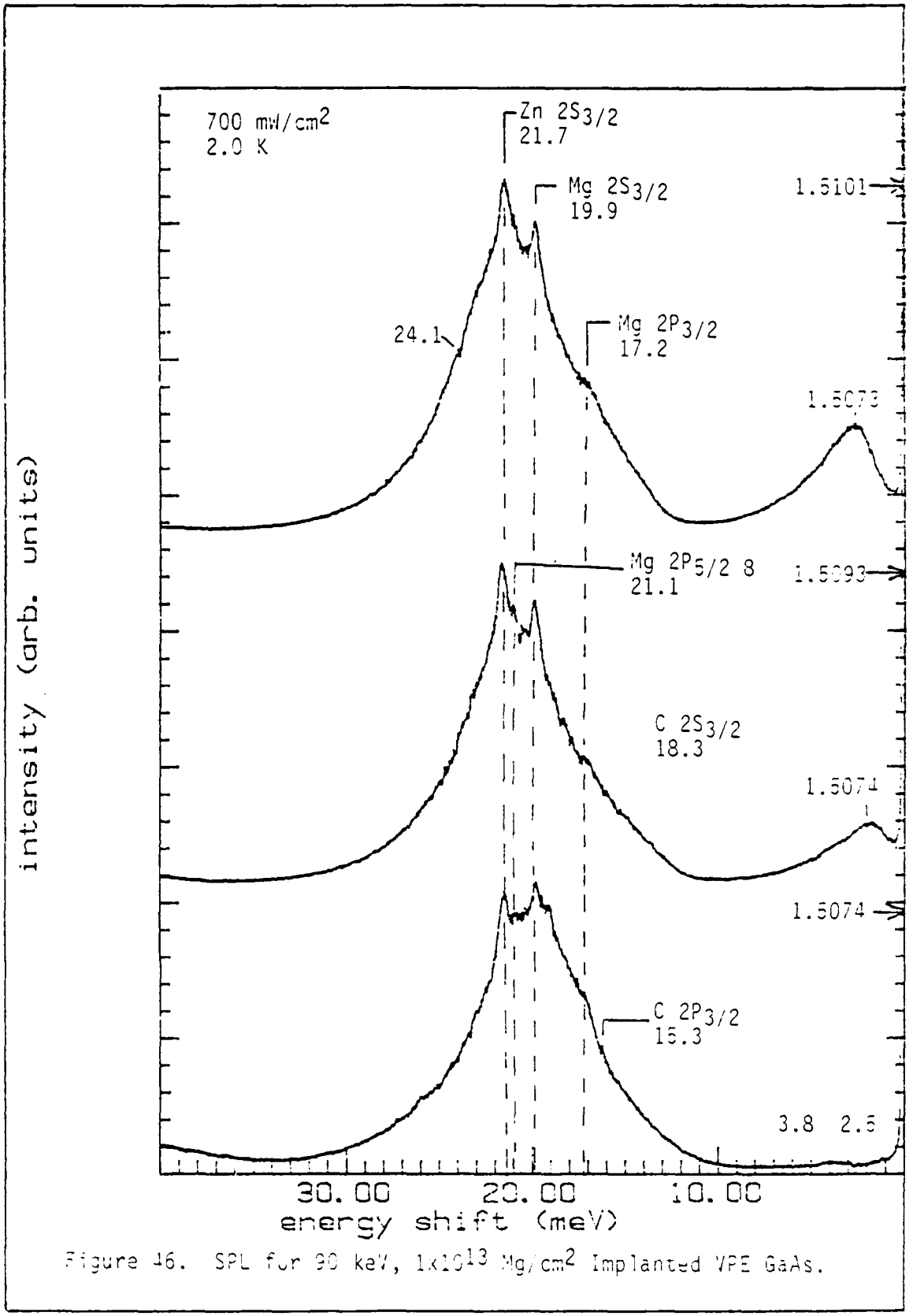

Figure 46. SPL for 90 keV, $1x10^{13}$ Mg/cm^2 Implanted VPE GaAs.

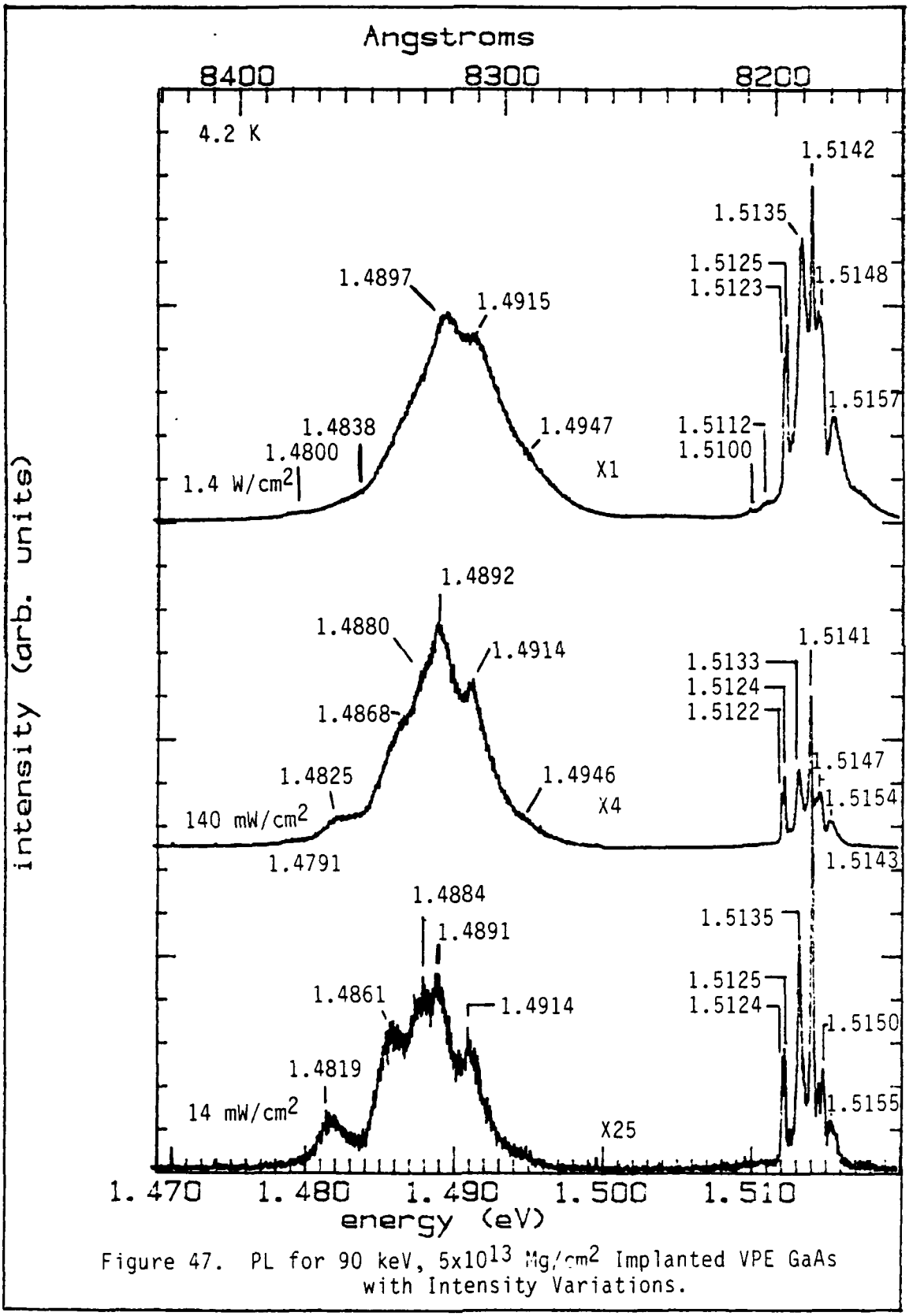

Figure 47. PL for 90 keV, 5×10^{13} Mg/cm^2 Implanted VPE GaAs with Intensity Variations.

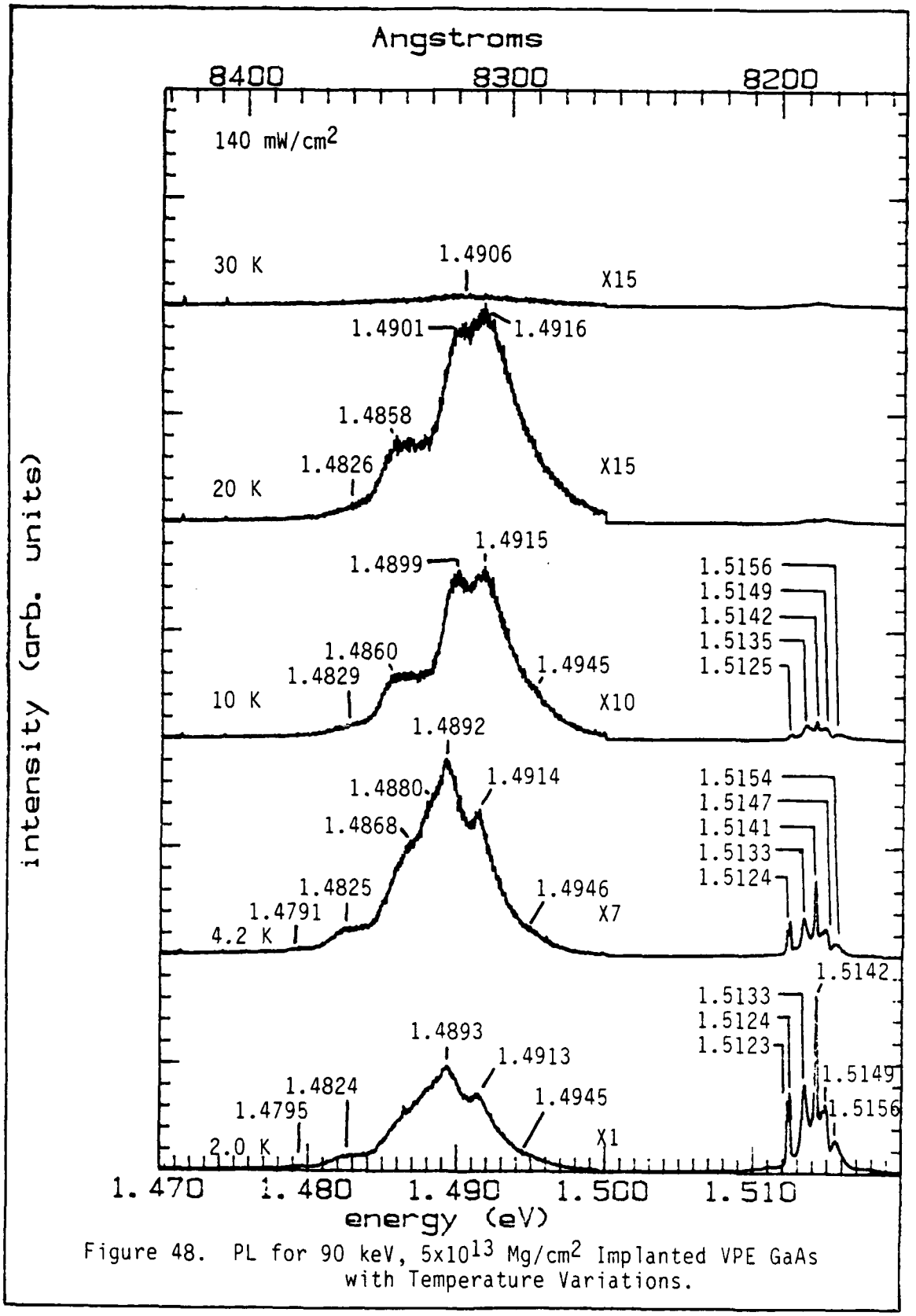

Figure 48. PL for 90 keV, 5×10^{13} Mg/cm^2 Implanted VPE GaAs with Temperature Variations.

intensity of the FB/DAP spectra by almost an order of magnitude. The spectra are well resolved, particularly the 14 mW/cm^2 spectrum. The Mg FB is visible at 1.4914 eV. In addition, the Mg DAP transition is resolvable at 1.4884 eV, which is now separate from the Zn FB transition at 1.4891 eV. The 1.4861 eV transition appears to be the Si FB and the Zn DAP transitions, but they are not separately resolvable. The transition at 1.4819 eV appears to be a DAP transition based on the temperature dependent data, probably the Si DAP. At temperatures of 4.2 K or less and under higher excitation intensities, the peak at 1.4893 eV dominates the spectra, and the Zn FB and Mg DAP transitions are no longer separately observable. Without the 14 mW/cm^2 spectra, the heavy overlap of these peaks can yield a misleading conclusion because it makes the Zn appear to be the dominant impurity in the sample.

The SPL spectra are shown in Figure 49. The Mg $2P_{3/2}$ and $2S_{3/2}$ transitions are visible at 17.1 and 19.9 eV, respectively. The observable Zn transitions are the $2P_{3/2}$ transition at 19.1 meV and the $2S_{3/2}$ transition at 21.6 meV. The transitions at 3.8 and 4.1 meV are once again weakly visible in this sample. However, no structures were observed in the PL below 1.511 eV, as were observed in other samples, and thus, the source of these transitions is uncertain.

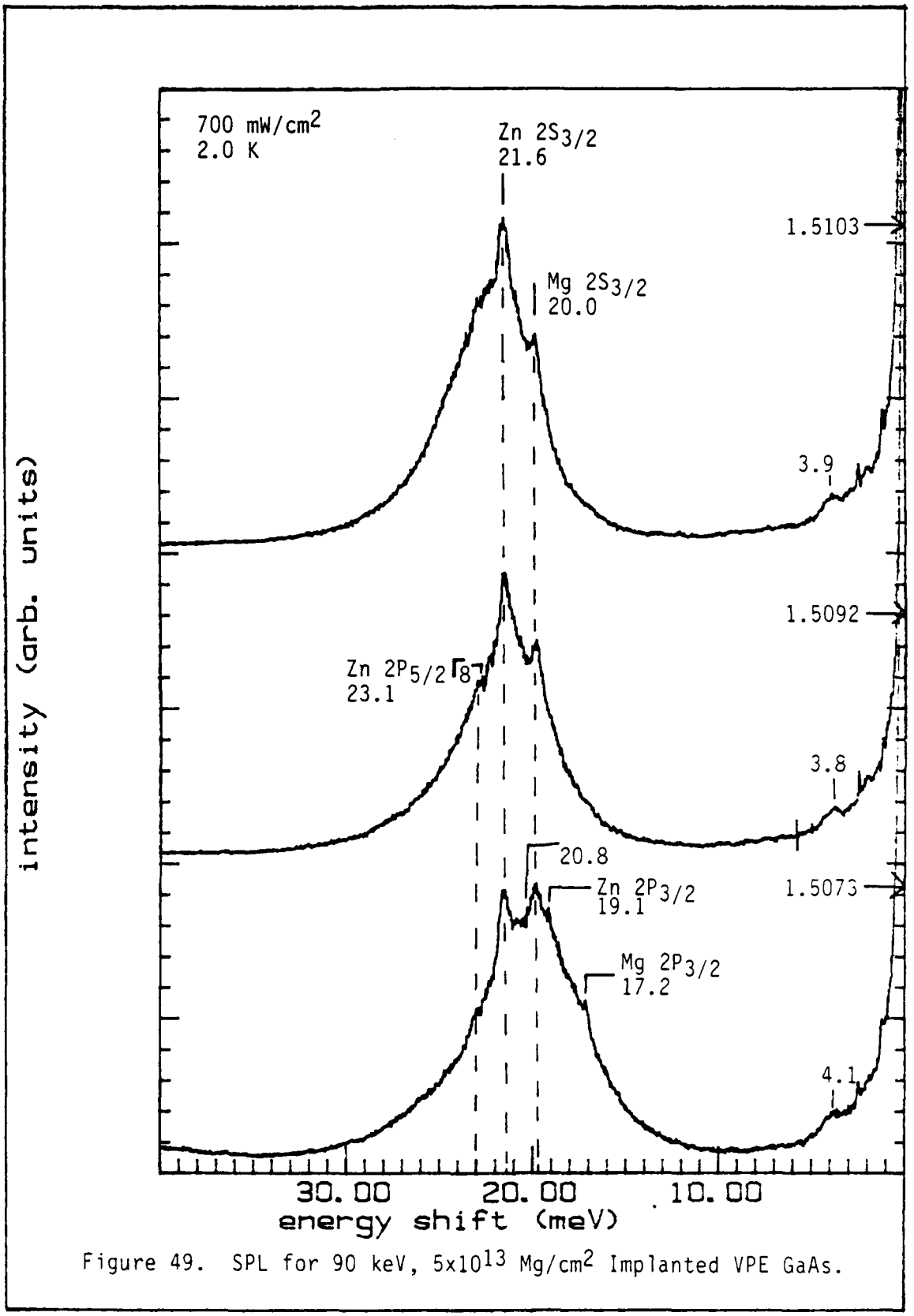

Figure 49. SPL for 90 keV, 5×10^{13} Mg/cm^2 Implanted VPE GaAs.

120 keV Ion Implants

For the 120 keV ion implant energy, only two samples implanted with doses of 10^{13} and 10^{14} Mg/cm^2 were investigated. Furthermore, the PL measurements were not made, and only the SPL analysis was performed.

1X10^{13} Implant. The SPL spectra for the 10^{13} cm^{-2} implant is shown in Figure 50. Five distinct peaks exhibiting SPL like behavior were observed from this sample. Two peaks, at 17.3 and 20.0 meV, from the pump energy appear to be the $2P_{3/2}$ and $2S_{3/2}$ transitions for Mg, respectively, and these values are well within the error limits of the measurement. The transitions at 21.6 meV closely matches the previously observed transition for the $2S_{3/2}$ transition for a Zn acceptor. The fifth peak at 26.0 meV is more difficult to identify. Two possible SPL sources exist for this peak, the Zn $3S_{3/2}$ transition or the Ge $2P_{3/2}$ transition. However, this peak appears at an absolute energy of 1.4813 eV, which is well below the minimum allowed energy of the Zn DAP. Therefore, the Zn $3S_{3/2}$ transition cannot be the source of this emission, leaving only the Ge $2p_{3/2}$ transition as a possible candidate.

Another spectral feature visible in two of the three SPL spectra is a peak at 1.5080 eV. The 1.5080 eV peak does not shift with the pumping energy, and as the laser is tuned through that peak, the component higher in energy than the

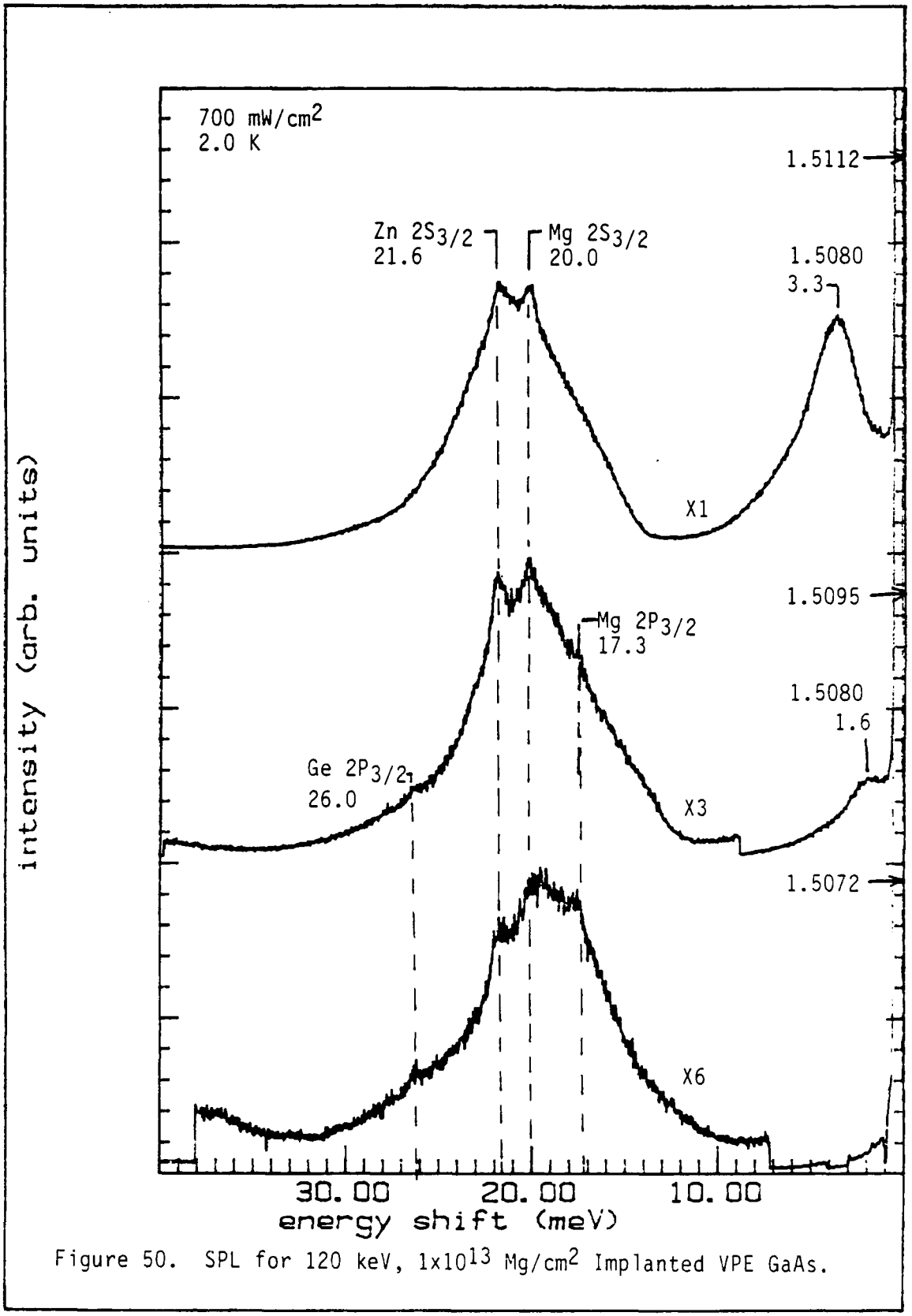

Figure 50. SPL for 120 keV, $1x10^{13}$ Mg/cm^2 Implanted VPE GaAs.

laser energy disappears. This is indicative of the peak being composed of a number of discrete transitions which are independent of each other. This peak behaves similar to the DAP bands when the laser energy coincides with part of the band. Thus, the 1.5080 eV peak is most probably a pair related structure which is associated with an unknown state in the material.

1X10^{14} Implant. The 10^{14} cm^{-2} SPL spectra is shown in Figure 51. Six distinct SPL peaks are visible in this sample. The first three peaks at 17.1, 20.0, and 21.2 meV are consistent with the previously measured energies for the Mg $2P_{3/2}$, $2S_{3/2}$, and $2P_{5/2}$ (Γ_8) transitions, respectively. The next two peaks at 19.1 and 21.6 meV match the observed transitions for the $2P_{3/2}$ and the $2S_{3/2}$ states of Zn, respectively. In addition, one other distinct transitions is visible at 26.1 meV. The 26.1 meV peak could be the $2P_{3/2}$ transition for Ge as discussed previously.

Comparisons and Evaluation

Photoluminescence. Several trends were noted from examination of the photoluminescence structure of the Mg implanted GaAs.

It appears that the annealing process introduces the Si impurity in the probed layer of these samples. The Si DAP band in the annealed substrate has an intensity of nearly

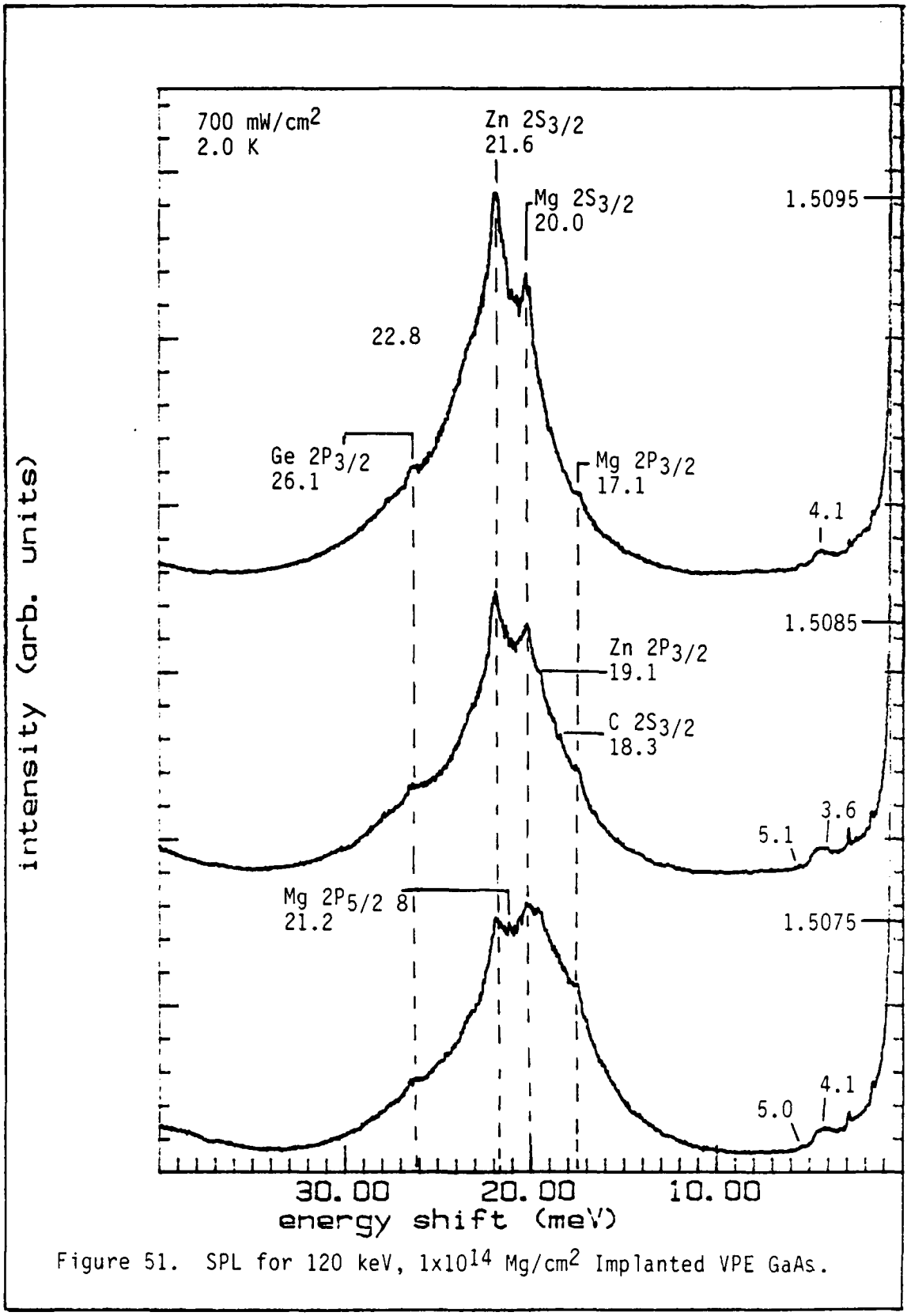

Figure 51. SPL for 120 keV, $1x10^{14}$ Mg/cm^2 Implanted VPE GaAs.

the same order of magnitude as the Zn impurity in the sample. This characteristic is consistent with the previous observations of capped and annealed samples. How much of the Si comes from the Cr-doped semi-insulating substrate, which usually contain Si, and how much Si diffuses from the Si_3N_4 cap is unknown.

No PL signal from the Mg acceptor has been observed in either the virgin VPE samples or the nonimplanted (but annealed) VPE samples. Also, PL from Mg was not detected in the samples implanted with 10^{12} Mg/cm^2. This characteristic is likely due to the very low Mg concentration. However, a clear PL signal began to appear at a dose of $5x10^{12}$ Mg/cm^2. Generally; however, the PL intensity for Mg increased with increasing ion dose. Unfortunately, further increases in the implantation dose have the effect of broadening the whole FB/DAP structure. The 60 keV, $5x10^{12}$ Mg/cm^2 implanted sample has a sufficiently large impurity concentration as well as unannealed damage to cause substantial impurity broadening. As a result, there is a complete lack of detail in the FB/DAP portion of the spectra for large implant doses. Examination of all the implanted samples reveals that, despite implant fluences as large as $5x10^{13}$ cm^{-2}, luminescent intensity of the Mg related structures appears not to exceed that of the Zn related structures. This characteristic is mainly due to the heavy overlap between the Zn FB and the Mg DAP bands. The overlap of these two

peaks causes the Zn FB to appear to grow in relation to the implant such that the Zn FB peak always appears larger than the Mg FB.

The PL results for the Mg implant, in general, suggest that the intensity of the optical luminescence from the sample does not accurately reflect the relative concentration of Mg relative to the other acceptors present in the material.

Another observation exists in the $5x10^{12}$ and $1x10^{13}$ cm^{-2} samples at both 60 and 90 keV implant energies. These samples show a strong peak in the vicinity of 1.5080 eV. A number of studies have been performed concerning the emissions between 1.5110 and 1.5040 eV (1,16,59). These studies were primarily accomplished considering a series of sharp emissions in the region where the 1.508 eV transition occurs, and not on a broad peak similar to the one seen in the implanted VPE samples. However, an observation was reported on what was termed the [g-g] transition exhibited in high purity samples implanted with C, Mg, Zn, and Cd (42). Reference 42 reported that the [g-g] transitions increased in intensity with implantation dose until a certain concentration was reached, and then it began to decline and eventually disappeared at higher concentrations. The optimum concentration for Zn was at $3x10^{17}$ cm^{-3}. The source of the [g-g] transition was hypothesized to be the formation of acceptor-acceptor pairs characterized by

overlapping of the excited states of the holes (42:2504). The [g-g] line matches the current observations of the 1.508 eV peak in the implanted VPE samples. The acceptor-acceptor pair theory would also explain the similarity in behavior between the 1.508 eV structure and DAP bands when environmental and pumping parameters were varied.

Selective Pair Luminescence. The analysis of the SPL from the virgin and implanted samples yields several important pieces of information. First, the presence of Mg was detected in the undoped virgin and annealed substrates by the SPL measurements, although its presence in the unimplanted samples was not indicated in the PL measurements. The presences of Mg was definitely confirmed in the SPL spectra by the presence of the 20.0 meV transition between the $2S_{3/2}$ and the $1S_{3/2}$ Mg acceptor states, which has been reported in the spectroscopy of the two- hole satellites. The presence of Mg raises questions as to why it appears in the SPL but not in the PL. Why is Mg present at all in the virgin VPE sample?

The quality of the substrate is demonstrated by the presence of the two electron structures just below the exciton region which have previously been associated with high purity materials containing $N_a+N_d < 10^{14}$ cm^{-3} (38:12.5). Other high purity GaAs samples grown by MBE using arsine as an As source (60:240) showed that Mg or Be were the dominant residual impurity in samples with a carrier concentration of

or less. A similar analogy may be drawn with respect to the high purity VPE samples used in this study. Mg may be a residual impurity in very small amounts in most GaAs samples, but it is masked by C and Zn impurities which are present in higher concentrations in most samples. The PL of the Mg would not be apparent until the Mg impurity level is comparable to C and Zn impurity levels. Reference 60 also indicated an uncertainty in the degree of incorporation and electrical activation of Mg in GaAs (60:241). This may explain the failure of the PL to show any indication of Mg in the virgin samples.

The presence of Mg as a background contaminant in the virgin material somewhat complicates the analysis of the effect on the SPL by the Mg ion implantation. Because of the nature of selective pair luminescence, it is very difficult to quantify how much residual or implanted Mg contributes to the SPL signal. In spite of this, the SPL spectra generally show slight increases in the relative intensities of the Mg peaks with increasing implantation dose for a given pump wavelength (Figures 52 and 53). The Mg implant is distributed within a relatively small region near the surface of the crystal. Thus, the number of implanted Mg acceptors involved in the SPL may be very limited, resulting in a limited contribution to the SPL intensity from the Mg. On the other hand, the Zn impurities are distributed throughout the epilayer and contribute more

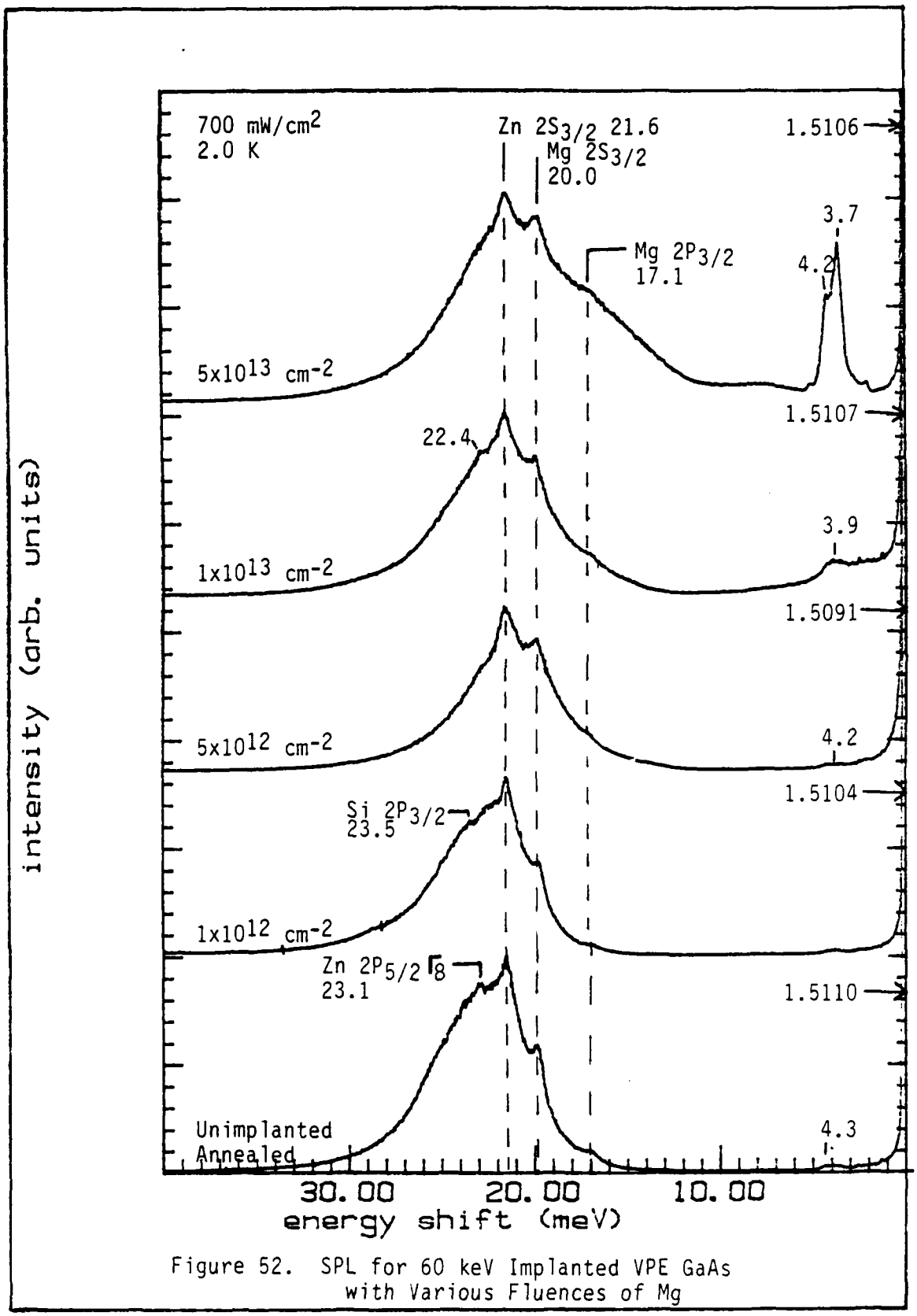

Figure 52. SPL for 60 keV Implanted VPE GaAs with Various Fluences of Mg

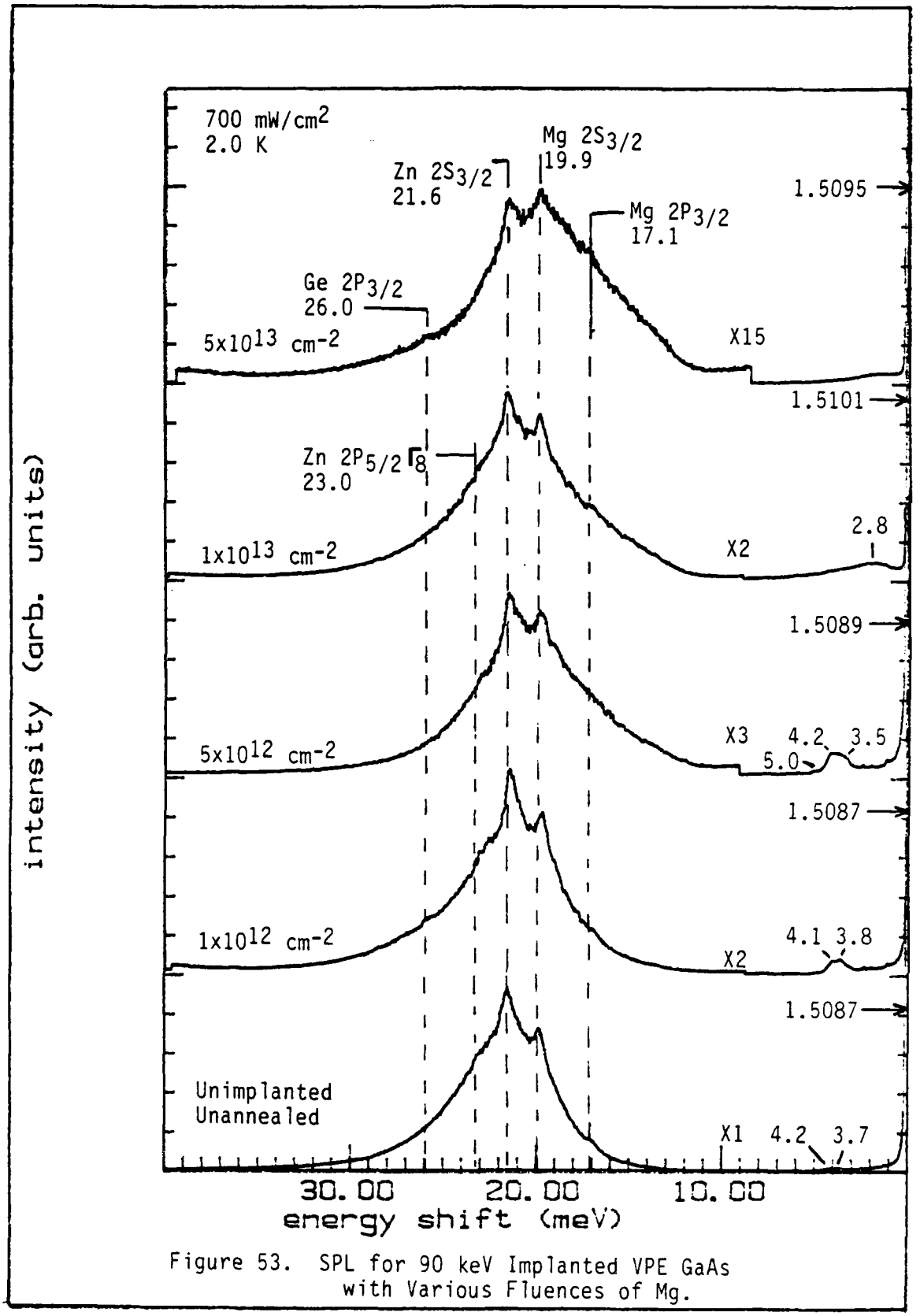

Figure 53. SPL for 90 keV Implanted VPE GaAs with Various Fluences of Mg.

effectively to the SPL intensity compared to the Mg which is abundant only in the thin implanted region. The higher energy implanted samples in Figure 54 also show a slight increase in the Mg SPL, which indicates the Mg acceptors have been distributed deeper into the material, and hence, more implanted Mg is involved in the SPL process. As shown in Figure 52, the $5x10^{13}$ cm^{-2}, 60 keV implanted sample shows a growth of the high energy side of the DAP background peak with indications that some FB structure from the Mg is showing. It appears that at higher implant doses the localized Mg concentration is sufficiently large for the FB transition to reappear in the spectra. Thus, acceptor populations in excess of the donor population in localized regions of the material begin to contribute to the FB transitions.

The real advantage of SPL was revealed in this study because it revealed nearly all the impurities present in the virgin material, even though the PL only showed Zn and a trace of C. The ability to identify traces of minority impurities in a material is the primary advantage of the SPL technique. Furthermore, the SPL technique can provide impurity information even when the FB/DAP PL structure is so intertwined, that information concerning he different impurities is not easily resolvable. The primary disadvantage of SPL, as observed in this study, is the inability to provide a measure of the relative

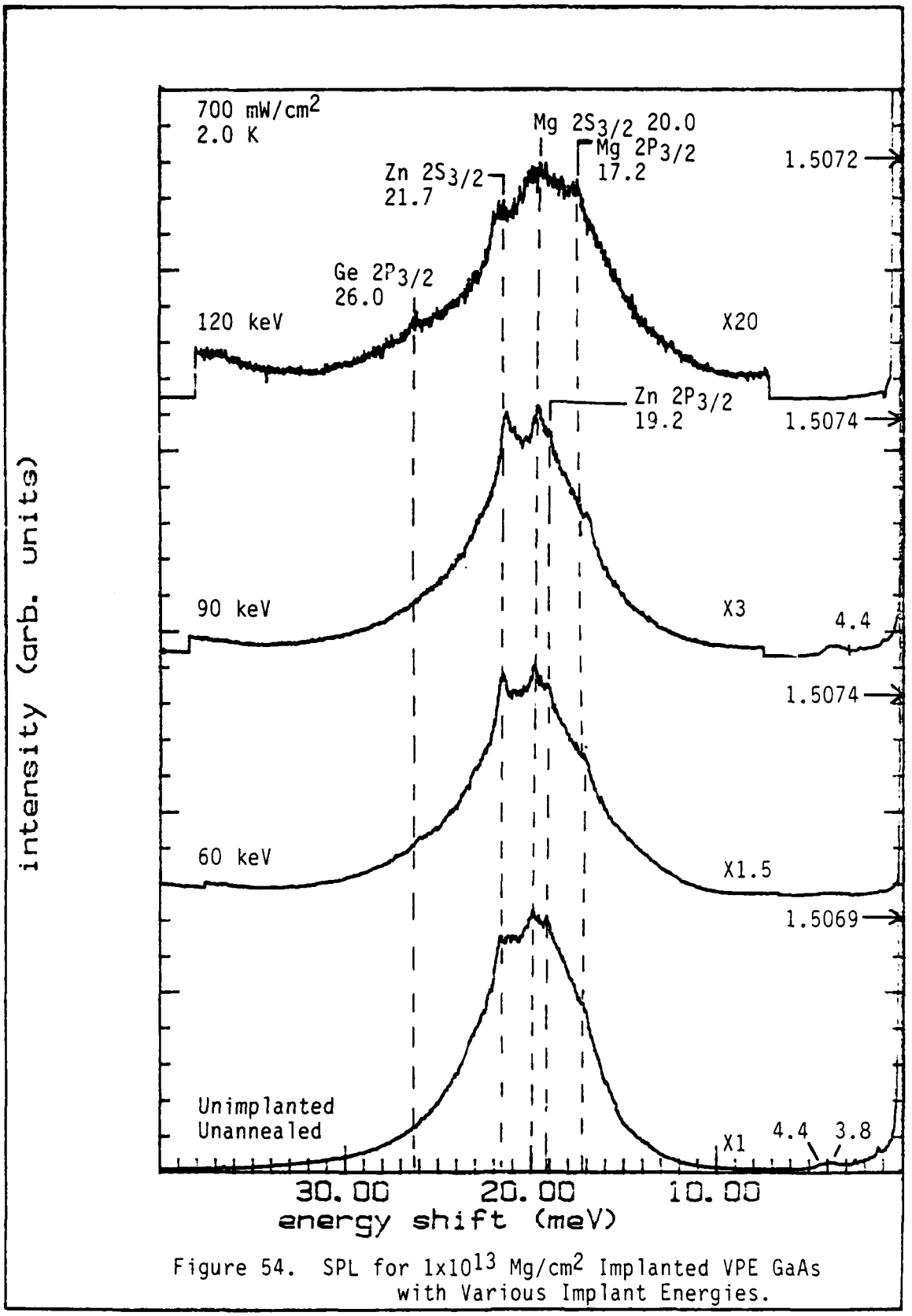

Figure 54. SPL for $1x10^{13}$ Mg/cm^2 Implanted VPE GaAs with Various Implant Energies.

concentrations of the existing impurities. Although, changes in the SPL transitions were observed as a result of ion implantation fluences, another impact from the ion implantation was an alteration in the background luminescence of the SPL signal.

The other very interesting observation in the SPL is the presence of transitions in the region 3.8 to 5.2 meV with respect to the pump energy. These transitions appear to be centered near the 1.5080 eV transition observed in the PL. The exact origin of these lines is unknown, but a number of possibilities exist. The first possibility is that the transitions represent the SPL transitions for donors in GaAs. The observed transitions at 4.2 and 5.2 meV closely match the expected values for the first two excited states of a donor in GaAs at 4.4 and 5.2 meV. Unfortunately, this argument does not explain the third transition at 3.8 meV, although it may be speculated that the 3.8 meV peak may correspond to the first excited state of other donor species. The second possibility is that these transitions are related to the [g-g] structure in some manner. Even so, the exact origin of this transition is not known since the exact nature of the [g-g] transition is not known. However, it can also be speculated that these features may be associated with transitions between various excited states of the acceptors, such as the C $2P_{5/2}(\Gamma_8)$-$2P_{3/2}$ transition (4.2 meV) and the Zn $2P_{5/2}(\Gamma_8)$-$2P_{3/2}$ transition (3.9 meV) with

subsequent recombination. Although this explanation seems unlikely, it does support the acceptor pair nature proposed for the [g-g] transition.

Chapter V

Conclusions and Recommendations

Photoluminescence (PL) and selective pair luminescence (SPL) studies have been accomplished concerning Mg ion-implanted VPE grown GaAs as a function of pump laser intensity, pump laser wavelength, and sample temperature.

The photoluminescence of the virgin VPE GaAs used in this study indicates that the epilayer is of high purity with $(N_A + N_D)$ on the order of 10^{14} cm^{-3}. This epilayer exhibited a high quality exciton spectra with resolution of all the major exciton lines, including two electron satellites of the neutral donor bound exciton. The dominant residual impurity visible in the PL was Zn with only traces of C and Ge. Si was also observed in the samples which had been capped (Si_3N_4) and annealed, which indicated that some thermal diffusion had occurred during the annealing process.

No FB or DAP transitions for Mg were noted in the PL from virgin VPE or nonimplanted annealed samples. The PL from Mg was barely resolvable in the 10^{12} Mg/cm^2 implanted samples. This observation is likely attributable to a relatively low concentration of Mg in the sample. However, a clear PL transition for Mg appeared at doses greater than or equal to $5x10^{12}$ Mg/cm^2. Generally, the PL intensity for Mg increased with increasing ion dose. However, further

increases in the implantation dose has the effect of broadening the entire FB/DAP structure. For example, the 60 keV, $5x10^{13}$ Mg/cm^2 implanted sample produced sufficient impurity concentration and unannealed damage to cause substantial impurity broadening of the PL. As a result, there is a complete lack of detail in the FB/DAP part of the spectra for higher implantation doses.

Through a comprehensive SPL study, the first three excited state of the Mg acceptor were determined by selective pair luminescence. The Mg states are the $2P_{3/2}$, $2S_{3/2}$, and the $2P_{5/2}\Gamma_8$ transitions observed at 17.2, 20.0, and 21.2 meV respectively. These values of 17.2 and 21.2 meV agree very well with the values reported for far-infrared Fourier Transform spectroscopy (32), and the 20.0 meV $2S_{3/2}$ Mg transition agrees very well with previously observed of through two hole spectroscopy (6:1051).

The presence of the Mg residual impurity was detected through SPL in the virgin VPE and nonimplanted annealed VPE samples. The same, but slightly stronger SPL signals from Mg excited states were observed in all the Mg implanted VPE samples. Furthermore, all of the first three excited states of Mg were usually observed in spectra from the Mg implanted samples. However, the effects of adding additional Mg to the epilayer through ion implantation cannot be determined quantitatively from the variations in SPL peak intensities. The addition of more Mg caused changes in the DAP background

that is visible in the SPL spectra. Small but detectable increases in intensities were observed in the Mg SPL transitions relative to other features of the spectra. There is some small increase in the SPL peak intensity from Mg with increasing Mg dose and implantation energy. The limited observability of the implants can be easily explained by the restricted implant region for the Mg, although activation of the Mg implant may also be a factor.

Several possibilities exist for the limited detection of SPL signals in the ion implanted region. The penetration depth of 1.500 eV radiation is less than the thickness of the epilayer of about 3 μm, but larger than 1 μm, while the LSS projected range (R_p) for the Mg implant is only 0.0925 μm. Thus, the implanted region constitutes only about 10% of the total material pumped by the laser. In addition, not all of the Mg in the implanted region is capable of contributing to the SPL, and only appropriately separated donor-Mg acceptor pairs may contribute to the SPL. Also, the total number of donor-acceptor pairs is limited by the donor population in the implanted region, further restricting the amount of selective pair luminescence contributed by the Mg implant.

The temperature variant measurements of the SPL spectra indicates the SPL transitions can be observed at temperatures as high as 20 K. Thus, it appears the temperature restrictions on SPL are not as critical as was

generally anticipated. A considerable amount of information is available even at temperatures up to 10 K, although the most detail is visible at 2.0 K. Essentially, the same restrictions that apply to DAP spectra from PL generally apply to SPL. Increasing temperature causes broadening of the SPL transitions, and as the temperature increases, fewer of the excited states are visible, and at 20 K, only the Zn and Mg $2S_{3/2}$ transitions are visible.

Intensity variations for the SPL measurements revealed the optimum pump intensity depends on the quality of the material. In general, the lowest intensity that yields a good signal to noise ratio is best. High pump intensities saturate the SPL transition, and the leftover photons can cause substantial increases in the DAP background. Under low pump intensities, the SPL transitions deplete the DAP background, yielding the best resolution of the SPL peaks.

The SPL technique has proven to be best suited for an unambiguous acceptor impurity identification of bulk grown, thick epilayer, or properly ion implanted GaAs material. Implanting acceptors deep into a high purity GaAs substrate with higher ion energy may produce an optimum pair population in the implanted region, and thus an optimum SPL peak signal.

The appearance of a strong transition at 1.5080 eV in samples implanted with fluences of $1x10^{13}$ and $5x10^{13}$ cm^{-3} is very interesting. The peak is consistent with previous

observations of the [g-g] transition which has been associated with acceptor-acceptor pairing (42:2503). However, a more detailed study is necessary for this particular peak.

A theoretical computational capability for calculating excited acceptor and donor states in GaAs should be developed for future research in this area. The ability to model the excited states of different impurities in semiconductors as a complement to the experimental work would be a great asset. In addition, the acquisition of software for processing the data in the form of curve fitting, smoothing, and filtering would be useful.

Appendix

Three programs were used during the course of this research. All software was written for Z-100 or IBM PC compatible machines with an RS-232C serial port. The first program in listing 1, Tracomm.bas, captures data from the Tracor Northern mainframe and writes the complete ASCII data file to the disk drives. Tracomm is written in basic.

The second program in Listing 2 is Traconv.pas. Traconv.pas is a data conversion program written in Turbo Pascal. The program reads in the Tracor data file stored on disk and removes all the channel markers from the file. It then writes the file back to the disk as an ASCII file with all extraneous spaces removed. This puts the file into a format that can be utilized in a variety of software analysis packages.

Listing 3 contains program Specplot.pas. Specplot is a program for plotting the reduced data from Traconv on an IBM PC compatible. The program is menu driven and can produce hard copy through a screen dump. In addition, the program has a cursor mode that will allow the examination of the data on a point by point basis.

Listing 1.

```
10 clear
20 dim dat$(1028)
30 f$=chr$(13)+chr$(10)
40 screen 0,0
50 key off:cls:close
60 defint a-z
70 locate 25,1
80 print string$(60," ")
90 xoff$=chr$(19):xon$=chr$(17):eot$=chr$(4)
100 speed$="1200"
110 wor$="7"
120 par$="O"
130 sto$="1"
140 locate 1,1
150 input "what would you like to name the file?
[.dat]",filnam$
160 print "what size file will you be transfering"
164 print "              0.  512 chs."
165 print "              1. 1024 chs."
170 print "              2. 2048 chs."
180 print "              3. 4096 chs."
190 print "              4. 8192 chs."
200 input size%
210 if size%=2 then size%=260
220 if size%=3 then size%=516
230 if sixe%=4 then size%=1028
235 if size%=1 then size%=132
236 if size%=0 then size%=68
240 filnam$="b:"+filnam$+".mca"
250 open filnam$ for output as #5
260 c$=","
270 comfil$="com1:"+spedd$+c$+par$+c$+wor$+c$+sto$
280 open comfil$ as #1
290 cls
300 locate 25,1:print "Tracor Communication Program"
310 locate 1,1
320 open "scrn" for output as #2
330 con%=0
340 for con%=1 to size%
350 input #1,dat$(con%)
360 print dat$(con%)
370 next con%
380 close #1
390 open comfil$ as #1
400 cls:locate 25,10:print "Writing data to disk"
410 locate 1,1:print "Working"
420 for x%=1 to size%
430 print #5, dat$(x%)
440 if x% mod 20 = 0 then print "."
450 next x%
```

```
460 close
470 goto 10
480 end
```

Listing 2.

```
program traconv;{Traconv removes channel markers from  }
      {Tracor data files}
type
  name = string [14];

var
  x : array [1..4096] of real;
  size : integer;
  filename : name;

procedure read_file (filename : name; var size : integer);
{Read in Tracor data file}
var
  datafile : text;
  dummy : string[255];
  i,j : integer;
  temp : real;
  openfile :string[14];

begin
  openfile := 'a:' + filename + '.mca';{get filename}
  assign (datafile,openfile);          {open file}
  reset (datafile);           {go to beginning of file}
  for i := 1 to 4 do readln (datafile,dummy);{First 4 lines}
  size := 0;                                 {throw away}
  j := 0;
  while not eof(datafile) do {read numbers throw away every}
  begin                      {ninth number}
    if j mod 9 <> 0 then
    begin
      size := size + 1;
      read (datafile,x[size]);
      j := j + 1;
    end
    else
    begin
      read (datafile,temp);
      j := j + 1;
    end;
  end;
  close (datafile);
end;

procedure write_file  (filename : name; size : integer);
{write reduce file back to disk}
var
  datafile : text;
  i : integer;
  newfile : string[14];
```

```
begin
  newfile := 'b:' + filename + '.dat';{get new file name}
  assign (datafile,newfile);          {open file}
  rewrite (datafile);                 {initialize file}
  for i := 1 to size do  {write dat in compressed format}
  begin
    if x[i]>=1.0E5 then write (datafile,x[i]:6:0,' ')
      else if x[i]>=1.0E4 then write (datafile,x[i]:5:0,' ')
        else if x[i]>=1.0e3 then write (datafile,x[i]:4:0,'
')
          else if x[i]>=1.0e2 then write
(datafile,x[i]:3:0,' ')
            else if x[i]>=10.0 then write
(datafile,x[i]:2:0,' ')
              else write (datafile, x[i]:1:0,' ');
     if size mod 100 = 0 then write ('.');
   end;
   close (datafile);
 end;

{MAIN}
begin{Main  program}
  writeln ('Place source disk in drive A: ');
  writeln ('Place destination disk in drive B:');
  repeat  {repeat conversion process unitl no filename}
  begin{enetered.}
    writeln;
    write ('enter filename of source file : ');
    readln (filename);
    if filename <> '' then
    begin
      read_file (filename,size);
      write_file (filename,size);
    end;
  end;
  until filename = '';
end.
```

Listing 3.

```
Program plot; {2-D PLOT PROGRAM}

TYPE DATA = ARRAY [1..4097,1..2] OF REAL;
     NUMB = INTEGER;
     ANSWER = CHAR;
     LETTER = STRING[80];
     userspec = string[64];
     registers = record
                   ax,bx,cx,dx,bp,si,di,ds,es,flags:integer;
                 end;
     filename = string[13];
     dtapointer = ^dtarecord;
     dtarecord = record
                   dosreserved : array[1..21] of byte;
                   attribute   : byte;
                   filetime,
                   filedate,
                   sizelow,
                   sizehigh    : integer;
                   foundname   :array [1..13] of char;
                 end;

CONST
  WINXMAX = 631; {HORIZONTAL SCREEN POSITION OF RIGHT HAND
                  SIDE}
  WINXMIN = 104; {HORIZONTAL SCREEN POSITION OF LEFT HAND
                  SIDE}
  WINYMAX = 26;  {VERTICAL SCREEN POSITION FOR TOP}
  WINYMIN = 167; {VERTICAL SCREEN POSITION FOR BOTTOM}
  nul = ^@;        {character 0}
  seekattrib = $10;{files and subdirectories}

VAR TEMP,nfiles
,J,K,L,cal,STEP,XTIC,YTIC,XSUBTK,YSUBTK:INTEGER;
    XMAX,XMIN,YMAX,YMIN,XSCALE,YSCALE,XSTEP,YSTEP:REAL;
    ach,lambda,DXMAX,DXMIN,DYMAX,DYMIN,TIMES:REAL;
    XY:DATA;
    Npoints:NUMB;
    MENU:INTEGER;
    SYMFLAG,GRIDFLAG,LINEFLAG:ANSWER;
    TITLE,XAXIS,YAXIS:LETTER;
    SCRTEXT:ARRAY [1..80,1..25] OF CHAR;
    START,FINISH,FILMIN,FILMAX,conflg:INTEGER;
    NAME : filename;
    transferrec : dtapointer;
    matchptrn   : userspec;
    retname     : filename;
    filsize     : real;
    count       : integer;
```

```
    nofind, lastfile,
    subdirec  : boolean;

PROCEDURE READINT (VAR X:INTEGER); {READS ASCII STRING FROM
                                    KEYBOARD AND}
                                   {CONVERTS TO INTEGER
                                    NUMBER.  ALLOWS }
VAR DUMMY : STRING[80];            {ERROR CHECKING OF INPUT
                                    TO AVOID    }
    RESULT :INTEGER;               {DATA TYPE ERROR}

BEGIN
  REPEAT
  BEGIN
    READ (DUMMY);  {READ DUMMY STRING FROM KEYBOARD}
    VAL (DUMMY,X,RESULT); {CONVERT FROM STRING TO INTEGER}
    IF RESULT<>0 THEN     {IF RESULT <>0 THEN THERE HAS BEEN
                           AN INPUT ERROR}
      WRITE (' DATA TYPE ERROR TRY AGAIN!! '); {TRY TO GET
                                                INPUT AGAIN}
  END;
  UNTIL RESULT=0;{IF INPUT WAS ACTUALLY INTEGER THEN LEAVE}
END;{READINT}

PROCEDURE READREAL (VAR X:REAL); {SAME AS READINT ONLY
                                  OUTPUT IS REAL NUMBER}

VAR DUMMY : STRING[80];
    RESULT : INTEGER;

BEGIN
  REPEAT
  BEGIN
    READ(DUMMY);
    VAL(DUMMY,X,RESULT);
    IF RESULT<>0 THEN
      WRITE (' DATA TYPE ERROR TRY AGAIN!! ');
  END;
  UNTIL RESULT=0;
END;{READREAL}

procedure pointdta (var dtarec : dtapointer);

const getdta = $2f00; {function number }

var regs : registers;

begin
  regs.ax := getdta;
  msdos(regs);
  dtarec := ptr (regs.es,regs.bx);
```

```
end; {pointdta}

function sizeoffile (hiword,loword :integer) : real;

var bigno,size : real;

begin
  bigno := (maxint*2.0) + 2;
  if hiword < 0 then size := (bigno + hiword) * bigno
    else size := hiword * bigno;
  if loword >= 0 then size := size + loword
    else size := size + (bigno + loword);
  sizeoffile := size;
end;

procedure findfirst (pattern : userspec; var found :
                     filename; var size : real;
                     var nomatch, lastone, subdir :
          boolean);

const findfirst = $4e00; {function number}

type asciiz = array [1..64] of char;

var
  filespec : asciiz;
  regs : registers;
  posinstr, count : integer;
  foundlen : byte absolute found;

begin
  for posinstr := 1 to length(pattern) do
    filespec[posinstr] := pattern [posinstr];
  filespec[length(pattern) + 1] := nul;
  with regs do
  begin
    ds := seg (filespec);
    dx := ofs (filespec);
    cx := seekattrib;
    ax := findfirst;
    msdos(regs);
    if (flags and 1) > 0 then
    begin
      case ax of
         2 : begin {no match}
               nomatch := true;
               lastone := true;
             end;
        18 : begin              {no more files}
               nomatch := false;
               lastone := true;
             end;
```

```
      else
        writeln (^G'Can"t interpret error return code');
        halt;
      end;
    end
    else
    begin               {no error return code}
      nomatch := false;
      lastone := false;
    end;
  end; {with regs}

  if (not nomatch) then
  with transferrec^ do
  begin
    found := foundname;
    count := 0;
    while found[count] <> nul do count := count + 1;
    foundlen := count;
    for count := length(found) + 1 to 13 do
      found := found + ' ';
    if (attribute and seekattrib) > 0
      then subdir := true
      else subdir := false;
    if not subdir
      then size := sizeoffile(sizehigh,sizelow)
      else size := 0.0;
  end; {with transferrec}
end;{findfirst}

procedure findnext (var found : filename; var size : real;
                    var lastone, subdir : boolean);

const findnext = $4f00;     {function number}

var
  regs : registers;
  count : integer;
  foundlen : byte absolute found;

begin
  with regs do
  begin
    ax := findnext;
    msdos(regs);
    if (flags and 1 ) > 0  then
      if ax = 18 then lastone := true
      else
      begin
        writeln (^G'Can"t interpret error return code');
        halt;
      end
```

```
    else lastone := false;
  end; {with regs}

  with transferrec^ do
  begin
    found := foundname;
    count := 0;
    while found[count] <> nul do count := count + 1;
    foundlen := count;
    for count := length(found) + 1 to 13 do found := found
+' ';
    if (attribute and seekattrib) > 0 then subdir := true
      else subdir := false;
    if not subdir then
      size := sizeoffile(sizehigh,sizelow)
      else size := 0.0;
  end; {with transferrec}
end; {findnext}

procedure directory (matchptrn : filename);

begin
  clrscr;
  writeln (' --  Directory  -- ');
  writeln;
  count := 0;
  pointdta (transferrec);
  findfirst(matchptrn,retname,filsize,
            nofind,lastfile,subdirec);
  if nofind or lastfile then writeln ('File not found.')
  else
  begin
    while (not lastfile) do
    begin
      if subdirec then lowvideo;
      write (retname,'  ',filsize:8:0,'   ');
      normvideo;
      count := count + 1;
      if (count mod 3) = 0 then writeln;
      findnext(retname,filsize,lastfile,subdirec);
    end;
  end;

  if (count mod 3) <> 0 then writeln;
  writeln;
  write ('*** ',count,' Files or  ');
  lowvideo;
  write ('Sub-Directories');
  normvideo;
  writeln (' found ***');
end;
```

```
PROCEDURE DUMP;{PERFORM SCREEN DUMP TO EPSON COMPATIBLE
                PRINTER}
TYPE RESULT = RECORD
               AX,BX,CX,DX,BP,SI,DI,DS,ES,FLAGS : INTEGER;
              END;
VAR REGS : RESULT;
BEGIN
  INTR(5,REGS); {CALL SCREEN DUMP INTERRUPT}
  WRITE(LST,CHR(12)); {FEED PRINTER A FORM FEED WHEN DONE}
END;


PROCEDURE INIT; {initialize ALL PLOT variables}
VAR I,J:INTEGER;
BEGIN
  MENU:=0;GRIDFLAG:='N';SYMFLAG:='N';XTIC:=0;YTIC:=0;XSTEP:=0;YSTEP:=
  LINEFLAG:='N';DXMAX:=100;DYMAX:=100;DXMIN:=0;DYMIN:=0;
  FOR I:=1 TO 80 DO FOR J:=1 TO 25 DO SCRTEXT[I,J]:=CHR(0);
  FILMIN:=1;
  FILMAX:=1;
  NPOINTS:=0;
  TITLE:=CHR(0);XAXIS:=TITLE;YAXIS:=TITLE;
  step:=1;XSUBTK:=0;YSUBTK:=0;CONFLG:=0;
  END;

PROCEDURE GINIT; {INITIALIZE GRAPHICS SCREEN AND DRAW BOX}
BEGIN
  HIRES;  {SET HIRES GRAPHICS MODE}
  HIRESCOLOR(15); {SET PLOT COLOR}
  DRAW (0,0,639,0,1);        {DRAW BOX AROUND SCREEN}
  DRAW (639,0,639,199,1);
  DRAW (639,199,0,199,1);
  DRAW (0,199,0,0,1);
END; {GINIT}

PROCEDURE BOX; {DRAW BOX AROUND PLOT REGION}
BEGIN
  DRAW (WINXMIN,WINYMIN,WINXMIN,WINYMAX,1);
  DRAW (WINXMIN,WINYMAX,WINXMAX,WINYMAX,1);
  DRAW (WINXMAX,WINYMAX,WINXMAX,WINYMIN,1);
  DRAW (WINXMAX,WINYMIN,WINXMIN,WINYMIN,1);
END; {BOX}

PROCEDURE INNUMB (I,J,L:INTEGER; X:REAL); {CONVERT NUMBER TO
                                           STRING AND PUT IT}
VAR NUM:STRING[10];                        {IN TEXT ARRAY FOR
                                           PRINTING TO SCREEN}
     K:INTEGER;                            {I AND J REPRESENT
                                           THE POSITION TO}
BEGIN                                      {PLACE THE NUMBER, L
                                           IS THE LENGTH OF}
```

```
  IF X<0 THEN  {FOR NEGATIVE NUMBER}     {THE NUMBER, AND X
                                          IS THE NUMBER}
  BEGIN
    STR(X:7:3,NUM);    {CONVERT STRING TO NUMBER}
    FOR K:=1 TO L+1 DO SCRTEXT[I+K-1,J]:=COPY(NUM,K,1);
{PLACE IN SCREEN ARRAY}
  END ELSE  {IF X<0}
  BEGIN       {FOR POSITIVE NUMBER}
    STR(X:6:3,NUM); {CONVERT STRING TO NUMBER}
    FOR K:=1 TO L DO SCRTEXT[I+K,J]:=COPY(NUM,K,1); {PLACE
IN SCREEN ARRAY}
  END;{IF X>=0}
END;{INNUMB}

PROCEDURE SORTDATA (VAR MAX,MIN:REAL; K:INTEGER);
                                    {SORT DATA FILES TO FIND}
BEGIN                               {FIND MAXIMUM AND MINIMUM}
MAX:=0;    {INITIALIZE MIN AND MAX VALUES}  {VALUES OF PLOT}
  MIN:=1E32;
  FOR L:=1 TO NPOINTS DO    {GO THROUGH DATA}
  BEGIN
    IF XY[L,K]>MAX THEN MAX:=XY[L,K]; {COMPARE MAX AND MIN
                VALUES}
    IF XY[L,K]<MIN THEN MIN:=XY[L,K];
  END; {FOR L}
END; {SORTDATA}

PROCEDURE GETDATA (VAR XY:DATA; VAR nfiles:INTEGER; VAR
Npoints:NUMB);
VAR DATAFILE:TEXT;
      X,Y:REAL;                          {READ AND SORT DATA
              FILE}
      J,I:INTEGER;
      DNAME : STRING[14];

BEGIN
  WRITELN;
  WRITE ('WHAT IS THE NAME OF THE FILE :'); {GET DATA FILE
                NAME}
  READLN (NAME);
  IF NAME<>'' THEN    {IF NO NAME LEAVE GETDATA}
  BEGIN
    NPOINTS:=0;
    DNAME:='B:'+NAME+'.DAT'; {CREATE DATA FILE NAME
B:DNAME.DAT}
    FOR I:=1 TO 4097 DO {INITIALIZE DATA ARRAY}
    BEGIN
      XY[I,1]:=I;
      XY[I,2]:=0;
    END; {FOR I}
    MATCHPTRN := DNAME;
    findfirst(matchptrn,retname,filsize,
```

```
              nofind,lastfile,subdirec);
    if nofind or lastfile then writeln ('File not found.')
    else
    begin
      ASSIGN (DATAFILE,DNAME); {OPEN DATA FILE}
      RESET (DATAFILE);        {RESET DATA FILE FOR READING}
      WHILE NOT EOF(DATAFILE) DO {READ DATA UNTIL END OF
              FILE}
      BEGIN
        Npoints:=Npoints+1;        {INCREMENT NUMBER OF
            POINTS}
        READ (DATAFILE,xY[NPOINTS,2]);{READ Y COORDINATE}
      END;{WHILE NOT EOF}
      NPOINTS:=NPOINTS-1;{DECREMENT NUMBER OF POINTS BY 1}
      CLOSE (DATAFILE);  {CLOSE DATA FILE}
      SORTDATA (YMAX,YMIN,2);  {SORT Y DATA }
      XMIN:=1.0; XMAX:=NPOINTS;
{RESET PLOT PARAMETERS}
      DXMAX:=XMAX;DXMIN:=XMIN;DYMAX:=YMAX;DYMIN:=YMIN;
      FILMIN:=1;FILMAX:=NPOINTS;step:=1;conflg:=0;
      START:=1;FINISH:=NPOINTS;TIMES:=1;
    END; {IF NOFIND ELSE}
  END;{IF NAME<>''}
END; {GETDATA}

PROCEDURE CHANGESCALE (VAR MIN,MAX,STEP:REAL;
         VAR TIC:INTEGER; DMAX,DMIN:REAL;
                          VAR SUBTK:INTEGER);
VAR CHANGE:ANSWER;        {USED TO CHANGE X OR Y AXIS SCALING}
BEGIN                     {PARAMTERS.}
  WRITELN ('THE DATA MAXIMUM IS ',DMAX);  {PRINT OUT CURRENT
                  DATA AND PLOT }
  WRITELN ('THE DATA MINIMUM IS ',DMIN);  {PARAMETERS}
  WRITELN;
  WRITELN ('THE PLOT MAXIMUM IS ',MAX);
  WRITELN ('THE PLOT MINIMUM IS ',MIN);
  WRITELN;
  WRITELN ('THE NUMBER OF TICS IS ',TIC);
  WRITELN ('THE TIC SPACING IS ',STEP);
  WRITELN;
  WRITE ('DO YOU WISH TO CHANGE THE PLOT REGION ? ');
                          {CHECK TO SEE IF YOU}
  READLN (CHANGE);        {REALLY WANT TO CHANGE THESE VALUES}
  IF CHANGE='Y' THEN
  BEGIN
    WRITE ('THE PLOT MINIMUM IS : ');   {READ NEW PLOT
              PARAMETERS FOR }
    READREAL (MIN);                     {THE AXIS}
    WRITELN;
    WRITE ('THE PLOT MAXIMUM IS : ');
    READREAL (MAX);
    WRITELN;
```

```
    WRITE ('THE NUMBER OF TIC MARKS IS : ');
    READINT (TIC);
    WRITELN;
    WRITE ('THE TIC MARK SPACING IS : ');
    READREAL (STEP);
    WRITELN;
    WRITE ('THE NUMBER OF SUBTICKS IS : ');
    READINT(SUBTK);
    WRITELN;
    IF MIN>MAX THEN STEP:=-STEP; {ADJUST STEP SIZE TO STEP
              BACKWARDS IF}
  END; {IF CHANGE}                {MIN > MAX}
END; {CHANGESCALE}

PROCEDURE MISCPARAMETERS;  {SET MISCELLANEOUS PLOT
          CONFIGURATIONS}
 BEGIN
   WRITE ('DO YOU WANT GRID LINES (Y OR N) ?');
   READLN (GRIDFLAG);
   WRITE ('CONNECT DATA POINTS WITH A LINE (Y OR N) ?');
   READLN (LINEFLAG);
   WRITE ('DO YOU WANT SYMBOLS PLOTTED (Y OR N) ?');
   READLN (SYMFLAG);
 END;

PROCEDURE SETSCALE (VAR XSCALE,YSCALE:REAL);
BEGIN                             {SET SCALE OF XY DATA }
  XSCALE:=(WINXMAX-WINXMIN)/(XMAX-XMIN); {FIND X SCALING
                VALUE}
  YSCALE:=(WINYMIN-WINYMAX)/(YMAX-YMIN); {FIND Y SCALING
                VALUE}
END; {SETSCALE}

FUNCTION XP (X:REAL):INTEGER;
  {FUNCTION CONVERTS X DATA TO X PIXEL POSITION}
VAR Z:REAL; {FOR X COORDINATE}
BEGIN
  Z:=WINXMIN+(X-XMIN)*XSCALE;  {COMPUTE PIXEL POSITION FROM
           X COORDINATE}
  IF Z<WINXMIN THEN Z:=WINXMIN; {CHECK TO SEE IF ITS TO FAR
            TO LEFT}
  IF Z>WINXMAX THEN Z:=WINXMAX;  {CHECK TO SEE IF ITS TO FAR
             TO RIGHT}
  XP:=ROUND(Z);
 END; {XP}

FUNCTION YP (Y:REAL):INTEGER; {SAME AS XP FOR Y COORDINATE}
VAR Z:REAL;
BEGIN
  Z:=WINYMIN-(Y-YMIN)*YSCALE;
  IF Z<WINYMAX THEN Z:=WINYMAX;
  IF Z>WINYMIN THEN Z:=WINYMIN;
```

```
  YP:=ROUND(Z);
END; {YP}

PROCEDURE SPLOT(X,Y:REAL);  {PLOT REAL WORLD NUMBERS, CALLS
           XP AND YP TO }
BEGIN                       {CONVERTS DATA TO PIXEL
           POSITION}
  PLOT(XP(X),YP(Y),1);
END; {SPLOT}

PROCEDURE SDRAW(X,Y,W,Z:REAL); {SAME AS SPLOT FOR LINES
           INSTEAD OF POINTS}
BEGIN
  DRAW (XP(X),YP(Y),XP(W),YP(Z),1);
END; {SDRAW}

PROCEDURE ANGMARK;  {DOES ANGSTROM AXIS ACROSS TOP}

VAR AXMX,AXMN,X,XE:REAL;
    XI,YI,I:INTEGER;

BEGIN
  YI:=TRUNC(WINYMAX/8); {COMPUTE POSITION OF TEXT LINE FOR
       SCALE}
  FOR I:=1 TO 80 DO SCRTEXT[I,YI]:=CHR(0); {ERASE TEXT IN
                    TEXT LINE}
  AXMN:=10.0*(TRUNC(12398.54/XMIN/10.0)+1); {COMPUTE MIN
                   ANGSTROM }
  AXMX:=10.0*TRUNC(12398.54/XMAX/10.0);     {COMPUTE MAX
                   ANGSTROM }
  X:=AXMN+10.0;                    {START AT NEAREST 10
                ANGTROMS}
  WHILE X>AXMX DO           { DO UNTIL REACH MAX OF AXIS}
  BEGIN
    X:=X-10.0;              {INCREMENT TIC MARKS BY 10
          ANGSTROMS}
    XE:=12398.54/X;         {CONVERT ANGSTROM TO eV (X
          SCALE)}
    XI:=XP(XE);             {FIND SCREEN POSITION OF TIC
          MARK}
    IF X=TRUNC(X/100)*100 THEN {WRITE WAVELENGTH AND BIG TIC
           EVERY}
    BEGIN                        {100 ANGSTROMS}
      DRAW (XI,WINYMAX,XI,WINYMAX+5,1); {DRAW LARGE TIC}
      XI:=ROUND(XI/8);                  {FIND TEXT POSITION}
      IF (XI<76) AND (XI>4)  THEN INNUMB(XI-2,YI,4,X);
    {WRITE TEXT TO SCREEN}
    END ELSE DRAW (XI,WINYMAX,XI,WINYMAX+3,1); {ELSE DRAW
                   SMALL TIC}
  END; {WHILE X}
END; {ANGMARK}
```

```
PROCEDURE XMARK (XTIC:INTEGER; XSTEP:REAL);{COMPUTE AND
PLACE TIC MARKS FOR}
VAR X,STICK:REAL;                                    {X AXIS}
    XI,YI,Y0,I:INTEGER;
BEGIN
  IF CONFLG=1 THEN ANGMARK;  {DO ONLY IF DATA IN eV INSTEAD
             OF CHANNELS}
  IF XSUBTK<>0 THEN STICK:=XSTEP/XSUBTK; {FIND STEP SIZE FOR
                  SMALL TIC}
  Y0:=YP(0);               {DOES Y AXIS GO THROUGH ZERO}
  YI:=ROUND((WINYMIN+11)/8);             {FIND Y POSITION
                FOR X AXIS TEXT}
  IF (Y0>WINYMAX) AND (Y0<WINYMIN) THEN
      DRAW (WINXMIN,Y0,WINXMAX,Y0,1);
  FOR J:=0 TO XTIC DO          {DO TIC MARKS}
  BEGIN
    X:=XMIN+J*XSTEP;           {COMPUTE X VALUE FOR TIC MARK}
    XI:=XP(X);                 {CONVERT TO SCREEN POSITION}
    IF GRIDFLAG='Y' THEN       {CHECK TO SEE IF DRAW TIC MARKS
          OR GRID}
    BEGIN
      DRAW (XI,WINYMIN,XI,WINYMAX,1); {IF YES DRAW GRID}
    END ELSE
    BEGIN           {IF NO DRAW TICS}
      IF (Y0>WINYMAX) AND (Y0<WINYMIN) THEN
             DRAW (XI,Y0+5,XI,Y0-5,1);
      DRAW (XI,WINYMIN,XI,WINYMIN-5,1);
    END; {IF GRIDFLAG}
    XI:=ROUND(XI/8);  {FIND X POSITION ON SCREEN FOR X AXIS
         TEXT}
    IF (XI<76) AND (XI>4) AND (YI<25) THEN
    INNUMB(XI- 2,YI,6,X);{PUT NUMBER IN}
    X:=X-STICK;  {DO SUBTICK}
{SCREEN ARRAY}
    FOR I:=0 TO XSUBTK DO
    BEGIN
      X:=X+STICK; {COMPUTE SUBTICK VALUE}
      XI:=XP(X);  {COMPUTE SCREEN POSITION OF SUBTICK}
      DRAW (XI,WINYMIN,XI,WINYMIN-3,1);{DRAW SUBTICK}
    END; {FOR I}
  END; {FOR J}
END; {XMARK}

PROCEDURE YMARK (YTIC:INTEGER; YSTEP:REAL); {SAME AS XMARK
                 FOR Y AXIS}
VAR Y,STICK:REAL;
    XI,YI,X0,I:INTEGER;
BEGIN
  IF YSUBTK<>0 THEN STICK:=YSTEP/YSUBTK;
  X0:=XP(0);
  IF (X0>WINXMIN) AND (X0<WINXMAX) THEN
DRAW(X0,WINYMIN,X0,WINYMAX,1);
```

```
  XI:=ROUND((WINXMIN-72)/8);
  FOR J:=0 TO YTIC DO
  BEGIN
    Y:=YMIN+J*YSTEP;
    YI:=YP(Y);
    IF GRIDFLAG='Y' THEN
    BEGIN
      DRAW (WINXMIN,YI,WINXMAX,YI,1);
    END ELSE
    BEGIN
      IF (X0>WINXMIN) AND (X0<WINXMAX) THEN
     DRAW (X0+5,YI,X0- 5,YI,1);
      DRAW (WINXMIN,YI,WINXMIN+10,YI,1);
      DRAW (WINXMAX,YI,WINXMAX-10,YI,1);
    END;{IF GRIDFLAG}
    YI:=ROUND((YI+3)/8);
    IF (YI<26) AND (YI>0) AND (XI>0) THEN INNUMB(XI,YI,6,Y);
    Y:=Y-STICK;
    FOR I:=0 TO YSUBTK DO
    BEGIN
      Y:=Y+STICK;
      YI:=YP(Y);
      DRAW (WINXMIN,YI,WINXMIN+6,YI,1);
      DRAW (WINXMAX,YI,WINXMAX-6,YI,1);
    END;{FOR I}
  END;  {FOR J}
END; {YMARK}

PROCEDURE CENTER (TITLE:LETTER; I,J:INTEGER);
  {CENTER A STRING OF TEXT HORIZ.}
VAR K:INTEGER;              {AND PLACE IN SCREEN ARRAY}
BEGIN    {TITLE IS STRING, I IS THE VERTICAL POSITION}
  J:=ABS(ABS(WINXMAX-WINXMIN) DIV 8
      - LENGTH(TITLE)) DIV 2 + WINXMIN DIV 8;
  FOR K:=1 TO LENGTH(TITLE) DO
SCRTEXT[J+K,I]:=COPY(TITLE,K,1);
END;{CENTER}

PROCEDURE VERTIC (TITLE:LETTEP; I,J:INTEGER);
  {SAME AS CENTER BUT WRITES TEXT}
VAR K:INTEGER;                                {VERTICALLY}
BEGIN
  J:=ABS(ABS(WINYMAX-WINYMIN) DIV 8
      - LENGTH(TITLE)) DIV 2 + WINYMAX DIV 8;
  FOR K:=1 TO LENGTH(TITLE) DO
SCRTEXT[I,K+J]:=COPY(TITLE,K,1);
END; {VERTIC}

PROCEDURE WRITEXT;   {PUT SCREEN TEXT ARRAY ON SCREEN}
VAR I,J:INTEGER;
    C:CHAR;
BEGIN
```

```
  FOR I:=1 TO 80 DO        {ROW}
  BEGIN
    FOR J:=1 TO 25 DO      {COLUMN}
    BEGIN
      C:=SCRTEXT[I,J];     {VALUE OF POSITION}
      GOTOXY(I,J);         {GOTO POSITION ON SCREEN}
      IF C<>CHR(0) THEN WRITE(C); {A NULL CHARACTER PRINTS
            NOTHING}
    END;{FOR J}
  END;{FOR I}
END; {WRITEXT}

PROCEDURE CONVERT(k:INTEGER);
  {CONVERTS CHANNEL NUMBERS TO eV}
VAR J:INTEGER;
    CH:CHAR;

BEGIN
  CONFLG:=1;   {SET FLAG SO PROGRAM KNOWS DATA HAS BEEN
      CONVERTED}
  cal:=k;      {CHANNEL NUMBER OF CALIBRATION LINE}
  GOTOXY(1,25);
  WRITE (' DO YOU WANT CALIBRATE SPECTRUM (Y OR N): ');
  READ (CH); {CHECK TO SEE IF YOU REALLY WANT TO DO  }
  IF (CH='Y') OR (CH='y') THEN                  {THIS}
  BEGIN
    GOTOXY(1,25);
    WRITE ('INPUT WAVELENGTH OF CALIBRATION LINE
      (IN ANGSTROMS) :');
    READREAL (LAMBDA);  {GET WAVELENGTH OF CAL LINE}
    GOTOXY(1,25);
    WRITE ('
');
    GOTOXY(1,25);
    WRITE ('INPUT NUMBER OF ANGSTROMS PER CHANNEL :');
    {GET NUMBER OF ANGSTROMS}
    READREAL (ACH);   {PER CHANNEL}
    FOR J:=1 TO NPOINTS DO XY[J,1]:=12398.54/(LAMBDA+
          (J- CAL)*ACH);{CONVERT X}
DXMAX:=XY[1,1];DXMIN:=XY[NPOINTS,1];XMAX:=DXMIN;XMIN:=DXMAX;conflg:=1
    SETSCALE(XSCALE,YSCALE);       {RESET X AXIS PARAMETERS}
    GOTOXY(1,25);
    WRITE ('                                              ');
  END;{IF CH}
END;{CONVERT}

PROCEDURE MAGNIFY;  {BLOWS UP PART OF DATA}
VAR I:INTEGER;
    NEWTIME:REAL;

BEGIN
  GOTOXY(1,25);                {GET MAGNIFICATION FACTOR}
```

```
  WRITE ('CURRENT MAGNIFICATION FACTOR IS ',TIMES,
      ', ENTER NEW FACTOR :');
  READ (NEWTIME);
  TIMES:=NEWTIME/TIMES;     {FIND CHANGE OF SCALE}
  GOTOXY(1,25);
  WRITE ('                                                  ');
  FOR I:=START TO FINISH DO XY[I,2]:=XY[I,2]*TIMES;
    {RESCALE DATA IN REGION}
  TIMES:=NEWTIME;                {FROM START TO FINISH}
END; {MAGNIFY}


PROCEDURE ADDTXT; FORWARD;

PROCEDURE CURSOR;{PROCEDURE MOVES CURSOR AROUND PLOT REGION}
VAR I,J,TAB:INTEGER;
    CH:CHAR;
    X,Y:INTEGER;
    X2,Y2:REAL;
  BEGIN
     TAB:=(FILMAX-FILMIN) DIV 20;    {SET TAB KEY TO ONE
           TWENTIETH OF PLOT}
     I:=FILMIN;                      {PUT INITIAL CURSOR
           POSITION TO PLOT MIN}
     WHILE CH<>#17 DO                {REMAIN IN CURSOR MODE
           UNTIL CNTRL-Q HIT}
     BEGIN
       X:=XP(XY[I,1]);               {CURRENT X POSITION OF
           CURSOR}
       Y:=YP(XY[I,2]);               {CURRENT Y POSITION OF
           CURSOR}
       DRAW (X,Y,X,Y-20,1);          {DRAW CURSOR}
       GOTOXY (1,25);                {MOVE TO CURSOR
           INFORMATION LINE}
       WRITE ('X = ',XY[I,1]:10:4,'   Y = ',XY[I,2]:10:3);
     {WRITE XY INFO TO}
       READ (KBD,CH);          {GET CHARACTER FROM KEYBRD}
          {SCREEN}
       CASE ORD(CH) OF         {FIGURE OUT WHAT TO DO}
          9:BEGIN              {INCREMENT CURSOR POSITION BY
           AMOUNT OF TAB}
             I:=I+TAB;
            END;
         67:CONVERT(I);        {IF LARGE C THEN CONVERT TO eV}
         99:CONVERT(I);        {IF SMALL c THEN CONVERT TO eV}
        115:START:=I;          {IF SMALL s THEN MARK START
          POSITION FOR MAGNIFY}
         83:START:=I;          {IF LARGE S THEN MARK START
          POSITION FOR MAGNIFY}
        102:FINISH:=I;         {IF SMALL f THEN MARK FINISH
          POSITION}
         70:FINISH:=I;         {IF LARGE F THEN MARK FINISH
```

```
          POSITION}
        109:MAGNIFY;        {IF SMALL m THEN MAGNIFY}
         77:MAGNIFY;        {IF LARGE M THEN MAGNIFY}
         27: BEGIN          {IF ESC THEN READ ADDITIONAL
              CHARACTER}
              READ(KBD,CH);{CURSOR KEYS NEED TWO CHARACTERS}
              CASE ORD(CH) OF
               77: I:=I+step;  {STEP RIGHT}
               75: I:=I-step;  {STEP LEFT}
              END; {CASE (ORD)}
            END; {27}
       END;{CASE}
       IF I>FILMAX THEN I:=FILMIN; {WRAP AROUND FROM ONE END
            TO THE OTHER}
       IF I<FILMIN THEN I:=FILMAX;
       DRAW (X,Y-1,X,Y-20,0);       {ERASE CURSOR}
     END; {WHILE NOT}
END; {CURSOR}


PROCEDURE GPLOT; {PLOT PROCEDURE}
VAR CH:CHAR;
    FP1:INTEGER;
BEGIN
  GINIT; {INITIALIZE GRAPHICS}
  BOX;   {DRAW BOX ON SCREEN}
  XMARK (XTIC,XSTEP);   {PLACE TIC MARKS AND AXIS MARKINGS
       ON SCREEN}
  YMARK (YTIC,YSTEP);
  IF LINEFLAG='Y' THEN
  BEGIN                 {CONNECT THE DOTS}
    SPLOT(XY[FILMIN,1],XY[FILMIN,2]);  {PLOT FIRST POINT}
    FP1:=FILMIN+1;
    FOR L:=FP1 TO FILMAX DO  {FROM FIRST POINT TO LAST DRAW
LINE}
      SDRAW(XY[L-1,1],XY[L-1,2],XY[L,1],XY[L,2]);
  END ELSE
    FOR L:=FILMIN TO FILMAX DO SPLOT(XY[L,1],XY[L,2]);
    {PLOT POINTS}
  WRITEXT;  {WRITE CHARACTERS TO SCREEN}
  WHILE CH<>#17 DO {GO TO ONE OF THE EDITING MODES UNTIL
      CTRL-Q}
  BEGIN
    READ(KBD,CH);
    CASE CH OF
      'A' : ADDTXT; {ADD TEXT TO SCREEN}
      'a' : ADDTXT;
      'C' : CURSOR; {MOVE CURSOR}
      'c' : CURSOR;
      'D' : DUMP;   {DUMP SCREEN TO PRINTER}
      'd' : DUMP;
    END; {CASE CH}
```

```
  END;{WHILE CH}
END;{GPLOT}

PROCEDURE ADDTXT; {ADD TEXT TO SCREEN}
VAR I,J:INTEGER;
    CH:CHAR;

BEGIN
  I:=1;J:=1; {INITIAL CURSOR POSITION}
  WHILE CH<>#17 DO {ADD TEXT UNTIL CTRL-Q}
  BEGIN
    GOTOXY(I,J); {GO TO POSITION I,J ON SCREEN}
    WRITE(CHR(219)); {WRITE CURSOR TO SCREEN}
    GOTOXY(I,J);     {GO BACK TO POSITION}
    READ(KBD,CH);    {GET CHARACTER FROM KEYBOARD}
    IF CH=#27 THEN   {IF CHAR = ESC THEN READ AGAIN FOR
        CURSOR KEYS}
    BEGIN
      READ(KBD,CH);
      WRITE(SCRTEXT[I,J]);
      CASE ORD(CH) OF
        77:I:=I+1;          {ADJUST SCREEN POSITION
            DEPENDING ON CURSOR KEY}
        75:I:=I-1;
        72:J:=J-1;
        80:J:=J+1;
      END;{CASE ORD}
      IF I>80 THEN I:=1;    {WRAP AROUND SCREEN}
      IF I<1 THEN I:=80;
      IF J>25 THEN J:=1;
      IF J<1 THEN J:=25;
    END ELSE
    CASE ORD(CH) OF      {IF NOT CURSOR KEY THEN CHECK TO
        SEE IF ALLOWED CHAR}
      32:BEGIN
           SCRTEXT[I,J]:=CHR(0); {SPACE}
           WRITE(CH);
           I:=I+1;
         END;
      33..123,125..255:BEGIN     {ALPHA NUMERICS}
                         SCRTEXT[I,J]:=CH;
                         WRITE(CH);
                         I:=I+1;
                       END;
      18:GPLOT;    {CTRL-R REDRAWS SCREEN}
    END;{CASE ORD}
  END;{IF CH}
END; {ADDTEXT}

PROCEDURE CLRTEXT; {ZERO OUT TEXT ARRAY WITH NULL
      CHARACTERS}
VAR I,J:INTEGER;
```

```
BEGIN
  FOR I:=1 TO 80 DO
     FOR J:=1 TO 25 DO SCRTEXT[I,J]:=CHR(0);
END;{CLRTEXT}

PROCEDURE CLRAXIS;  {CLEAR TEXT FROM JUST THE X AND Y AXIS}
VAR I,J:INTEGER;
BEGIN
  FOR I:=3 TO 10 DO        {CLEAR COLUMNS 3 TO 10 OF ROWS 2
          TO 23 FOR Y AXIS}
    FOR J:=2 TO 23 DO SCRTEXT[I,J]:=CHR(0);
  FOR I:=3 TO 79 DO SCRTEXT [I,22]:=CHR(0); {CLEAR ROW 22
                FOR X AXIS}
END;{CLRAXIS}

PROCEDURE GRAPH; {DRAW THE GRAPH}
VAR CH:CHAR;
 BEGIN
  CLRAXIS;                {CLEAR AXES OF TEXT}
  CENTER(TITLE,1,80);     {ADD TITLE}
  CENTER(XAXIS,24,80);    {ADD X AXIS TEXT}
  VERTIC(YAXIS,2,25);     {ADD Y AXIS TEXT}
  SETSCALE(XSCALE,YSCALE); {FIND SCALING PARAMETERS FOR PLOT
          LIMITS}
  GPLOT;                    {PLOT THE GRAPH}
END; {GRAPH}

PROCEDURE PLOTFILE;
  {WRITE AN INFORMATION FILE FOR DRIVING THE PROGRAM THAT}
                    {OUTPUTS TO THE HOUSTAN INSTR. PLOTTER}
VAR DATAFILE : TEXT;
    I,J : INTEGER;
    PNAME,NEWNAME : STRING[14];

BEGIN
  WRITELN;
  WRITE ('ENTER NAME FOR PLOTTER INFORMATION FILE (RETURN
    FOR DEFAULT):');
  READLN (NEWNAME); {ENTER NAME OF FILE FOR PIF, DEFAULT
       WILL DERIVE NAME}
  IF NEWNAME='' THEN NEWNAME:=NAME; {FROM DATA FILE};
  PNAME:='B:'+NEWNAME+'.PLT'; {DEFAULT NAME}
  ASSIGN (DATAFILE,PNAME);  {OPEN FILE}
  REWRITE (DATAFILE);       {RESET FILE FOR WRITING AND
            WRITE INFORMATION}
  WRITE (DATAFILE,XMAX,' ',XMIN,' ',XTIC,' ',XSTEP,'
      ',XSUBTK,' ');
  WRITE (DATAFILE,YMAX,' ',YMIN,' ',YTIC,' ',YSTEP,'
      ',YSUBTK,' ');
  WRITE (DATAFILE,LAMBDA,' ',CAL,' ',ACH,' ');
  WRITELN (DATAFILE,FILMAX,' ',FILMIN,' ',CONFLG,' ',START,'
     ',FINISH,' ',TIMES);
```

```
  WRITE (DATAFILE,LINEFLAG,GRIDFLAG);
  FOR I:=1 TO 80 DO
    FOR J:=1 TO 25 DO WRITE(DATAFILE,SCRTEXT[I,J]);
  CLOSE (DATAFILE);
END;{PLOTFILE}

PROCEDURE XYDUMP; {DUMPS CALIBRATED XY DATA TO DISK}

VAR
  DATAFILE : TEXT;
  I,J : INTEGER;
  NEWNAME : STRING [14];

BEGIN   {CHECK AND SEE IF FILE IS CONVERTED TO ENERGY SCALE}
  IF CONFLG = 1 THEN
    WRITELN ('WARNING !!!!!!!! FILE IS STILL IN CHANNEL
    FORMAT AND HAS NOT BEEN CONVERTED TO ENERGY');
  WRITE ('INSERT DISK IN DRIVE B: AND HIT RETURN');
    {GIVE CHANCE TO CHANGE }
  READLN; {DISK                    }
  NEWNAME := 'B:'+ NAME + '.PXY';  {CREATE FILE NAME FOR  }
  ASSIGN (DATAFILE,NEWNAME);       {OUTPUT FILE           }
  REWRITE (DATAFILE);              {OPEN NEW FILE         }
  FOR I := 1 TO NPOINTS DO
    WRITELN(DATAFILE,XY[I,1]:6:4,' ',XY[I,2]:6);
      {WRITE POINTS TO FILE}
  CLOSE (DATAFILE);        {CLOSE FILE            }
END;  {END OF XYDUMP}



PROCEDURE READFILE;
  {REVERSE OF PLOTFILE, READ IN PREVIOUSLY USED PIF}

VAR DATAFILE : TEXT;
    I,J,DUMMYI : INTEGER;
    PNAME,NEWNAME : STRING[14];
    DUMMYR :REAL;

BEGIN
  WRITELN;
  WRITE ('ENTER NAME FOR PLOTTER INFORMATION FILE (RETURN
       FOR DEFAULT):');
  READLN (NEWNAME);
  IF NEWNAME='' THEN NEWNAME:=NAME;
  PNAME:='B:'+NEWNAME+'.PLT';
  matchptrn:=pname;
  findfirst(matchptrn,retname,filsize,
            nofind,lastfile,subdirec);
  if nofind or lastfile then writeln ('File not found.')
  else
  begin
```

```
    ASSIGN (DATAFILE,PNAME);
    RESET (DATAFILE);
    READ (DATAFILE,XMAX,XMIN,XTIC,XSTEP,XSUBTK);
    READ (DATAFILE,YMAX,YMIN,YTIC,YSTEP,YSUBTK);
    READ (DATAFILE,DUMMYR,DUMMYI,DUMMYR);
    READLN (DATAFILE,FILMAX,FILMIN,
            CONFLG,START,FINISH,TIMES);
    READ (DATAFILE,LINEFLAG,GRIDFLAG);
    FOR I:=1 TO 80 DO
      FOR J:=1 TO 25 DO READ(DATAFILE,SCRTEXT[I,J]);
    CLOSE (DATAFILE);
  end; {if nofind else}
END;{READFILE}

BEGIN   {MAIN PROGRAM}
 INIT;
 WHILE MENU<>14 DO        {REPEAT UNTIL THE PROGRAM ENDS}
 BEGIN
   WRITELN ('                                    MENU');
   WRITELN;
   WRITELN ('                 1.  GET NEW FILES');
   WRITELN ('                 2.  PLOT FILES');
   WRITELN ('                 3.  CHANGE X AXIS SCALE');
   WRITELN ('                 4.  CHANGE YAXIS SCALE');
   WRITELN ('                 5.  LABEL GRAPH');
   WRITELN ('                 6.  LABEL X AXIS');
   WRITELN ('                 7.  LABEL Y AXIS');
   WRITELN ('                 8.  SET MISCELLANEOUS
             PARAMETERS');
   WRITELN ('                 9.  CLEAR TEXT');
   WRITELN ('                10.  WRITE PLOTTER FILE');
   WRITELN ('                11.  READ PLOTTER FILE');
   WRITELN ('                12.  DIRECTORY');
   WRITELN ('                13.  CREAT XY DATA FILE');
   WRITELN ('                14.  END PROGRAM');
   WRITE ('INPUT CHOICE : ');
   READINT (MENU);
   CASE MENU OF
     1: GETDATA(XY,NFILES,NPOINTS);     {INPUT DATA FILE}
     2: GRAPH;                          {PLOT DATA FILE}
     3: BEGIN           {CHANGE THE PARAMETERS ON X AXIS}
          WRITELN;
          WRITELN ('X AXIS PARAMETERS');
          WRITELN;
          CHANGESCALE(XMIN,XMAX,XSTEP,
                      XTIC,DXMAX,DXMIN,XSUBTK);
          IF CONFLG=1 THEN     {ADJUST SCALING}
          BEGIN
            FILMIN:=CAL+TRUNC((12398.54/XMIN
                               -LAMBDA)/ACH);
      {FIND FILMIN AND}
            FILMAX:=CAL+TRUNC((12398.54/XMAX
```

```
                                        -LAMBDA)/ACH);
      {FILMAX FOR CURRENT}
            IF FILMIN>FILMAX THEN    {ADJUST FOR FORWARD}
             {SCALE}
            BEGIN                    {OR BACKWARD PLOTTING}
              TEMP:=FILMAX;
              FILMAX:=FILMIN;
              FILMIN:=TEMP;
              STEP:=-1;
            END ELSE STEP:=1;
            IF FILMAX>NPOINTS THEN FILMAX:=NPOINTS;
          {MAKE SURE FILMIN AND }
            IF FILMIN<1 THEN FILMIN:=1; {FILMAX REMAIN IN
              LIMITS}
          END;{IF CONFLG}              {OF ARRAY}
        END;{3}
     4: BEGIN     {Y AXIS PARAMTER ADJUSTMENT}
          WRITELN;
          WRITELN ('Y AXIS PARAMETERS');
          WRITELN;
          CHANGESCALE(YMIN,YMAX,YSTEP,
                      YTIC,DYMAX,DYMIN,YSUBTK);
        END;
     5: BEGIN      {INPUT GRAPH TITLE}
          FOR J:=1 TO 80 DO SCRTEXT [J,1]:=CHR(0);
          WRITELN;
          WRITELN ('ENTER GRAPH TITLE (80 CHARACTERS):');
          READLN (TITLE);
        END;
     6: BEGIN    {INPUT X AXIS LEGEND}
          WRITELN;
          WRITELN ('ENTER X AXIS TITLE (80 CHARACTERS):');
          READLN (XAXIS);
        END;
     7: BEGIN    {INPUT Y AXIS LEGEND}
          WRITELN;
          WRITELN ('ENTER Y AXIS TITLE (25 CHARACTERS):');
          READLN (YAXIS);
        END;
     8: MISCPARAMETERS;
      {INPUT MISC PARAMETERS (GRID,LINES, ETC.)}
     9: CLRTEXT;          {CLEAR TEXT ARRAY}
    10: PLOTFILE;         {WRITE PLOTTER INFO FILE}
    11: READFILE;         {READ PLOTTER INFO FILE}
    12: BEGIN
          MATCHPTRN:='B:*.*';
          DIRECTORY (MATCHPTRN);
          WRITELN ('PRESS ANY KEY TO CONTINUE');
          REPEAT UNTIL KEYPRESSED;
        END;{12}
    13: XYDUMP;
  END;
```

```
    TEXTMODE;          {CLEAR SCREEN AND RETURN TO TEXT MODE}
    END;
END.{END PROGRAM SPECPLOT}
```

Bibliography

1. Aboubaker, C. B., Neu G. "Nature of the 1.5040-1.5110 eV Emission Band in GaAs," Journal of Applied Physics, 58(9):3549-3555, (1 November, 1985).

2. Adachi, S., "GaAs, AlAs, and $Al_xGa_{1-x}As$: Material Parameters for Use in Research and Device Applications," Journal of Applied Physics, 58(3):R1-R29, (1 August, 1985).

3. Almassy, R.J., Reynolds, D.C. Solid State Comm., vol. 38, 1981, pg 1053-6.

4. Almassy, R., et al. "Observation of Shallow Residual Donors in High Purity Epitaxial GaAs by Means of Photoluminescence Spectroscopy," Solid State Communications, 38:1053-1056, (1981).

5. Ashcroft N. W., and N. David Mermin, Solid State Physics. Philadelphia: Holt, Rinehart, and Winston, 1976.

6. Ashen, D.J. et al. "The Incorporation and Characterization of Acceptors in Epitaxial GaAs," Journal of Physics and Chemistry of Solids, 36:1041-1053 (October 1975).

7. Baldereschi, A., Lipari, N. O., "Spherical Model of Shallow Acceptor States in Semiconductors," Physical Review B, 8(6):2697-2709, (15 September, 1973).

8. Baldereschi, A., Lipari, N. O., "Cubic Contributions to the Spherical Model of Shallow Acceptor States," Physical Review B, 9(4):1525-1539, (15 February, 1974).

9. Baldereschi, A., Lipari,, N. O., "Binding Energy of Shallow Acceptors in Group IV Elements and II-V Compounds," Journal of Luminescence, 12/13:489-493, (1976).

10. Baldereschi, A., et al. "Central Cell Effects on Acceptor Spectra in Si and Ge," Solid State Communications, 33:277-279, (1980).

11. Barthruff, D., Haspeklo, H., "Excited State of Shallow Acceptors in InP," Journal of Luminescence, 24:181-184, (1981).

12. Battacharya, P. K., et al. "Impurity and Defect Levels in Beryllium-Doped GaAs Grown by Molecular Beam Epitaxy," Journal Applied Physics, 53(9):6391-6398, (September, 1982).

13. Bogardus, E. H., Bebb H. B., "Bound-Exciton, Free-Exciton, Band-Acceptor, Donor-Acceptor and Auger Recombination in GaAs," Physical Review, 176(3):993-1002, (15 December 1968).

14. Chiang, S. Y., Pearson, G. L., "Photoluminescence Studies of Vacancies and Vacancy-Impurity Complexes in Annealed GaAs," Journal of Luminescence, 10:313-322, (1975).

15. Cone, Major Milton L. Cathodoluminescence Characterization of Ion Implanted GaAs. PhD dissertation. School of Engineering, Air Force Institute of Technology (AU), Wright-Patterson AFB, OH, May 1980.

16. Contour, J. P., et al. "Optical Characterization of Defect Levels Induced by MBE Growth of GaAs," Journal of Vacuum Science and Technology, 1(3):811-815, (July-Sept 1983).

17. Covington, D. W., et al. "Photoluminescence and Electrical Characterization of MBE GaAs Epilayers: A Recent Survey," Institute of Physics Conference, 45(3):171-180, (1979).

18. Dean, P. J., et al. "Donor Bound Exciton Excited States in Zinc Selenide," Physical Review B, 23(10):4888-4901, (15 May, 1981).

19. Dean, P. J., "Photoluminescence as a Diagnostic of Semiconductors," Progress in Crystal Growth Characterization, 5:88-174, (1982).

20. Dean, P. J., Skolnick, M. S., "Donor Discrimination and Bound Exciton Spectra in InP," Journal of Applied Physics, 54(1):346-359, (January, 1983).

21. Dean, P. J., et al. "Acceptor Excited States in Indium Phosphide," Solid State Communications, 32:379-384, (1979).

22. Dean, P. J., et al. "Dye Laser Selective Spectroscopy in Bulk-Grown Indium Phosphide," Journal of Physics C, 12:5567-5575, (1979).

23. Dingle, R., et al. "Characterization of High Purity GaAs Grown by Molecular Beam Epitaxy," Applied Physics Letters, 40(6):507-510, (15 March, 1982).

24. Dingle, R. "Radiative Lifetimes of Donor-Acceptor Pairs in p-Type Gallium Arsenide," Physical Review, 184(3):788-796, (15 August 1969).

25. Dobson, P. J., et al. "The Occurrence of Sharp Exciton-Like Features in Low Temperature Photoluminescence Spectra from MBE Grown GaAs," Solid State Communications, 43(12):917-919, (1982).

26. Henning, J. C. M., et al. "Excited States of the Zn and C Acceptors in $Al_{0.47}Ga_{0.53}As$," Physical Review B, 27(12):7451-7459, (15 June, 1983).

27. Hetzler, S. R., et al. "Selective Excitation Luminescence and Electronic Raman Scattering Study of the 78 meV Acceptor in GaAs," Applied Physics Letters, 44(8):793-795, (15 April, 1984).

28. IIegems, M., et al. "Optical and Electrical Properties of Mn-Doped GaAs Grown by Molecular Beam Epitaxy," Journal of Applied Physics, 46(7):3059-3065, (July 1975).

29. Johnson, E. J., et al. "Deep Center EL2 and Anti-Stokes Luminescence in Semi-Insulating GaAs", Applied Physics Letters, 40(11):993-995, (1 June, 1982).

30. Kamiya, T., Wagner, E., "Optical Determination of Impurity Compensation in n-Type Gallium Arsenide," Journal of Applied Physics, 48(5):1928-1934, (May, 1977).

31. Kazuhiro, K., et al. "Photoluminescence Spectra of Undoped GaAs Grown by Molecular-Beam Epitaxy at Very High and Low Substrate Temperatures," Journal of Applied Physics, 59(3):888-891, (1 February, 1986).

32. Kirkman, R. F., et al. "An Infrared Study of Shallow Acceptor States in GaAs," Journal of Physics C, 11:419-433, (1978).

33. Kisker, D. W., "Luminescence Study of C, Zn, Si, and Ge Acceptors in GaAs," Journal of Applied Physics, 54(3):1332-1336, (March, 1983).

34. Kunzel, H., Ploog, K., "The Effect of As_2 and As_4 Molecular Beam Species on Photoluminescence of Molecular Beam Epitaxially Grown GaAs," Applied Physics Letters, 37(4):416-418, (15 August, 1980).

35. Letterman, R. C. C., DiGiovanni, A. E., "Frequency Shift with Temperature as Evidence for Donor-Acceptor Pair Recombination in Relatively Pure n-Type GaAs," Physical Review, 153(3):841-843.

36. Luttinger, J. M., "Quantum Theory of Cyclotron Resonance in Semiconductors: General Theory," Physical Review, 102:1030, (1956).

37. Lyons, Lt Robert P. Ion Implantation of Diatomic Sulfur into GaAs. MS Thesis, AFIT/GE/EE/74-54. School of Engineering, Air Force Institute of Technology, Wright-Patterson AFB OH, December 1974.

38. Medland, J.D. Photoluminescence Spectra of VPE GaAs. EMIS Datareview, January 1986, section 12.5.

39. Metze, G. M., et al. "An Investigation of GaAs Films Grown by MBE at Low Substrate Temperatures and Growth Rates," Journal of Vacuum Science and Technology B, 1(2):166-169, (April 1983).

40. Nakashima, S., et al. "Excitation Spectra of Donor-Acceptor Pair Photoluminescence of ZnTe," Solid State Communications, 25:137-139, (1978).

41. Nam, S. B., et al. "Exciton Energy Spectrum in GaAs in a Magnetic Field," Journal of Luminescence, 12:277-284, (1976).

42. Nobukazu, O., et al. "Selective Optical Compensation Effect for a Newly Discovered Acceptor-Associated Emission in Zn^+ Ion-Implanted GaAs," Journal of Applied Physics, 60(7):2502-2504, (1 October, 1986).

43. Nomura, T., et al. "Concentration Ratio Dependence of Selective Optical Compensation Effect of Dually Zn^+ and Se^+ Ion-Implanted GaAs," Applied Physics Letters, 48(25):1745-1747, (23 June, 1986).

44. Ozeki, M., et al. "Residual Donors in High Purity Gallium Arsenide Epitaxially Grown from Vapor Phase," Japanese Journal of Applied Physics, 16(9):1617-1622, (September 1977).

45. Quagliano, L. G., Nather, H., "Up Conversion of Luminescence Via Deep Centers in High Purity GaAs and GaAlAs Epitaxial Layers," Applied Physics Letters, 45(5):555-557, (1 September, 1984).

46. Reynolds, D. C., et al. "Anomalies Observed in the Shallow Acceptor States in GaAs," Physical Review B, 32(12):8242-8245, (1985).

47. Reynolds, D. C., et al. "Observation of Discrete Donor-Acceptor Pair Spectra in MBE Grown GaAs," Solid State Communications, 52(7):685-688, (1984).

48. Reynolds, D. C., et al. "Lifetimes, Ionization Energies, and Discussion of the Emission Lines in the 1.5040-1.5110 eV Range in GaAs," Journal of Applied Physics, 60(7):2511-2516 (1 October, 1986).

49. Reynolds, D. C., et al. "Radiative Transitions Associated with Two-Acceptor-One-Donor Complexes in Epitaxial GaAs and InP," Physical Review B, 28(2):1117-1131.

50. Reynolds, D. C., et al. "Zeeman Studies of Photoluminescence of Excited Terminal States of a Bound-Exciton-Donor Complex in GaAs," Physical Review B, 12(12):5723-5728, (15 December, 1975).

51. Rossi, J. A., et al. "Identification of Exciton-Neutral Donor Complexes in the Photoluminescence of High Purity GaAs," Solid State Communications, 8:2021-2024, (1970).

52. Roth, A. P., et al. "New Photoluminescence Lines in GaAs Layers Grown by Metalorganic Vapor Phase Epitaxy," Journal of Applied Physics, 54(6):3427-3430, (June, 1983).

53. Samuelson, L., et al. "Electrical and Optical Properties of Deep Levels in MOVPE Grown GaAs," Journal of Crystal Growth, 55:164-172, (1981).

54. Schairer, W., Yep, T. O., "Two-Hole Transition in the Luminescence of Excitons Bound to Neutral Acceptors in GaAs," Solid State Communications, 9:421-424, (1971).

55. Schairer, W., et al. "Piezoelectric and Magneto-Optical Study of the Sn-Acceptor in GaAs," Physical Review B, 13(8):3452-3467, (15 April, 1976).

56. Scott, G. B., Roberts, J. S., "Photoluminescence in III-V Compounds Grown by MBE," Institute of Physics Conference Series, 45(3):181-189, (1979).

57. Shah, J., et al. "Donor-Acceptor Pair Recombination Involving the First Excited State of a Donor in GaAs," Physical Review, 176(3):938-942, (15 December 1968).

58. Skromme, B. J. et al. "Characterization of High-Purity Si-Doped Molecular Beam Epitaxial GaAs," Journal of Applied Physics, 58:4685-4702 (15 December 1985).

59. Skromme, B. J., et al. "Characterization of High-Purity Si-Doped Molecular Beam Epitaxial GaAs," Journal of Applied Physics, 58(12):4685-4702, (15 December 1985).

60. Skromme, B. J., et al. "Photoluminescence Characterization of Molecular Beam Epitaxial GaAs Grown Using Cracked AsH_3" Applied Physics Letters, 44(2):240-242, (15 January, 1984).

61. Skromme, B. J., Stillman, G. E., "Excited-State-Donor-to-Acceptor Transitions in the Photoluminescence Spectrum of GaAs and InP," Physical Review B, 29(4):1982-1992, (15 February, 1984).

62. Stangel, Capt James E. Growth of Epitaxial Gallium Arsenide by the Vapor Phase Process. MS thesis, AFIT/GE/EE/72-24. School of Engineering, Air Force Institute of Technology (AU), Wright-Patterson AFB OH, December 1972.

63. Street, R. A., Senske W., "Spectroscopy of Excited States in GaP," Physical Review Letters, 37(19):1292-1295, (8 November, 1976).

64. Stringfellow, G. B., et al. "Carbon in Molecular Beam Epitaxial GaAs," Applied Physics Letters, 38(3):156-157, (1 February, 1981).

65. Tews, H., "Zeeman Study of Donor-Acceptor Pairs in ZnTe," Physical Review B, 23(2):587-598, (15 January, 1981).

66. Tews, H., et al. "Excited States of Shallow Acceptors in ZnSe," Physical Review B, 19(10):5178-5184, (15 May, 1979).

67. Tews, H., Venghaus, H., "Selective Pair Luminescence in Semiconductors," Solid State Communications, 30:219-221, (1979).

68. Venghaus, H., "Excitation Intensity Dependence of Shallow Donor Bound Exciton Luminescence in n-GaAs", Journal of Luminescence, 16:331-341, (1978).

69. Wagner, J., Ramsteiner, M., "Residual Acceptor Assessment in As-Grown Bulk GaAs by Raman and Selective Pair Luminescence Spectroscopy: A Comparative Study," Applied Physics Letters, 49(20):1369-1371, (17 November, 1986).

70. White, A. M., "The Photoluminescence Spectrum of Bound Excitons in Indium Phosphide and Gallium Arsenide," Journal of Physics C, 5:1727-1738, (1972).

71. White, A. M., et al. "Acceptor Levels in Gallium Arsenide," Journal of Physics C, 6:L243-L246, (1973).

72. White, Guy K. Experimental Techniques in Low-Temperature Physics. Oxford: Clarendon Press, 1968.

73. Williams, E. W. and H. Barry Bebb, Semiconductors and Semimetals Volume 8. edited by R. K. Willardson and Albert C. Beer. New York and London: Academic Press, 1972.

74. Wolfe, C. M., et al. "Silicon as a Residual Donor in High-Purity GaAs," Applied Physics Letters, 24(2):78-80, (15 January, 1974).

75. Yu, P. W., "Photoluminescence Excitation of the 1.441 eV Cation Antisite Emission in p-Type GaAs," Physical Review B, 27(12):7779-7781, (15 June, 1983).

Jeffrey Cavins [redacted] Upon graduation from Florida Technological University in 1978, he received a Bachelor of Science degree in Physics and a commission in the United States Air Force. He served as a Project Officer for the Pulsed Laser Systems Branch at the Air Force Weapons Laboratory until he entered the Air Force Institute of Technology for his Masters degree in 1981. After receiving his Masters degree in Engineering Physics he was assigned to the Air Force Foreign Technology Division at Wright-Patterson AFB, Ohio, as a Laser Weapons Intelligence Analyst. In 1983 he returned to AFIT to pursue a doctorate. He is currently assigned to HQ USAF at Patrick AFB, Florida.

[redacted]

URITY CLASSIFICATION OF THIS PAGE

REPORT DOCUMENTATION PAGE

REPORT SECURITY CLASSIFICATION UNCLASSIFIED	1b. RESTRICTIVE MARKINGS
SECURITY CLASSIFICATION AUTHORITY	3. DISTRIBUTION/AVAILABILITY OF REPORT Approved for public release; distribution unlimited.
DECLASSIFICATION/DOWNGRADING SCHEDULE	
PERFORMING ORGANIZATION REPORT NUMBER(S) AFIT/DS/ENP/88-2	5. MONITORING ORGANIZATION REPORT NUMBER(S)
NAME OF PERFORMING ORGANIZATION: School of Engineering 6b. OFFICE SYMBOL (If applicable): AFIT/ENP	7a. NAME OF MONITORING ORGANIZATION
ADDRESS (City, State and ZIP Code) Air Force Institute of Technology (AU) Wright-Patterson AFB, Ohio 45433-6583	7b. ADDRESS (City, State and ZIP Code)
NAME OF FUNDING/SPONSORING ORGANIZATION 8b. OFFICE SYMBOL (If applicable)	9. PROCUREMENT INSTRUMENT IDENTIFICATION NUMBER
ADDRESS (City, State and ZIP Code)	10. SOURCE OF FUNDING NOS. PROGRAM ELEMENT NO. / PROJECT NO. / TASK NO. / WORK UNIT NO.
TITLE (Include Security Classification) See Box 19	
PERSONAL AUTHOR(S) Jeffrey R. Cavins, B.S., M.S., Capt, USAF	
a. TYPE OF REPORT: PhD Dissertation 13b. TIME COVERED: FROM _____ TO _____ 14. DATE OF REPORT (Yr., Mo., Day): 88 December 15. PAGE COUNT: 188	
SUPPLEMENTARY NOTATION	

COSATI CODES			18. SUBJECT TERMS (Continue on reverse if necessary and identify by block number)
FIELD	GROUP	SUB. GR.	Gallium Arsenides, Ion Implantation, Photoluminescence, Magnesium. (JES)
07	02		Theses, Ion Implantation

ABSTRACT (Continue on reverse if necessary and identify by block number)

Title: SELECTIVE PAIR LUMINESCENCE OF MAGNESIUM IN GALLIUM ARSENIDE

Dissertation Chairman: Yung Kee Yeo, PhD
Associate Professor of Physics

DISTRIBUTION/AVAILABILITY OF ABSTRACT UNCLASSIFIED/UNLIMITED ☒ SAME AS RPT. ☐ DTIC USERS ☐	21. ABSTRACT SECURITY CLASSIFICATION UNCLASSIFIED
NAME OF RESPONSIBLE INDIVIDUAL Yung Kee Yeo, PhD	22b. TELEPHONE NUMBER (Include Area Code) (513) 255-2012 22c. OFFICE SYMBOL AFIT/ENP

FORM 1473, 83 APR EDITION OF 1 JAN 73 IS OBSOLETE.

SECURITY CLASSIFICATION OF THIS PAGE

Photoluminescence (PL) and selective pair luminescence (SPL) studies were performed on vapor phase epitaxial (VPE) GaAs. The GaAs included both undoped and Mg ion implanted samples, with fluences of 10^{12}, $5x10^{12}$, 10^{13}, $5x10^{13}$, and 10^{14} Mg/cm^2, respectively.

PL from the unimplanted samples indicated Zn was the dominant impurity with slight traces of C and Si also evident. In addition, the SPL spectra contained three peaks at 17.2, 20.0, and 21.1 meV, which coincide with the values expected for the $2P_{3/2}$, $2S_{3/2}$, and $2P_{5/2}\Gamma_8$ states of Mg, respectively. This assignment was confirmed during SPL measurements of the ion implanted samples. The effect of the Mg implant on the relative intensities of the Mg related SPL transitions was small but discernible. Photoluminescence of the ion implanted materials showed strong Mg impurity spectra; however, the Zn impurity spectra was still dominant.

Additionally, a parametric study was performed on the effects of temperature and laser pump intensity on the SPL spectra. Temperature behavior of the SPL spectra was similar to the PL with the strongest SPL transitions visible at temperatures as high as 30 K. Analysis of the intensity behavior of the SPL spectra indicated pump intensity should be minimized (less than 70 mW/cm^2) for best results.